Surface photometry of galaxies

UGC 9133

NGC 5533

SA(rs)ab

cz=3866 km/s

3.1 x 1.9 arcmin

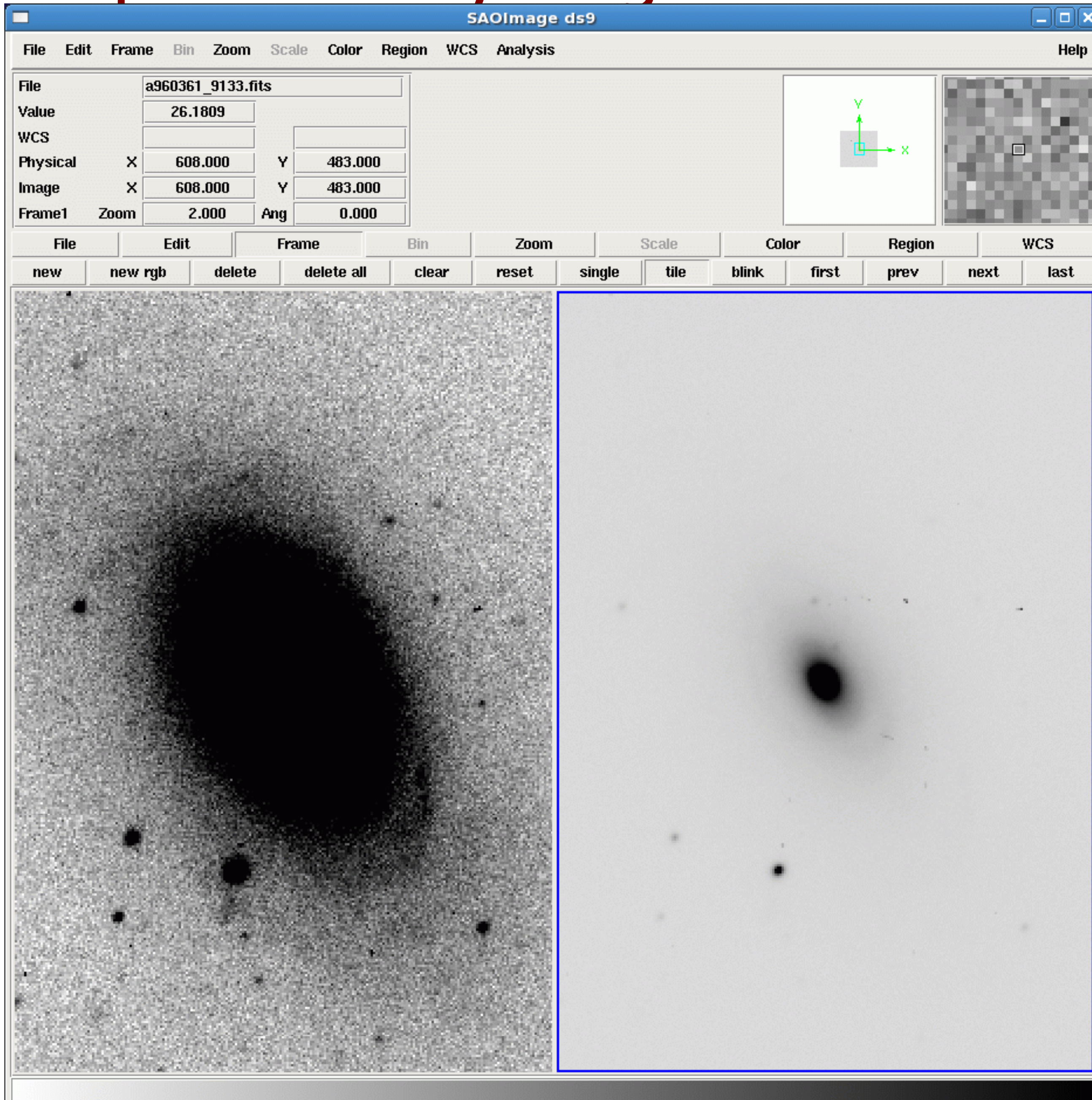

EGG resources

During the 1980's-90's, the EGG and friends undertook a number of studies which established the "gold standard" (according to a referee) of Tully-Fisher studies. The projects were dubbed:

- SFI: Spiral Field I-band
- SCI: Spiral Cluster I-band
- SC2, SFI++ (2nd generation studies, final datasets)

Since the early 1980's, we developed digital archives of all these data. They still exist (Long live ASCII!)

- Targeted observations of 9000 galaxies observed with Arecibo, Green Bank 42m/91m, Nancay, Effelsberg
- Optical (long slit) rotation curves notably from Palomar but also many from the literature
- I-band surface brightness profiles (ellipse fitting)
- + AL

These data exist

UGC 9133 = NGC 5533

Table 1

CITED IN TEXT | DATA | TYPESET IMAGE   Go to: Table 2

Additional Photometric Parameters

Number (1)	Other (2)	R.A. (J2000.0) (3)	Decl. (J2000.0) (4)	T (5)	$r_{23.5}$ (6)	r_{83L} (7)	$\mu_{\rm out}$ (8)	e (9)	ϵ_e (10)	P.A. (11)	$\epsilon_{\rm P.A.}$ (12)	$m_{\rm obs}$ (13)	ϵ_m (14)	Code (15)
331060...	478-009b	00 00 03.4	+23 05 15	5	24.7	21.7	23.43	0.762	0.009	64	2	15.20	0.05	
12898...		00 00 37.4	+33 36 02	5	21.4	20.5	24.27	0.646	0.035	11	5	15.23	0.05	
12900...	456-015	00 00 55.9	+20 20 17	5	46.3	37.4	24.30	0.820	0.009	110	1	13.73	0.04	
36544...	349 G 17	00 00 57.7	-33 36 47	5	35.3	29.3	25.41	0.219	0.110	120	12	12.91	0.05	
12901...	499-035	00 00 58.9	+28 54 41	3	41.5	32.1	24.30	0.570	0.042	46	1	12.84	0.02	
12913...	M+001018	00 01 36.7	+03 30 21	5	38.0	37.3	23.37	0.817	0.009	5	1	14.62	0.08	
36558...	409 G 4	00 01 57.6	-27 59 53	3	33.4	29.4	23.71	0.614	0.015	56	1	13.78	0.05	
12920...	478-014	00 02 23.0	+27 12 38	4	33.9	28.5	24.14	0.737	0.020	49	1	14.24	0.04	
400001...	M-101024	00 02 34.7	-03 42 37	4	31.6	23.2	23.83	0.439	0.094	0	4	12.90	0.02	
100002...	408-013	00 02 39.8	+08 44 13	3	32.7	22.1	24.58	0.734	0.012	23	1	13.61	0.02	

Notes.—Units of right ascension are hours, minutes, and seconds, and units of declination are degrees, arcminutes, and arcseconds. Table 1 is available in its entirety via the link to the machine-readable version above.

```
 30526 579 G  9 14 15 33.5 -20 39 48     3  29.3   26.7   24.64 0.501 0.025  117  2   13.85 0.04
 30527 511 G 16 14 15 43.4 -24 25 17     5  26.2   21.5   24.58 0.632 0.019  114  1   14.39 0.04
  9133 N5533    14 16 07.6 +35 20 36     3 102.7   83.1   24.24 0.407 0.022   27  3   10.54 0.03
 30535 579 G 10 14 16 24.1 -21 19 53     3  30.2   29.9   24.07 0.461 0.080    1  4   13.70 0.05
  9138 133-023  14 16 47.1 +23 00 09     4  46.5   36.3   23.81 0.810 0.005  168  4   13.63 0.04
241267 M+631092 14 17 11.7 +35 24 30     3  25.8   16.1   23.07 0.591 0.015   15  1   13.74 0.02
540063 I 991    14 17 48.8 -13 52 22     5  48.7   37.0   23.86 0.421 0.070  108  5   12.01 0.04
 30549 I4393    14 17 49.4 -31 20 54     5  75.1   58.4   23.91 0.875 0.019   77  1   12.86 0.05
```

"Activity" in galaxies

- Tides, collisions, mergers
  - Distorted appears due to gravitational forces
- Starburst
  - Star formation rate much higher than "normal" (i.e. the average in Milky Way today)
  - Large amounts of molecular gas
  - $L_{FIR}/M(H_2)$ like prototypical starburst galaxies (M82, N253)
- "Active Galactic Nucleus" (AGN; Seyfert galaxies; Quasar/QSO)
  - Presence of extremely bright, star-like nucleus which shows evidence (fast moving gas clouds; high energy photons) of SMBH
  - Broad line widths indicate AGN
  - Low H-recombination line fluxes => not enough OB stars to support luminosity

Sometimes more than one of these applies in the same system => cause and effect

Star formation history of the universe

- Observations of external galaxies reveal global and local star formation events ranging over >10^7x in absolute scale--- over a far wider range of physical environments than can be found in the Milky Way
- Star formation is a primary component of galaxy evolution and cosmic evolution
- Despite its central role, galactic-scale SF as a physical process is barely understood

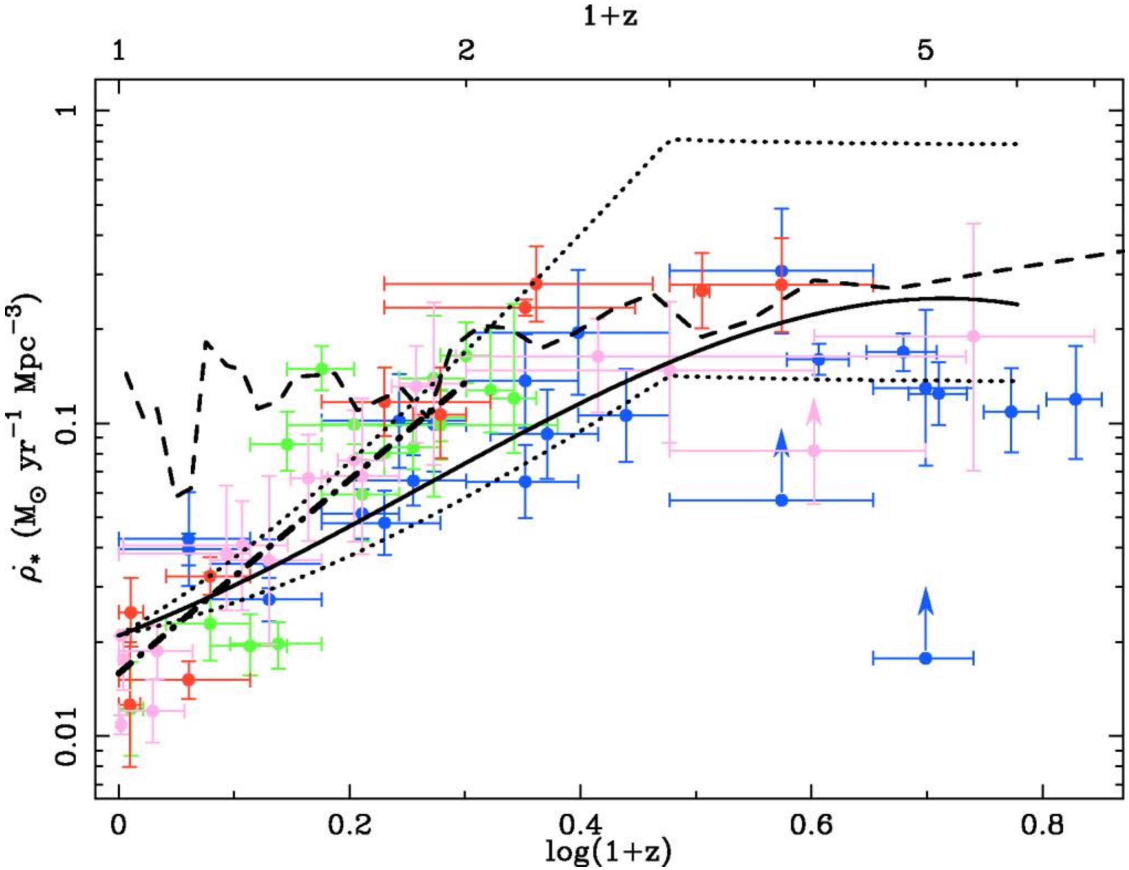

Hopkins 2004, ApJ, 615, 209

Dust extinction plays a key role in the interpretation of multiwavelength observations

Spectral diagnostics

- For nearby, resolved objects, HST can provide color-magnitude diagrams, but for more distant objects, we must deduce the star formation history from spectra (if we're lucky…)
- Does the spectrum show the characteristics of a static, evolved, old stellar population?
  - Age of the stellar population?
  - e.g. Hydrogen Balmer absorption: A-stars but no emission lines means no O,B stars
- Does the spectrum contain emission lines as expected for HII regions?
  - Current massive star formation
- Does the spectrum show absorption lines that are much broader than normal => SMBH

AGN diagnostics

- Miller et al. 2003, ApJ 597, 142: SDSS
  - See Osterbrock's book
  - Red circles: AGN
  - Blue triangles: Star forming galaxies
  - Differences in the spectral characteristics of the ionizing photons yield differences in the line ratios

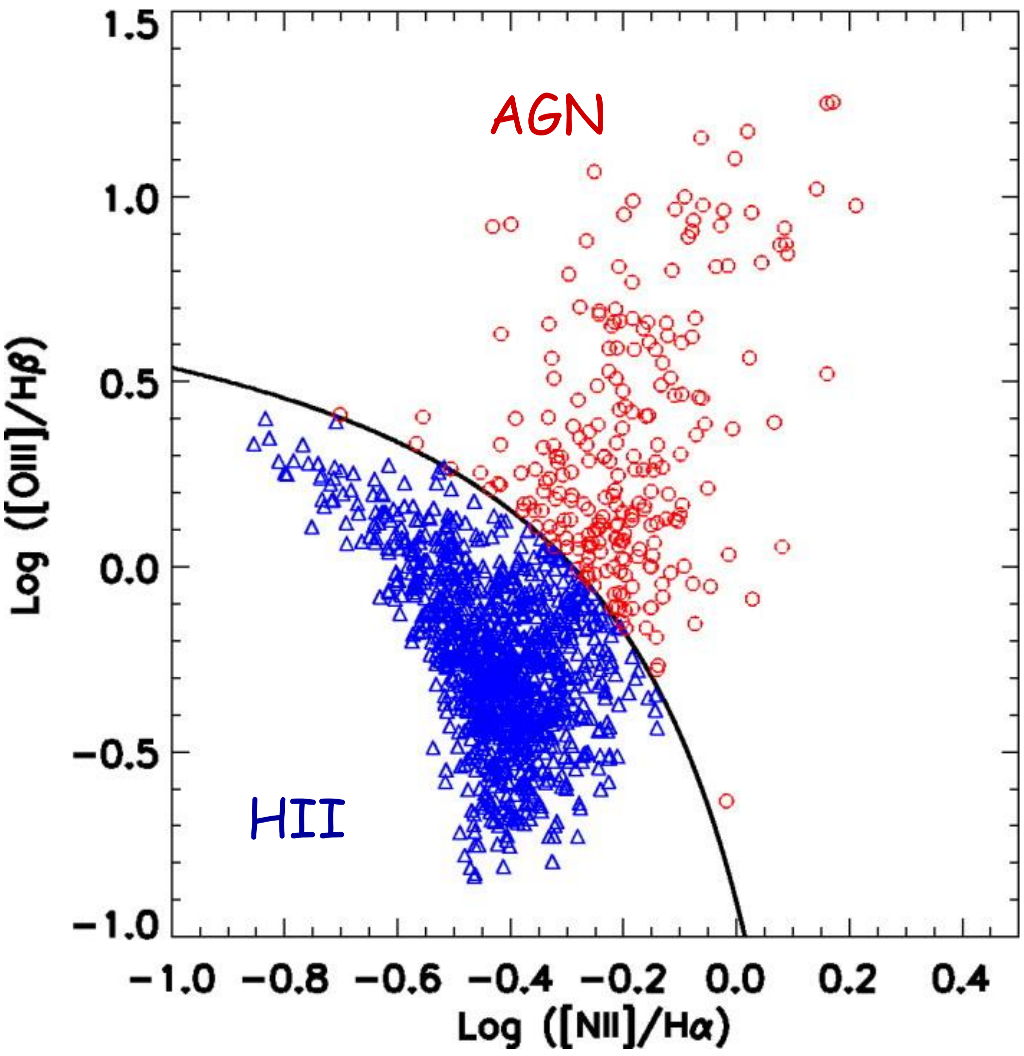

Star formation rate estimators

- Kennicutt 1998, ARAA 36, 189
- Condon 1992, ARAA 30, 575
- Hopkins et al. 2003, ApJ 599, 971 (SDSS)
- Bell et al. 2005, ApJ 625, 23 (Spitzer MIPS)
- Calzetti 2012 astro-ph 1208.2997

Star formation rate indicators:

- H-alpha => massive stars
- 1.4 GHz continuum => thermal HII + SNe
- L(FIR) => IRAS => dust heated by UV photons
- L(UV) => massive stars

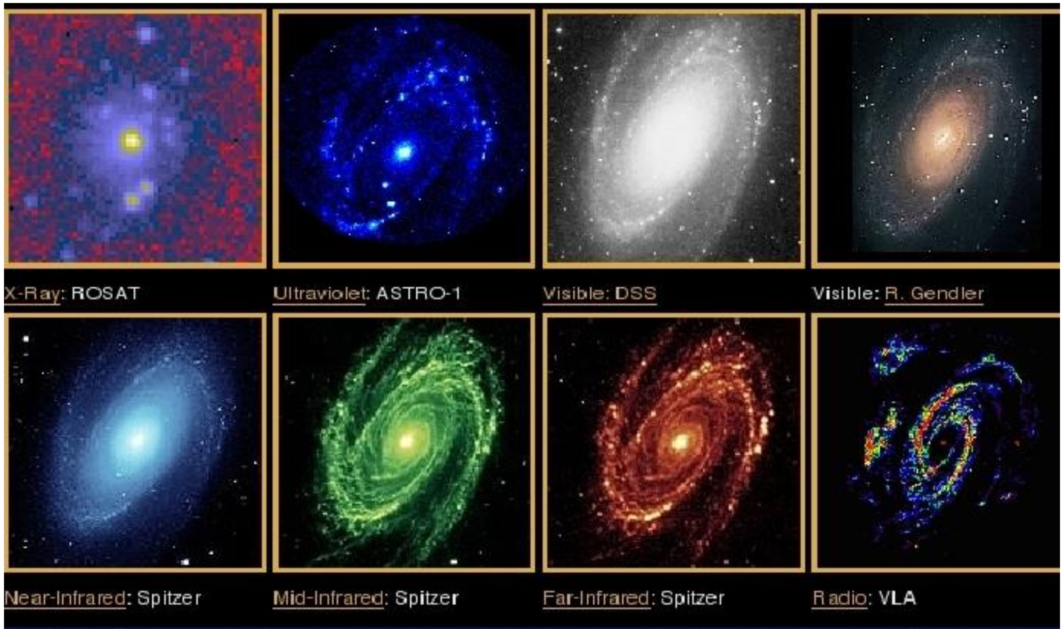

Wanted: indicators of young stars

- Observables produced by massive stars (short-lived population)

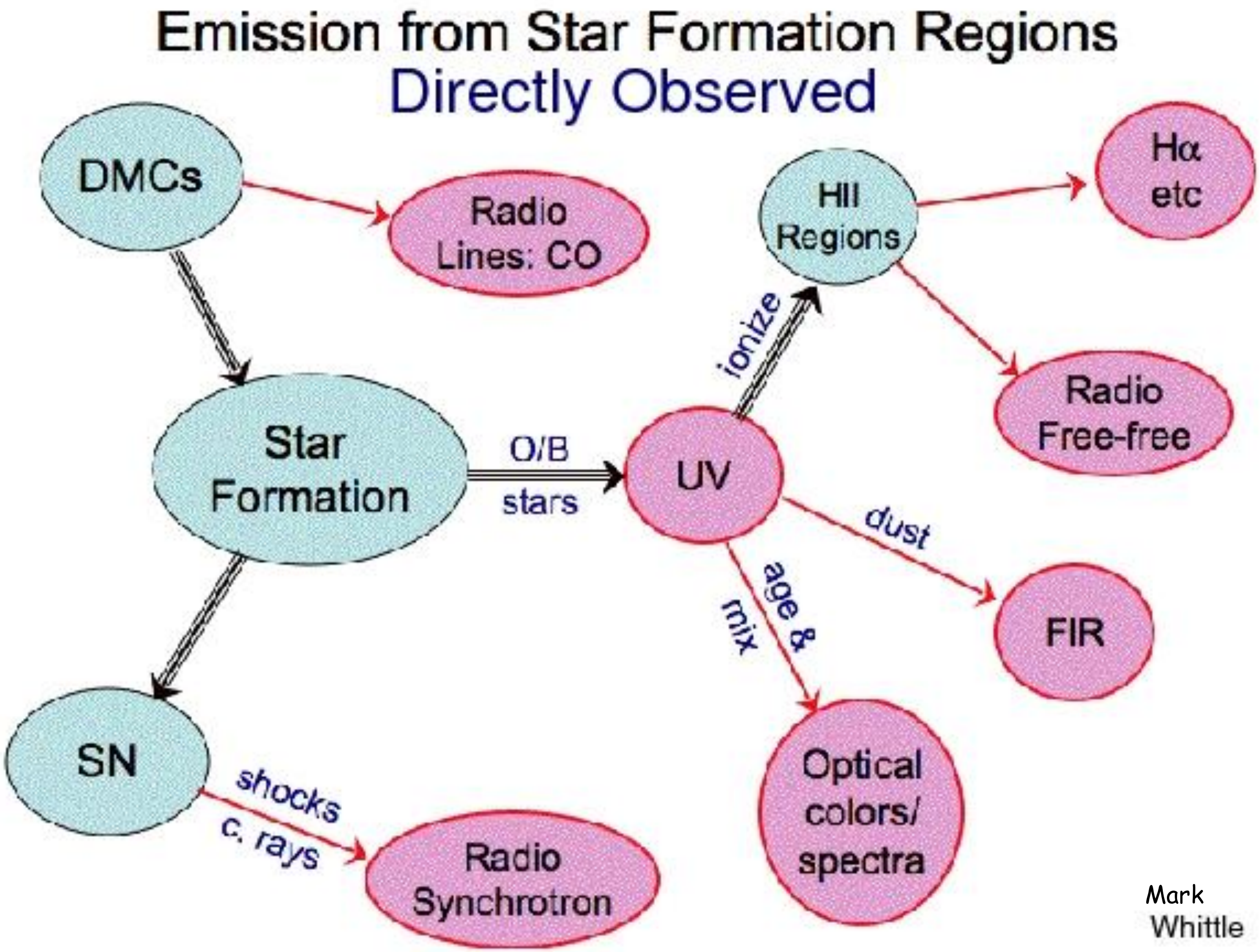

But remember: low mass stars dominate the mass

Star formation in disks and nuclei

- Kennicutt 1998, ARAA 36, 189

TABLE 1 Star formation in disks and nuclei of galaxies

Property	Spiral disks	Circumnuclear regions
Radius	1–30 kpc	0.2–2 kpc
Star formation rate (SFR)	0–20 $M_\odot$ year^{-1}	0–1000 $M_\odot$ year^{-1}
Bolometric luminosity	10^6–10^{11} $L_\odot$	10^6–10^{13} $L_\odot$
Gas mass	10^8–10^{11} $M_\odot$	10^6–10^{11} $M_\odot$
Star formation time scale	1–50 Gyr	0.1–1 Gyr
Gas density	1–100 $M_\odot$ pc^{-2}	10^2–10^5 $M_\odot$ pc^{-2}
Optical depth (0.5 μm)	0–2	1–1000
SFR density	0–0.1 $M_\odot$ year^{-1} kpc^{-2}	1–1000 $M_\odot$ year^{-1} kpc^{-2}
Dominant mode	steady state	steady state + burst
Type dependence?	strong	weak/none
Bar dependence?	weak/none	strong
Spiral structure dependence?	weak/none	weak/none
Interactions dependence?	moderate	strong
Cluster dependence?	moderate/weak	?
Redshift dependence?	strong	?

Two regimes of SFR

Range in galaxy star formation rates: $10^{-4} - 10^{3}\ M_\odot\ yr^{-1}$

- **Normal** galaxies (~75% of local SF) have SFRs : 0 - few $M_\odot\ yr^{-1}$
- **Starburst** galaxies (~25% of local SF) range from :

few $M_\odot\ yr^{-1}$ (SB) to 50 $M_\odot\ yr^{-1}$(LIGs) to $10^{2\text{-}3}\ M_\odot\ yr^{-1}$ (ULIGs)

Starburst: intense burst of short duration (< 10^{8} years)

often located in circumnuclear region

often in interacting systems (accumulation of gas)

different relationships may apply

Relevant observables

UV flux	High mass stars dominate UV luminosity => visible if not dusty
$H\alpha$ line flux	B0 and hotter create ionizing flux < 912 Å
Radio free-free flux	Ionized gas radiates bremsstrahlung at ~5 GHz
FIR flux	Dust absorbs UV and reradiates in FIR

For $H\alpha$ to emit, we need 1 ionizing photon per H atom

Photoionization rate: $Q_H = dN_{ion}/dt \;\; s^{-1}$

Assuming α @T=10^4 K = 3×10^{-13} $cm^3\ s^{-1}$ (recombination coeff)

Recombination rate: $\sim 3 \times 10^{-13}\, n_e^2 V \;\; s^{-1}$

1 in 4 recombinations yields $H\alpha$ photon so

$L(H\alpha) = 1.3 \times 10^{-12}\, Q_H$ erg/s

$L_\nu(ff) = 7.3 \times 10^{-39}\, n_e^2 V = 2.4 \times 10^{-26}\, Q_H$ (erg/s/Hz @T=10^4 K)

L(FIR) acts like a bolometer

UV Continuum Emission

Andromeda Galaxy
GALEX

Andromeda Galaxy
Visible light image (John Gleason)

Extinction is important!

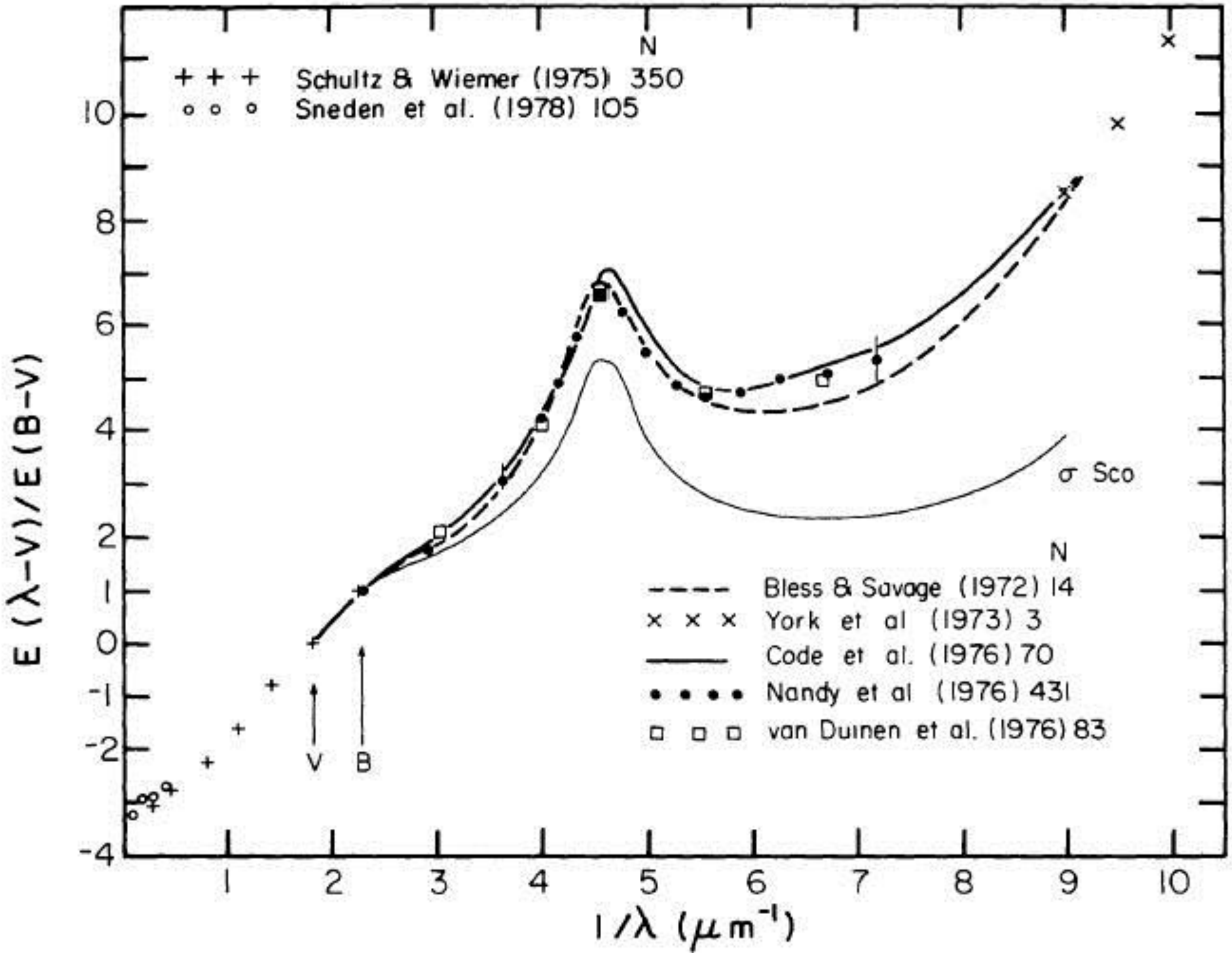

Ultraviolet continuum

Directly observing young stars with $M > 5\ M_\odot$

(i) Near-UV (1500 - 2800) Luminosity

hot high mass young stars dominate the NUV emission, yielding :

$$\mathrm{SFR}\ \ (M_\odot\ \mathrm{yr}^{-1}) \ = \ 1.4\times10^{-28}\ L_{NUV} \ \ (\mathrm{erg\ s}^{-1}\mathrm{Hz}^{-1})$$

strengths : for moderate-strong SFR, very little contamination from non-SB stars;

useful for high-z galaxies (where UV is redshifted into optical)

weaknesses : sensitive to IMF and to dust

- Salpeter IMF applies to galaxies with continuous SF over 10^8 years or longer.
- Starbursts seem to have smaller SFR/L_{NUV}.

-Direct photospheric measure of young massive stars

-Primary groundbased SFR tracer for galaxies at $z>2$

Photoionization Methods: Emission Lines

• for ionization-bounded region observed recombination line flux scales with ionization rate

• ionization dominated by massive stars ($M > 10\ M_o$), so nebular emission traces SFR in last 3-5 Myr

• ionizing UV reprocessed through few nebular lines, detectable to large distances

• only traces massive SFR, total rates sensitive to IMF extrapolation

• SFRs subject to systematic errors from extinction, escape of ionizing radiation from galaxy

SINGG survey
G. Meurer et al.

Hydrogen recombination lines

Observing effect on ISM of young stars with $M > 10\ M_\odot$

Ultraviolet flux (<912A) ionizes surrounding hydrogen cloud,
--> recombination emission

Photoionization rate = Recombination rate

$$Q_H = dN_{ion} / dt \ \ s^{-1} = 3 \times 10^{-13}\, n_e^{\,2} V \, s^{-1}$$

n_e = electron density, V = volume, 3×10^{-13} = recombination coeff at $T = 10^4$ K

1 in 4 recombinations yields Hα photon : $L_{H\alpha} = 1.3 \times 10^{-12}\, Q_H$ erg/s

Other Emission Lines

- Hβ (0.48 μm)
- Paschen-α (1.9 μm)
- Brackett-γ (2.2 μm)
- [OII] (0.37 μm)
- Lyman-α (0.12 μm)

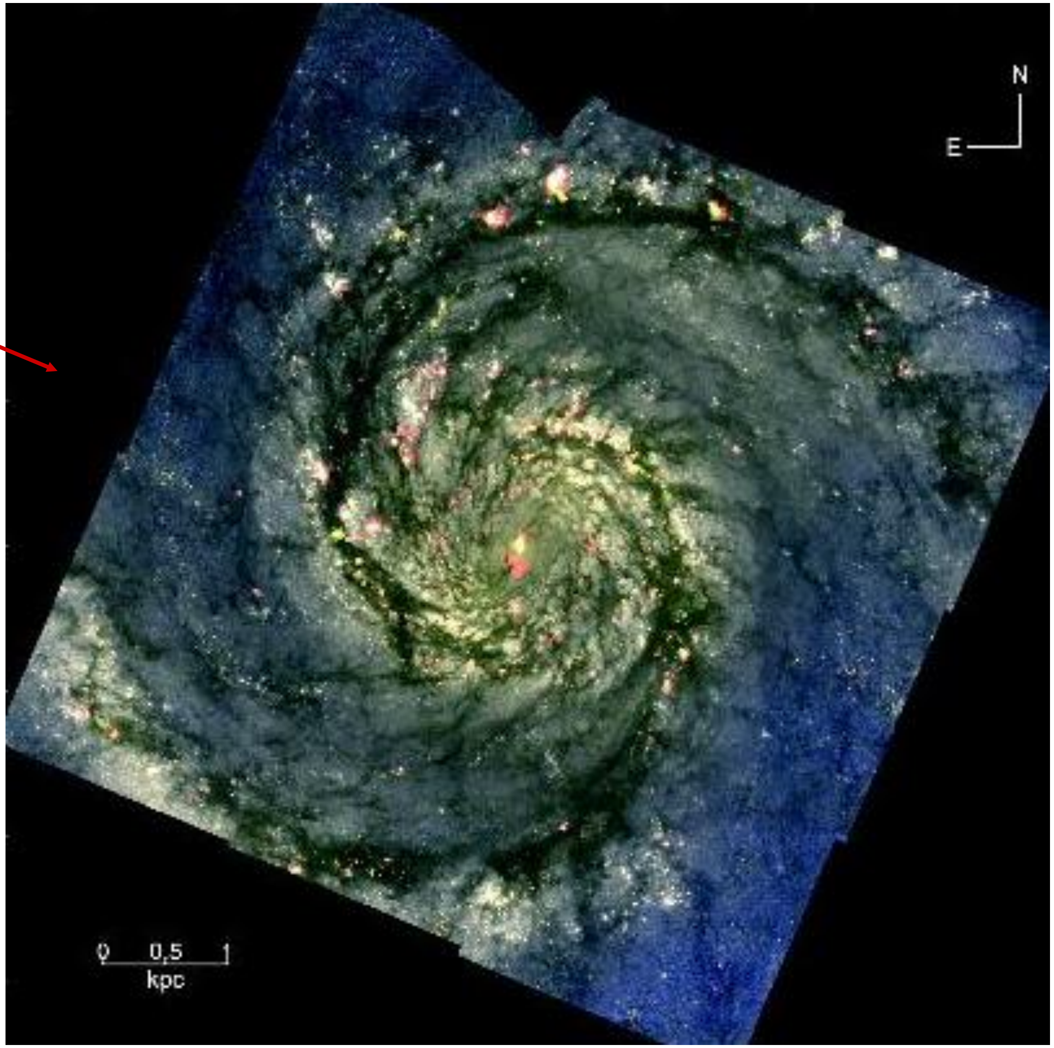

Scoville et al. 2000, AJ, 122, 3017

Hydrogen recombination lines

Observing effect on ISM of young stars with $M > 10\ M_\odot$

- The table gives some useful Hydrogen line wavelengths and relative strengths (Case B: $T = 10^4$ K):

Series (lower level)	α wav ratio/Hβ	β wav ratio/Hβ	γ wav ratio/Hβ	ζ wav ratio/Hβ	Series Limit wav
1: Lyman	1216 A_{vac} 23	1026 A_{vac} ??	973 A_{vac} ??	950 A_{vac} ??	912 A_{vac}
2: Balmer	$\boxed{6563\ A\ \ 2.86}$	4861 A 1.00	4340 A 0.47	4101 A 0.26	3646 A
3: Paschen	1.87 μ 0.339	1.28 μ 0.163	1.09 μ 0.090	1.00 μ 0.055	0.82 μ
4: Brackett	4.05 μ 0.080	2.63 μ 0.045	2.16 μ 0.028	1.94 μ 0.018	1.45 μ

Note that the Ly-α flux is often difficult to predict:
it is resonantly scattered and either:

it is absorbed by dust, or
the $2 \rightarrow 1$ transition goes via 2-photon decay

1 in 4 recombinations yields Hα photon

$L_{H\alpha} = 1.3 \times 10^{-12}\ Q_H$ erg/s

- Cascades between very high n (~100) give **radio recombination lines**
e.g. H109α at 5.8cm comes from transitions **n**=109 → 108
These lines are useful since they are unaffected by dust; though they are quite weak.

Whittle

HII regions

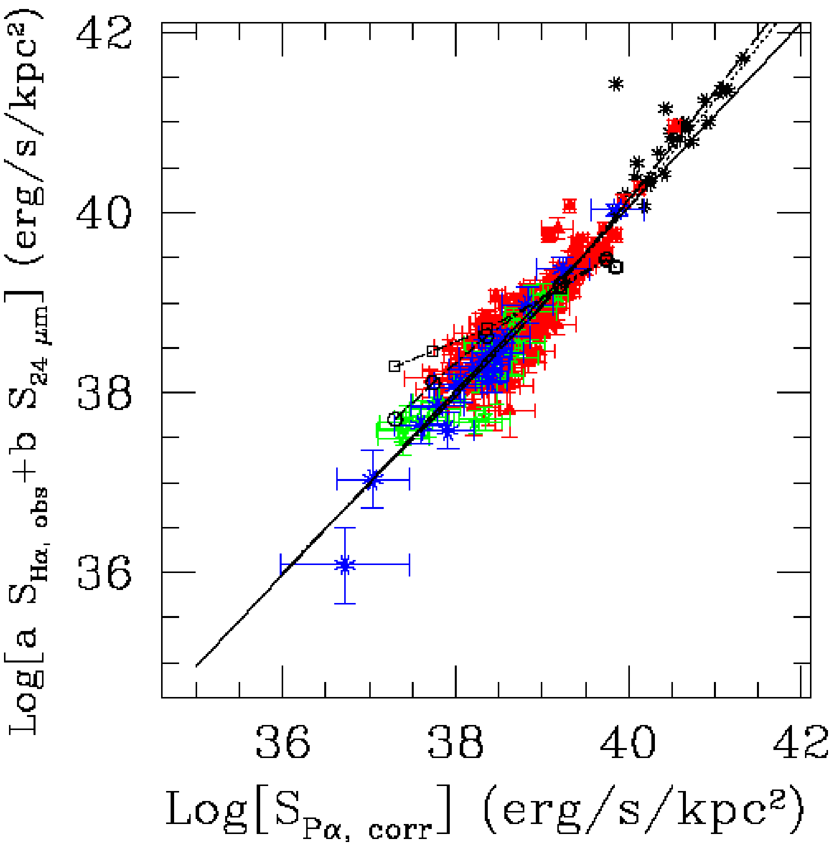

galaxies (integrated fluxes)

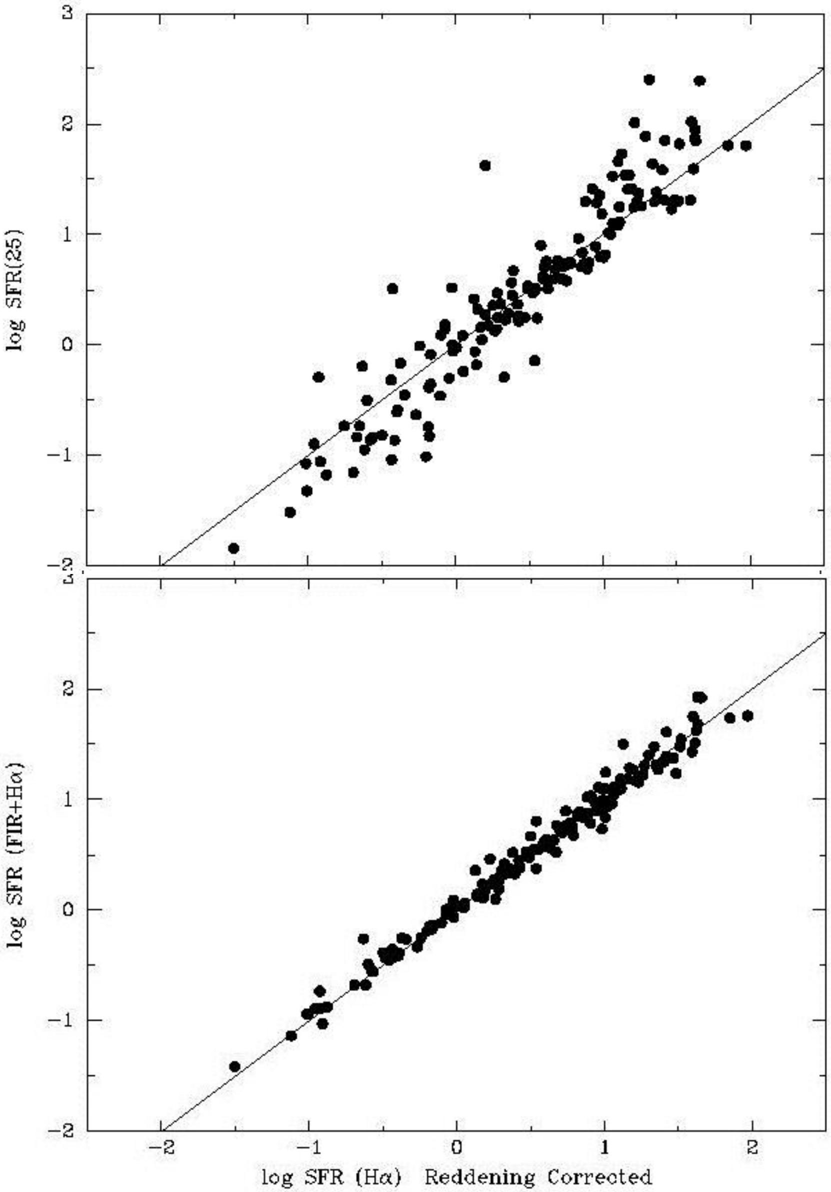

Calzetti et al. 2007
Kennicutt & Moustakas 2007

Recombination lines

(ii) Hα Luminosity

In principle this applies to other recombination lines : eg Brγ & Paα & H109 etc

Significant ionizing radiation only comes from stars with $M > 10M_\odot$

lifetime of these stars is < 20 Myr → Hα measures *current* SFR

$$\mathrm{SFR}\ (M_\odot\ \mathrm{yr}^{-1}) = 7.9\times10^{-42}\ L_{H\alpha}\ \ (\mathrm{erg\ s}^{-1})$$

$$= 8.2\times10^{-40}\ L_{Br\gamma}\ \ (\mathrm{erg\ s}^{-1})$$

$$= 1.1\times10^{-53}\ Q_H\ \ (\mathrm{s}^{-1})$$

strengths : sensitive; direct; high spatial resolution; useful out to $z \lesssim 2$

weaknesses : sensitive to reddening (typical $A_{H\alpha} \approx 0.5$ - 1.5 mags), IMF slope and M_{up}

5 - 50% of the ionizing radiation *escapes* the HII regions

→ must include Hα from the *diffuse ionized medium* (DIM) emission

(only ≈3% ionizing flux escapes the *galaxy*)

at higher z (when Hα too redshifted), a less precise relation is :

$$\mathrm{SFR}\ (M_\odot\ \mathrm{yr}^{-1}) = 1.4{+/-}0.4\times10^{-41} L_{[OII]\lambda3727}\ \ (\mathrm{erg\ s}^{-1})$$

Other lines e.g. [OII] λ3727Å used esp for higher redshift

Mark Whittle webpages

Hα+[NII] EW vs T

- Kennicutt 1998, ARAA 36, 189

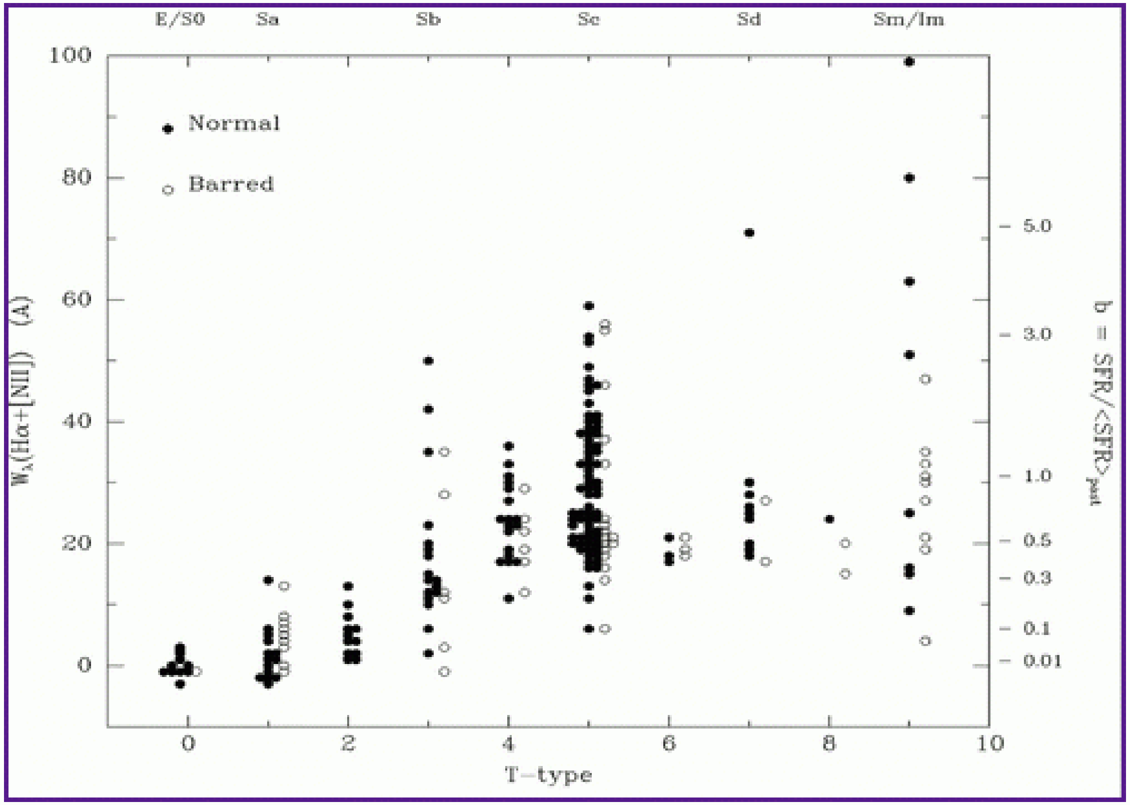

View larger version (71K)

Figure 3 Distribution of integrated Hα + [NII] emission-line equivalent widths for a large sample of nearby spiral galaxies, subdivided by Hubble type and bar morphology. The *right axis scale* shows corresponding values of the stellar birthrate parameter *b*, which is the ratio of the present SFR to that averaged over the past, as described in Section 5.1.

Stellar birthrate b

(iii) Equivalent Width : EW(Hα)

Recall EW(Hα) measures the *relative* strength of Hα to the continuum under the line

It therefore acts like a long baseline color index UV(Hα) $\leftrightarrow$ λ6550 A

Although it cannot be converted to a current SFR, it has another important use :

It measures the ratio of the current SFR (from Hα) to the integrated past SF (from the continuum)

Using synthesis models, this relation can be *quantified*, to give :

EW(Hα) $\rightarrow$ (current SFR) / (mean past SFR) ; written SFR/<SFR> or "b"

$$b = SFR/\langle SFR \rangle$$

Mark Whittle webpages

Evolution of the birthrate with T

- Kennicutt 1998, ARAA 36, 189

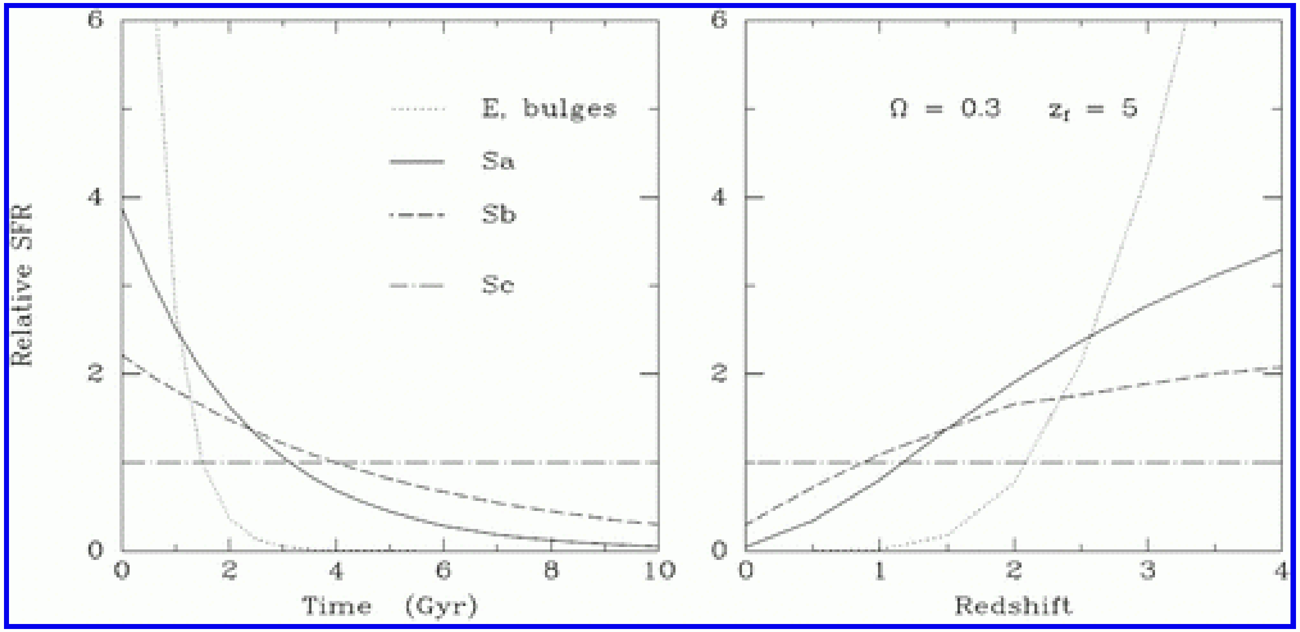

View larger version (61K)

Figure 8 A schematic illustration of the evolution of the stellar birthrate for different Hubble types. The *left panel* shows the evolution of the relative SFR with time, following Sandage (1986). The curves for spiral galaxies are exponentially declining SFRs that fit the mean values of the birthrate parameter *b* measured by Kennicutt et al (1994). The *curve* for elliptical galaxies and bulges is an arbitrary dependence for an e-folding time of 0.5 Gyr, for comparative purposes only. The *right panel* shows the corresponding evolution in SFR with redshift, for an assumed cosmological density parameter $\Omega = 0.3$ and an assumed formation redshift $z_f = 5$.

M82 at 6 cm

Figure: A λ 6cm MERLIN/VLA image of nearby starburst galaxy M82. The discrete sources are mostly supernova remnants with ages less than 1000 years and compact HIIregions. The non-thermal extended background is mainly due to relativistic electrons generated by older remnants.

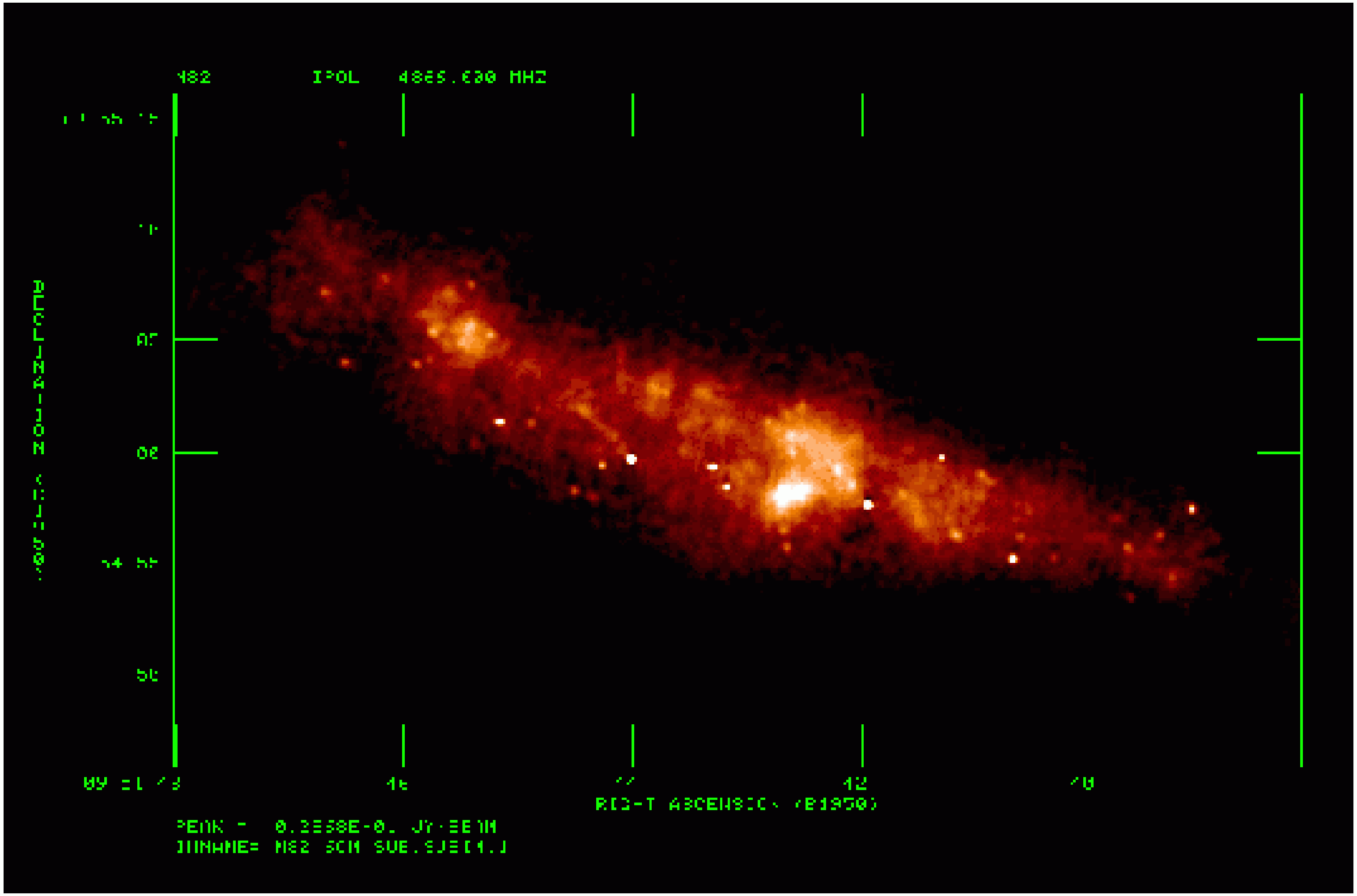

Radio continuum

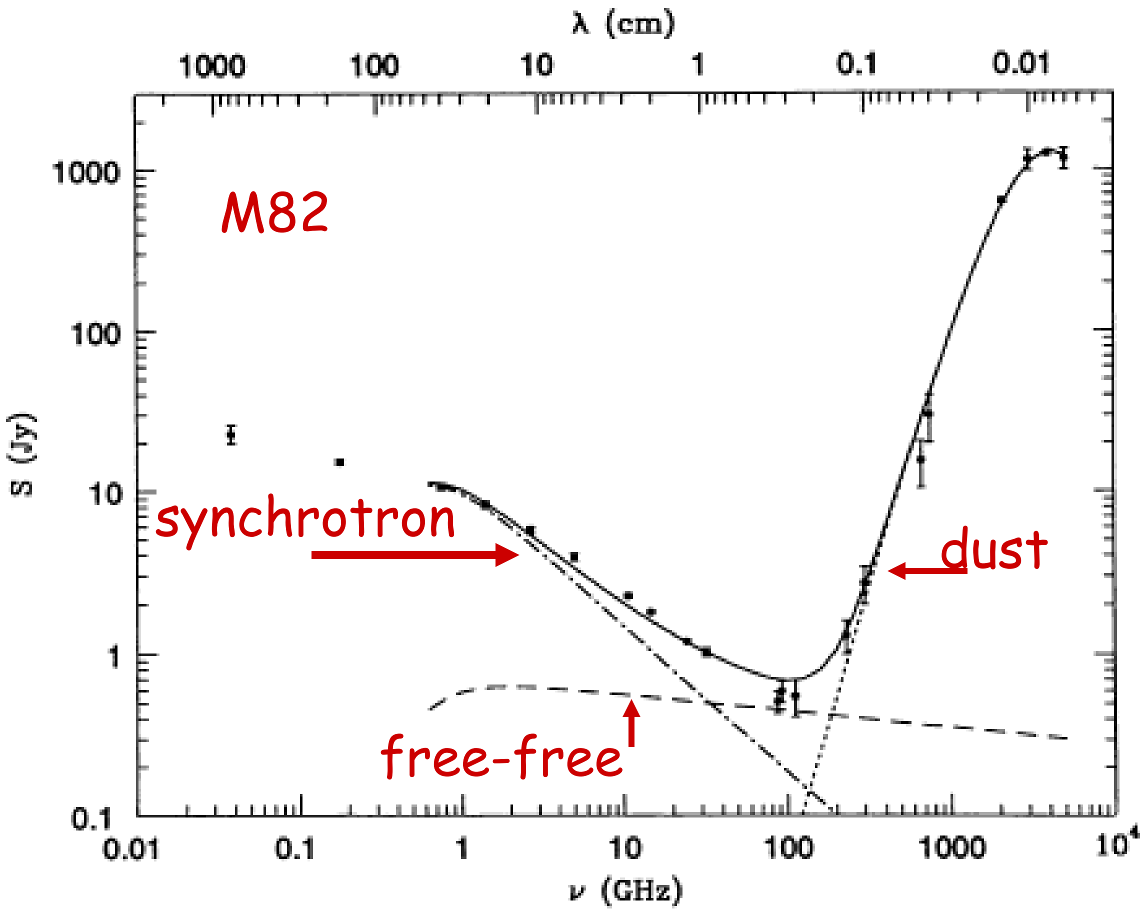

Figure 1 The observed radio/FIR spectrum of M82 (Klein et al 1988, Carlstrom & Kronberg 1991) is the sum (*solid line*) of synchrotron (*dot-dash line*), free-free (*dashed line*), and dust (*dotted line*) components. The H II regions in this bright starburst galaxy start to become opaque below $\nu \sim 1$ GHz, reducing both the free-free and synchrotron flux densities. The free-free component is largest only in the poorly observed frequency range 30–200 GHz. Thermal reradiation from $T \sim 45$ K dust with opacity proportional to $\nu^{1.5}$ swamps the radio emission at higher frequencies. Lower abscissa: frequency (GHz). Upper abscissa: wavelength (cm). Ordinate: flux density (Jy).

Condon 1992 and references therein

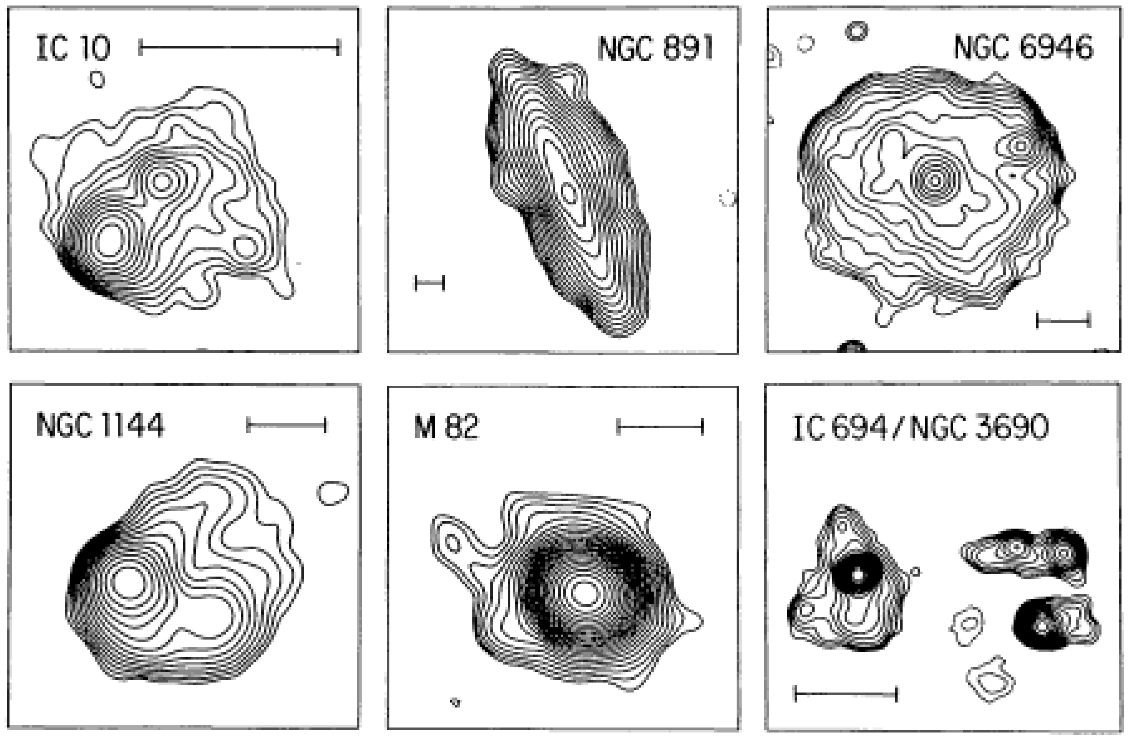

Figure 2 Contour maps (Condon 1987, Condon et al 1990) illustrating the range of source morphologies, sizes, and luminosities found in normal galaxies. The bars are $2h^{-1}$ kpc long. The logarithmic contours are separated by $2^{1/2}$ in brightness, and the 1.49 GHz brightness temperatures T_b of the lowest contours are 0.25 K (IC 10, NGC 891, NGC 6946), 0.5 K (M82), 8 K (NGC 1144), and 128 K (IC 694+NGC 3690).

(v) Radio Free-Free Luminosity

$$\mathrm{SFR}\ \ (M_{\odot}\ \mathrm{yr}^{-1}) = 4.3\times10^{-28}\ L_{\nu ff}\ \ (\mathrm{erg\ s^{-1}Hz^{-1}}\ @\ 5\ \mathrm{GHz})$$

strengths : direct link to HII regions (like Hα); zero reddening

weaknesses : usually weak w.r.t. synchrotron; requires separation using spectral indices.

(vi) Radio Synchrotron Luminosity

This *cannot* be calibrated *directly* because of the uncertainties of SNR & CR production not to mention the synchrotron efficiencies

One could use the L_{cm} vs $L_{H\alpha}$ or L_{cm} vs L_{FIR} correlations to derive an SFR vs L_{cm} relation but it would not be an independent relation.

Mark Whittle webpages

Far-infrared

Observing (re-)radiation from dust heated by UV (strong absorption by dust at UV wavelengths)

"Ultimate" SF tracer for case of UV-visible radiation field dominated by young stars and dust opacity high everywhere => starburst

$L_{FIR} = L_{bol}$

Star	Mass	Log Q_H	Log $L_{\nu ff}$	Log $L_{H\alpha}$	Log L_{bol}
O5	40	50.0	24.4	38.1	39.0
B0	16	48.7	23.1	36.8	38.0
A0	4	42.7	17.1	30.8	35.5

FIR Luminosity

(iv) FIR Luminosity

For Starbursts, where SF dominates the FIR emission, we have :

$$\text{SFR} \quad (M_{\odot}\,\text{yr}^{-1}) \quad = \quad 4.5\times10^{-44}\, L_{IR}\,(8-1000\mu) \quad (\text{erg s}^{-1})$$

Unfortunately, FIR can contain *two other* components :

- *cirrus* : diffuse emission @ $\approx$100μ from dust warmed by *normal optical starlight*
  this may dominate in E, S0, Sa, Sab $\rightarrow$ so FIR is *not* good SFR measure for these early types
  However, for Sb and later, we have a rough relation :

  $$\text{SFR} \quad (M_{\odot}\,\text{yr}^{-1}) \quad = \quad 8(+8/-3)\times10^{-44}\, L_{IR}\,(8-1000\mu) \quad (\text{erg s}^{-1})$$

- *AGN* : important in Seyferts & many ULIGS
  AGN generates hotter dust, so spectrum is "warmer" (eg fig 2 SM 96)
  eg $S_{25}/S_{60} > 3$ &/or $S_{60}/S_{100} > ??$

Mark Whittle webpages

Near/Mid-IR (Spitzer)

Bell et al. 2005

Estimate total IR from 24 micron MIPS and combine with UV to obtain SFR

- Hidden star formation: near IR and mid IR imaging can reveal optically invisible star formation regions
- In normal spirals, obscured SF knots can be seen in spiral arms (M51)
- In starbursts, dust obscures the optical light
  - Buried superstarclusters seen in IR
  - From SB to LIG to ULIG: L_{FIR} by 10^3 while L_{opt} up only by X 3
- At the highest luminosity, there is a population of optically invisible ULIGs at z ~ 2 => probably young, buried SB/QSO before blow-out

Composite SFR Indices

<u>Basic Idea</u>:

- calibrate 24μm emission (vs Pα, radio, etc) as tracer of dust-reprocessed SFR component

- use <u>observed</u> Hα emission to trace unprocessed SFR component

- total SFR derived from weighted sum of 24μm + Hα, calibrated empirically

- applied to UV+FIR SFRs, “flux ratio method”
 (Gordon et al. 2000)

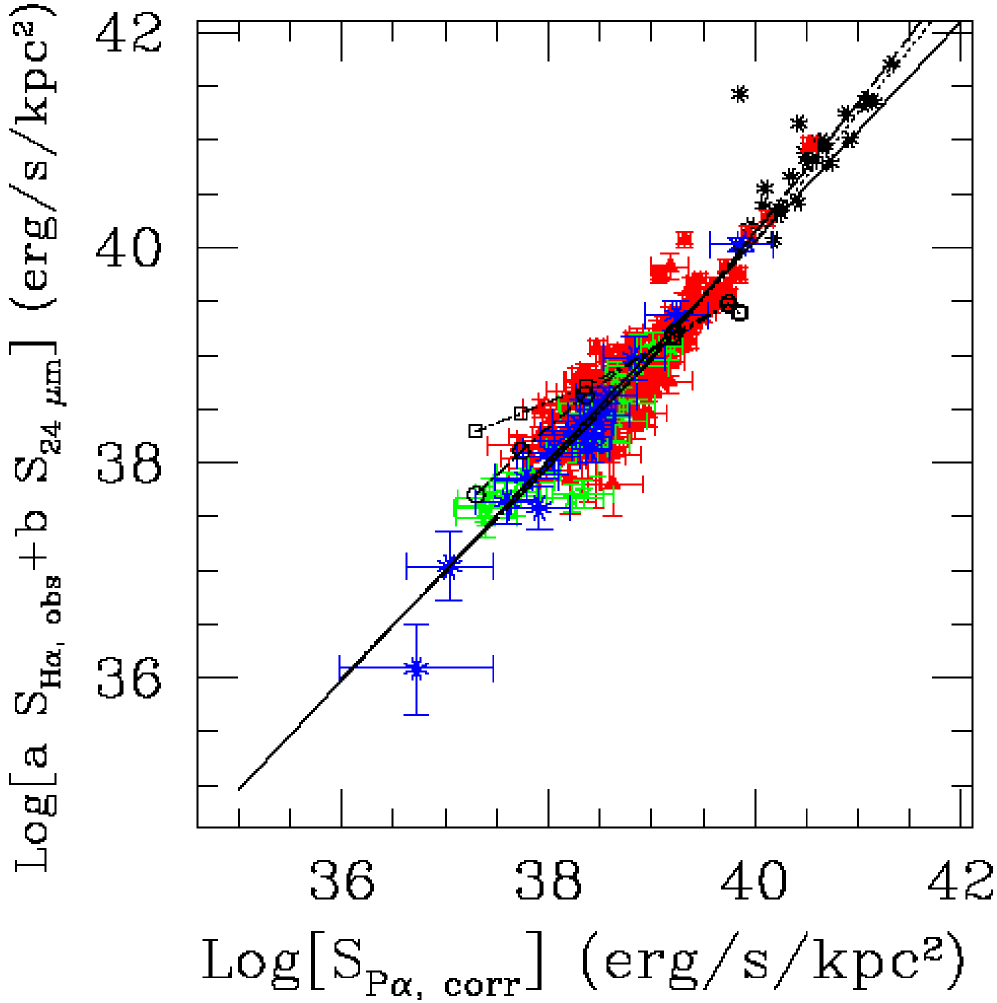

Calzetti et al. 2007, ApJ

Cookbooks

Extinction-Free Limit (Salpeter IMF, $Z=Z_\odot$)

$SFR\ (M_o\ yr^{-1}) = 1.4 \times 10^{-28}\ L_n(1500)$ ergs/s/Hz

$SFR\ (M_o\ yr^{-1}) = 7.9 \times 10^{-42}\ L(Ha)$ (ergs/s)

Extinction-Dominated Limit; SF Dominated

$SFR\ (M_o\ yr^{-1}) = 4.5 \times 10^{-44}\ L(FIR)$ (ergs/s)

$SFR\ (M_o\ yr^{-1}) = 5.5 \times 10^{-29}\ L(1.4\ GHz)$ (ergs/Hz)

Composite: SF Dominated Limit

$SFR\ (M_o\ yr^{-1}) = 7.9 \times 10^{-42}\ [L_{H\alpha,\ obs} + a\ L_{24\mu m}]\ (erg\ s^{-1})$

$[a = 0.15 - 0.31]$

$SFR\ (M_o\ yr^{-1}) = 4.5 \times 10^{-44}\ [L(UV) + L(FIR)]$ (ergs/s)

General Points and Cautions

- Different emission components trace distinct stellar populations and ages
  - nebular emission lines and resolved 24 mm dust sources trace ionizing stellar population, with ages <5-10 Myr
  - UV starlight mainly traces "intermediate" age population, ages 10-200 Myr
  - diffuse dust emission and PAH emission trace same "intermediate" age and older stars– 10 Myr to 10 Gyr(!)

- Consequence: it is important to match the SFR tracer to the application of interest
  - emission lines – Schmidt law, early SF phases
  - UV – time-averaged SFR and SFR in low surface brightness systems
  - dust emission – high optical depth regions

- Multiple tracers can constrain SF history, properties of starbursts, IMF, etc.

Calzetti review 1208.2997

Table 1.1. **Model-based luminosity-to-SFR calibrations**

Luminosity[a]	C[b]	Assumptions[c]
L(UV)	$3.0\times10^{-47}\lambda$	0.1–100 $M_\odot$, $\tau \geq$100 Myr
L(UV)	$4.2\times10^{-47}\lambda$	0.1–30 $M_\odot$, $\tau \geq$100 Myr
L(UV)	$4.3\times10^{-47}\lambda$	0.1–100 $M_\odot$, τ=10 Myr
L(UV)	$1.0\times10^{-46}\lambda$	0.1–100 $M_\odot$, τ=2 Myr
L(TIR)	1.6×10^{-44}	0.1–100 $M_\odot$, τ=10 Gyr
L(TIR)	2.8×10^{-44}	0.1–100 $M_\odot$, τ=100 Myr
L(TIR)	4.1×10^{-44}	0.1–30 $M_\odot$, τ=100 Myr
L(TIR)	3.7×10^{-44}	0.1–100 $M_\odot$, τ=10 Myr
L(TIR)	8.3×10^{-44}	0.1–100 $M_\odot$, τ=2 Myr
L(Hα)	5.5×10^{-42}	0.1–100 $M_\odot$, $\tau \geq$6 Myr, T_e=10^4 k, n_e=100 cm^{-3}
L(Hα)	3.1×10^{-41}	0.1–30 $M_\odot$, $\tau \geq$10 Myr, T_e=10^4 k, n_e=100 cm^{-3}
L(Brγ)	5.7×10^{-40}	0.1–100 $M_\odot$, $\tau \geq$6 Myr, T_e=10^4 k, n_e=100 cm^{-3}

[a] Luminosity in erg s^{-1}. Stellar and dust continuum luminosities are given as $\nu L(\nu)$; total IR=TIR is assumed to be equal to the stellar population bolometric luminosity.

[b] The constant C appears in the calibration as: SFR(λ)= $CL(\lambda)$, where SFR is in units of $M_\odot$ yr^{-1}. The constant is derived from stellar population models, with constant star formation and solar metallicity (Starburst99, Leitherer *et al.* 1999). For SFR(UV), the numerical value is multiplied by the wavelength λ in Å.

[c] Assumptions for mass range of the stellar IMF, which we adopt to have the expression derived by Kroupa (2001), see Section 1.2.2 and for the timescale τ over which star formation needs to remain constant, for the calibration constant to be applicable. For nebular lines, the adopted values of electron temperature and density are also listed.

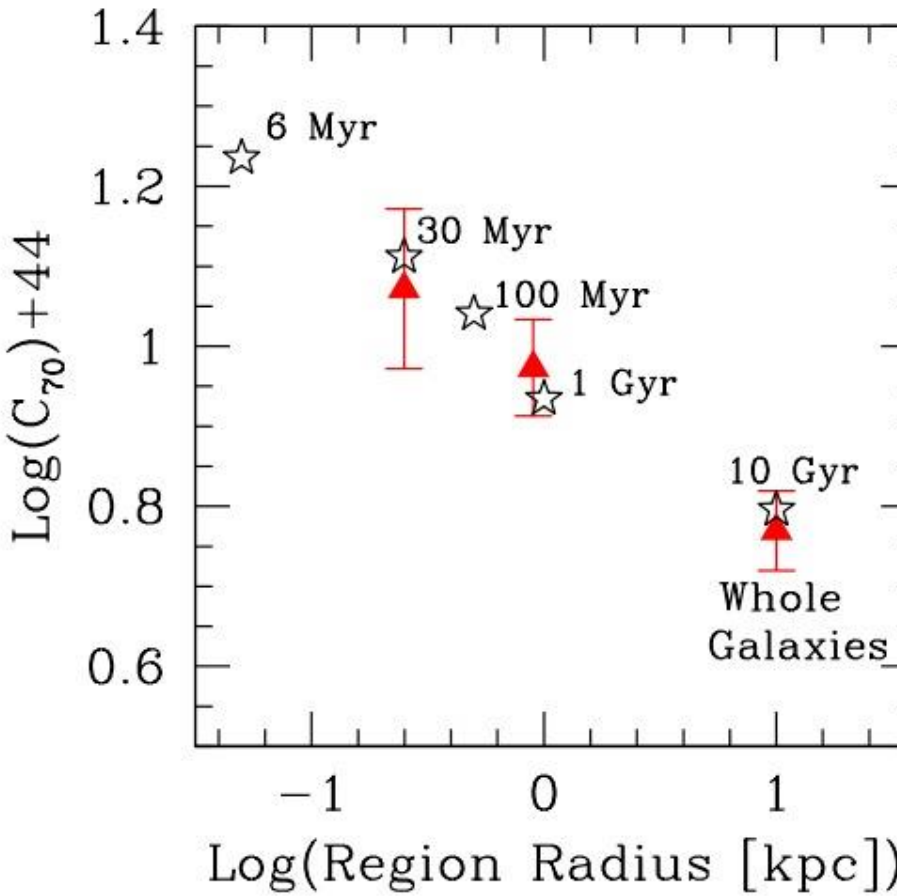

Fig. 1.1. The calibration constant, C_{70}, between SFR and the 70 μm luminosity, expressed as SFR(70)=C_{70} $L(70)$, as a function of the physical size of the regions used to derive the calibration. The filled red triangles are observed values from Li *et al.* (2010, 2012) and Calzetti *et al.* (2010), using both *Spitzer* and *Herschel* data. The black stars are from stellar population synthesis models, for constant star formation and a Kroupa IMF, in the stellar mass range 0.1–100 $M_\odot$; the mean age of the population that best approximates the observed C_{70} values is shown. The scaling between bolometric light and 70 μm emission is discussed in Calzetti *et al.* (2010). The association between star formation timescale and region size is based on a region crossing time with a 1–3 km s^{-1} speed.

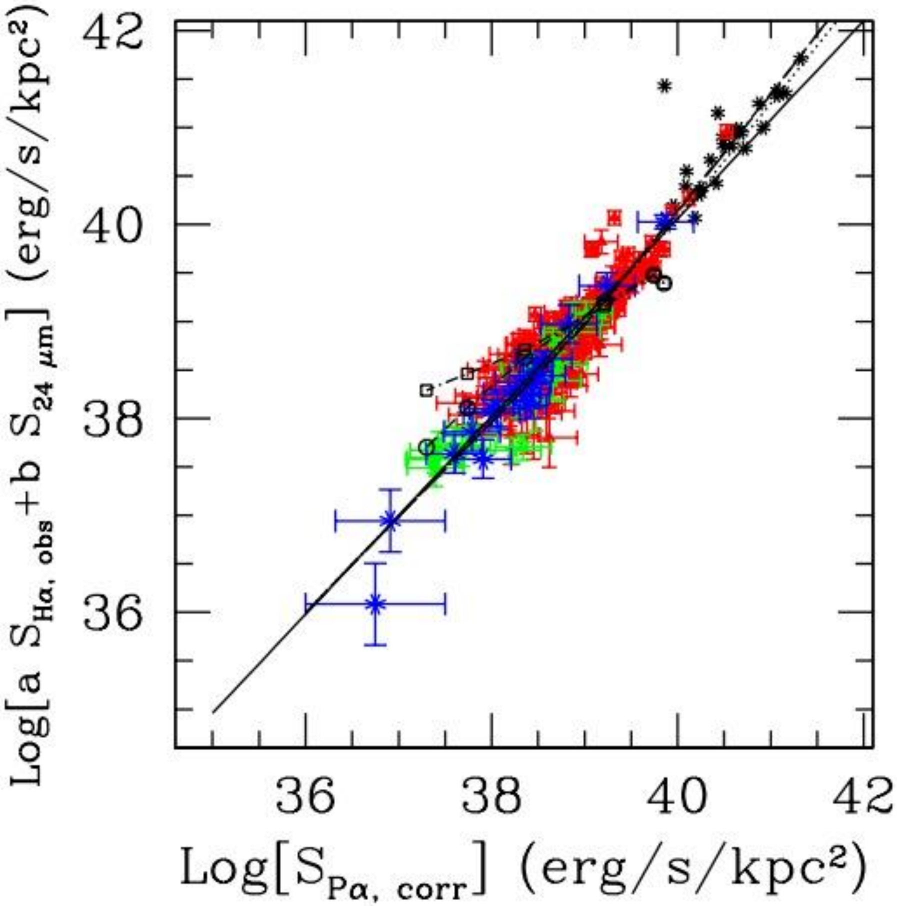

Fig. 1.2. An example of the calibration for a mixed SFR indicator, from Calzetti *et al.* (2007). This specific example is for a *local* SFR indicator: the data points include star-forming regions in nearby galaxies (red triangles, green squares, blue crosses) and local LIRGs (black stars, from Alonso-Herrero *et al.* 2006). The horizontal axis is the luminosity/area of the regions/galaxies in the hydrogen recombination line Pα (1.8756 μm), the vertical axis is a linear combination of the luminosity/area of the observed Hα and 24 μm luminosity. The star-forming regions include low (blue), intermediate (green), and high (red) metallicity. All the points align basically along a one-to-one relation (straight continuous line) suggesting that this calibration is fairly independent of the metallicity (dust content) and luminosity of the source. Other lines mark the position of models as described in Calzetti *et al.* (2007).

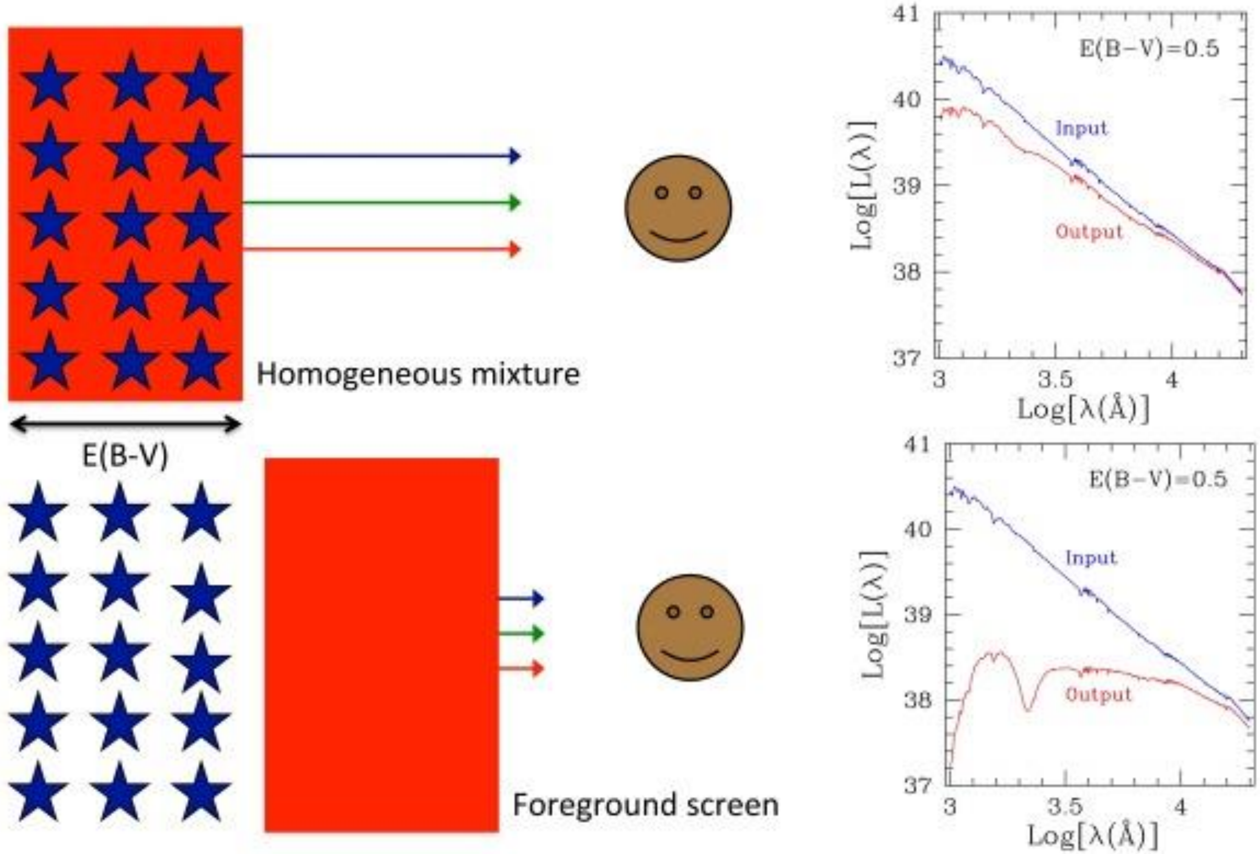

Fig. 1.4. The top and bottom panels show cartoon representations of the same extended distribution of stars and dust, but with a different geometrical relation between each other. In the top panel the dust and stars are homogeneously mixed, while in the bottom panel the dust is completely foreground to the stars. The characteristics of the stars are the same in the two panels. I have assumed that in both cases the dust obeys the Milky Way extinction curve (which has a prominent absorption feature at 2175 Å) with a thickness of $E(B-V)=0.5$. The panels to the right show the input stellar SED, which is the same for the two cases (blue; top spectrum), and the output SED (red; bottom spectrum). All other characteristics being equal, the different geometric relation between dust and stars has considerable impact on the emerging spectrum ('Output').

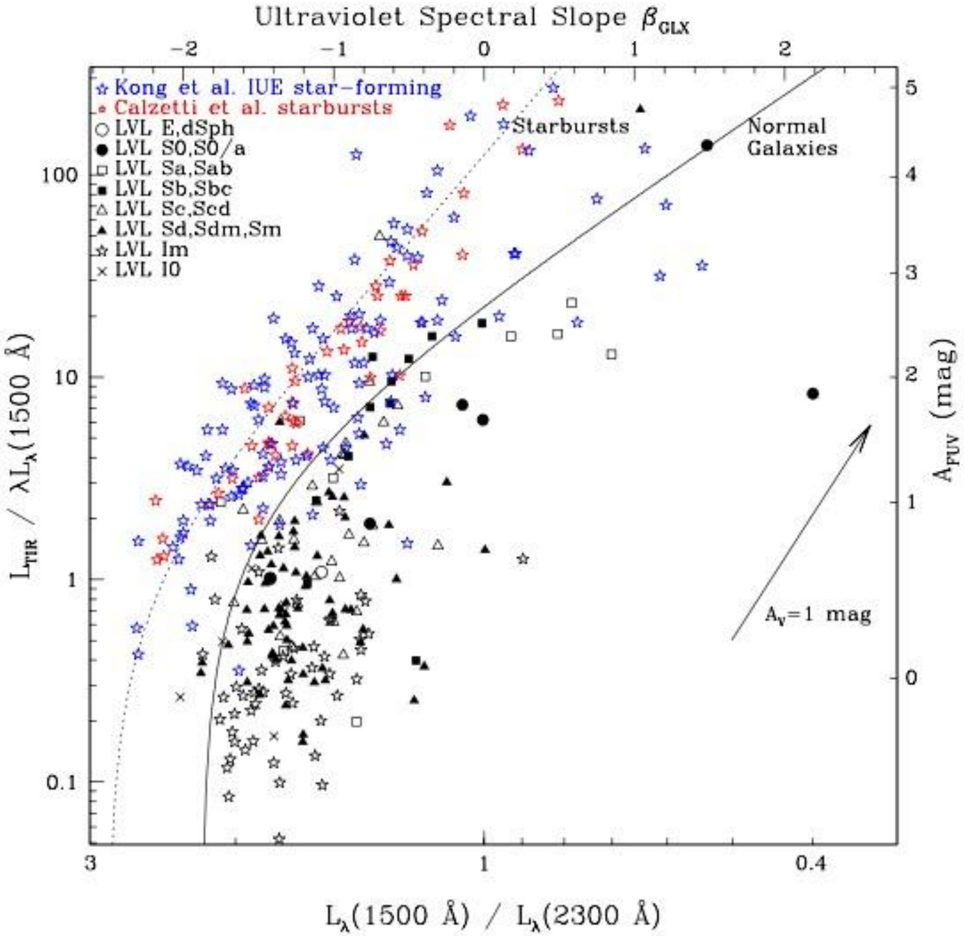

Fig. 1.5. The IRX-β plot for local starburst and star-forming galaxies, from Dale *et al.* (2009). The vertical axis is the IR excess over the UV, where the UV is the *GALEX* FUV (0.15 μm) band. The horizontal axis is the *GALEX* FUV−NUV colour, expressed as luminosity ratio, with the corresponding values of the UV spectral slope β shown at the top of the plot. The red points are the UV-bright starburst galaxies used by Meurer *et al.* (1999) to derive the IRX-β relation, shown by the dotted line (Equation 1.22). The blue and black points give the location of normal star-forming galaxies from samples of the local Universe. These galaxies have a much larger spread in the IRX-β plane than the UV-bright starbursts, and typically lower IR excesses at constant UV slope. Their mean trend is shown by the continuous line. An A_V=1 mag attenuation vector is also shown. Reproduced with permission from Dale *et al.* (2009).

Radio-IR correlation

UV and optical SFR indicators are sensitive to dust

IR emission easy to understand in optically thick case in vigorous star-forming galaxy

Radio emission arises from complex physics of cosmic ray generation and confinement

But…. Astonishingly tight relationship between radio-IR flux

- But… does not apply at low luminosities
- Radio flux from low L galaxies is suppressed relative to brighter galaxies

Bell, 2003, ApJ 586, 794

Radio – FIR correlation

- exploits tight observed relation between 1.4 GHz radio continuum (synchrotron) and FIR luminosity
- correlation may reflect CR particle injection/acceleration by supernova remnants, and thus scale with SFR
- no *ab initio* SFR calibration, bootstrapped from FIR calibration
- valuable method when no other tracer is available

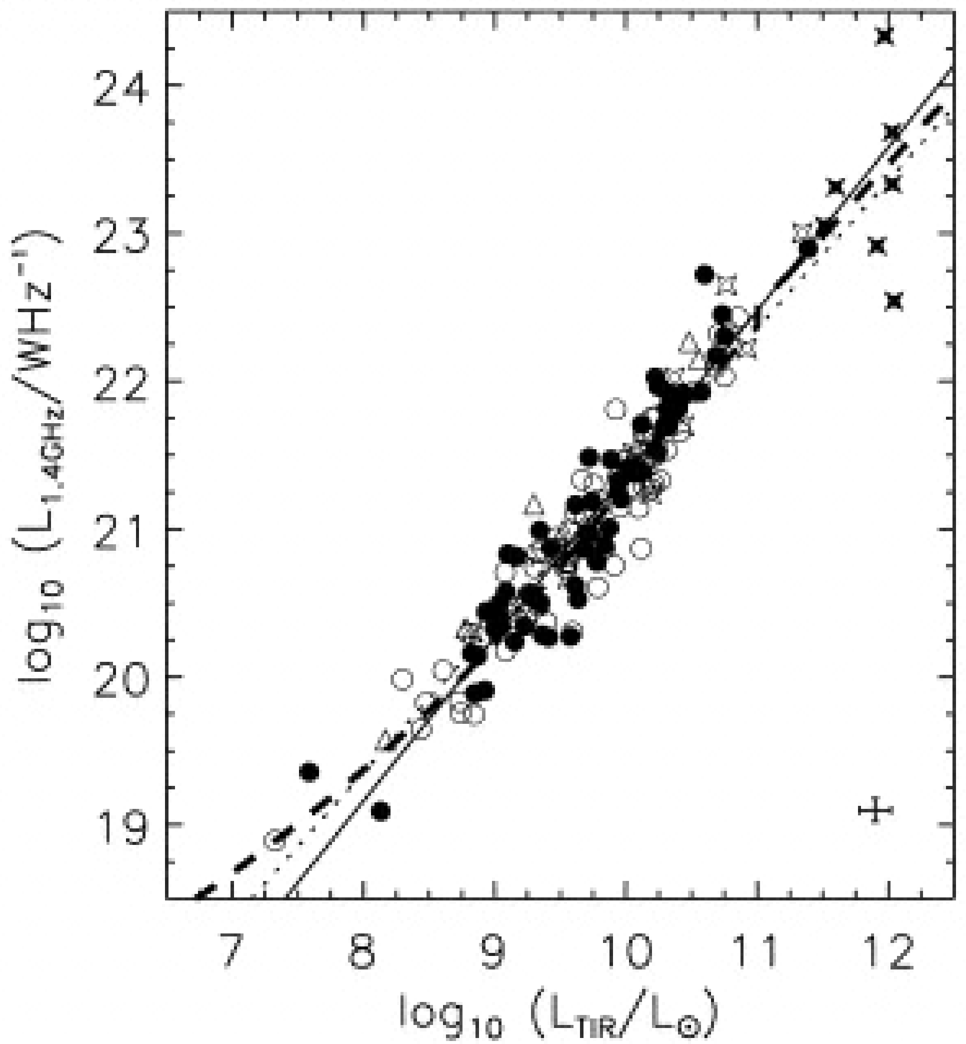

Bell 2003, ApJ, 586, 794

Star formation indicators from SDSS

- Hopkins et al. 2003, ApJ 599, 971 (SDSS)

APPENDIX B

SDSS SFR FORMULAE

For ease of reference, the formulae for deriving SFRs using the measured SDSS parameters, as well as the SFR calibrations used, are all collected together here. The sections in which each formula is derived are also given. All SFRs are calibrated based on a Salpeter IMF and a mass range of $0.1 < M_\odot < 100$.

The Hα luminosity–to–SFR calibration used is

$$\mathrm{SFR}_{\mathrm{H}\alpha}(M_\odot\ \mathrm{yr}^{-1}) = \frac{L_{\mathrm{H}\alpha}}{1.27 \times 10^{34}\ \mathrm{W}} . \qquad \text{(B1)}$$

For Hα SFRs, using the aperture correction method of equation (5), the derivation in § 3.2.2 gives

$$\mathrm{SFR}_{\mathrm{H}\alpha}(M_\odot\ \mathrm{yr}^{-1}) = [\mathrm{EW}(\mathrm{H}\alpha) + \mathrm{EW}_c]10^{-0.4(M_r-34.10)} \frac{3 \times 10^{18}}{[6564.61(1+z)]^2} \left(\frac{S_{\mathrm{H}\alpha}/S_{\mathrm{H}\beta}}{2.86}\right)^{2.114} \frac{1}{1.27 \times 10^{34}} , \qquad \text{(B2)}$$

where $S_{\mathrm{H}\alpha}$ and $S_{\mathrm{H}\beta}$ are the stellar absorption–corrected line fluxes, calculated as in equation (4). The exponent on the Balmer decrement term (in all the equations given here) is equal to $k(\lambda)/[k(\mathrm{H}\beta) - k(\mathrm{H}\alpha)]$ and depends on the assumed obscuration curve. For obscuration corrections to emission-line luminosities, we assume the obscuration curve of Cardelli et al. (1989) as recommended by Calzetti (2001). $\mathrm{EW}_c = 1.3$ Å is a reasonable approximation for the stellar absorption correction when using the SDSS pipeline spectral line measurements and corresponds roughly to a 2.6 Å EW stellar absorption in the SF galaxies.

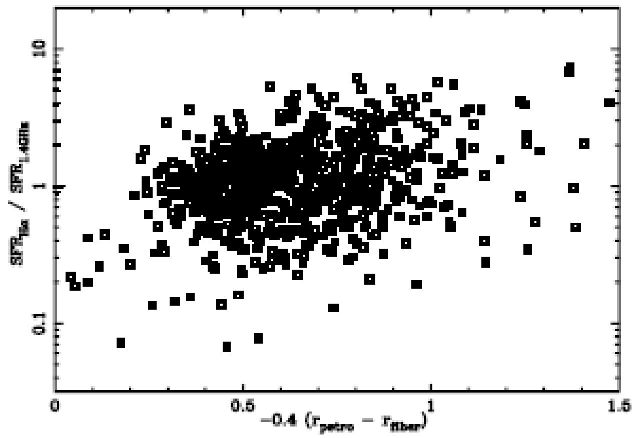

FIG. 26.—Ratio of SFRs from Hα and 1.4 GHz luminosities as a function of the aperture correction (from eq. [A1]). The implicit assumption of a uniform SF distribution made through the aperture correction results in the slight positive slope seen in this relation.

Star formation indicators from SDSS

Using the alternative aperture correction given in Appendix A results in

$$\mathrm{SFR}_{\mathrm{H}\alpha}(M_\odot\ \mathrm{yr}^{-1}) = 4\pi D_l^2 S_{\mathrm{H}\alpha} 10^{-0.4(r_{\mathrm{Petro}} - r_{\mathrm{fiber}})} \left(\frac{S_{\mathrm{H}\alpha}/S_{\mathrm{H}\beta}}{2.86}\right)^{2.114} \frac{1}{1.27 \times 10^{34}} , \tag{B3}$$

where D_l is the luminosity distance and $S_{\mathrm{H}\alpha}$ is the stellar absorption–corrected Hα line flux.

The [O II] luminosity–to–SFR calibration used is

$$\mathrm{SFR}_{[\mathrm{O\,II}]}(M_\odot\ \mathrm{yr}^{-1}) = \frac{L_{[\mathrm{O\,II}]}}{2.97 \times 10^{33}\ \mathrm{W}} , \tag{B4}$$

where $L_{[\mathrm{O\,II}]}$ incorporates the obscuration correction valid for the wavelength of Hα. For [O II] SFRs the derivation of § 3.3 gives

$$\mathrm{SFR}_{[\mathrm{O\,II}]}(M_\odot\ \mathrm{yr}^{-1}) = \mathrm{EW}(\mathrm{O\,II}) 10^{-0.4(M_u - 34.10)} \frac{3 \times 10^{18}}{[3728.30(1+z)]^2} \left(\frac{S_{\mathrm{H}\alpha}/S_{\mathrm{H}\beta}}{2.86}\right)^{2.114} \frac{1}{2.97 \times 10^{33}} , \tag{B5}$$

and using the alternative aperture correction given in Appendix A results in

$$\mathrm{SFR}_{[\mathrm{O\,II}]}(M_\odot\ \mathrm{yr}^{-1}) = 4\pi D_l^2 F_{[\mathrm{O\,II}]} 10^{-0.4(u_{\mathrm{Petro}} - u_{\mathrm{fiber}})} \left(\frac{S_{\mathrm{H}\alpha}/S_{\mathrm{H}\beta}}{2.86}\right)^{2.114} \frac{1}{2.97 \times 10^{33}} . \tag{B6}$$

The u-band luminosity–to–SFR calibration used is

$$\mathrm{SFR}_U(M_\odot\ \mathrm{yr}^{-1}) = \left(\frac{L_U}{1.81 \times 10^{21}\ \mathrm{W\ Hz}^{-1}}\right)^{1.186} . \tag{B7}$$

The derivation given in § 3.5 gives

$$\mathrm{SFR}_U(M_\odot\ \mathrm{yr}^{-1}) = \left[\frac{10^{-0.4(M_u - 34.10)}}{1.81 \times 10^{21}} \left(\frac{S_{\mathrm{H}\alpha}/S_{\mathrm{H}\beta}}{2.86}\right)^{2.061}\right]^{1.186} . \tag{B8}$$

The exponent on the Balmer decrement term here uses the obscuration curve of Calzetti et al. (2000) and incorporates the factor of 0.44 necessary for obscuration corrections of the stellar continuum (see also Calzetti 2001).

For completeness, the SFR calibrations from 1.4 GHz and FIR luminosities that give consistent SFR estimates with the above formulae are also given here (from Bell 2003). The calibration for 1.4 GHz luminosities is

$$\mathrm{SFR}_{1.4\mathrm{GHz}}(M_\odot\ \mathrm{yr}^{-1}) = \begin{cases} \dfrac{L_{1.4\,\mathrm{GHz}}}{1.81 \times 10^{21}\ \mathrm{W\ Hz}^{-1}} & (L_{1.4\,\mathrm{GHz}} > L_c) \\[2ex] \dfrac{L_{1.4\mathrm{GHz}}}{\left[0.1 + 0.9(L_{1.4\mathrm{GHz}}/L_c)^{0.3}\right] 1.81 \times 10^{21}\ \mathrm{W\ Hz}^{-1}} & (L_{1.4\,\mathrm{GHz}} \le L_c) , \end{cases} \tag{B9}$$

with $L_c = 6.4 \times 10^{21}\ \mathrm{W\ Hz}^{-1}$, and that for FIR luminosities is

$$\mathrm{SFR}_{\mathrm{FIR}}(M_\odot\ \mathrm{yr}^{-1}) = \frac{L_{\mathrm{FIR}}\left[1 + \sqrt{(2.186 \times 10^{35}\ \mathrm{W})/L_{\mathrm{FIR}}}\right]}{1.85 \times 10^{36}\ \mathrm{W}} . \tag{B10}$$

Star formation history

Strength of the 4000 Å break => star formation history
Balogh et al. 1999; Brinchmann et al. 2004

Kauffmann et al. 2003

- Use dereddened SDSS spectra
- $D_n(4000\text{Å}) = \dfrac{\int F_+ \, d\lambda}{\int F_- \, d\lambda}$

where $F_{+,-}$ are two narrow ($\Delta\lambda$~100 Å) bands centered at 4050 and 3900 Å.

- Use f_{nearUV} and f_{farUV} from GALEX
- Calculate IRX = log (L_{dust}/L_{farUV})
- Colored lines show a fit to median value of IR excess (IRX) in the bin of corresponding color

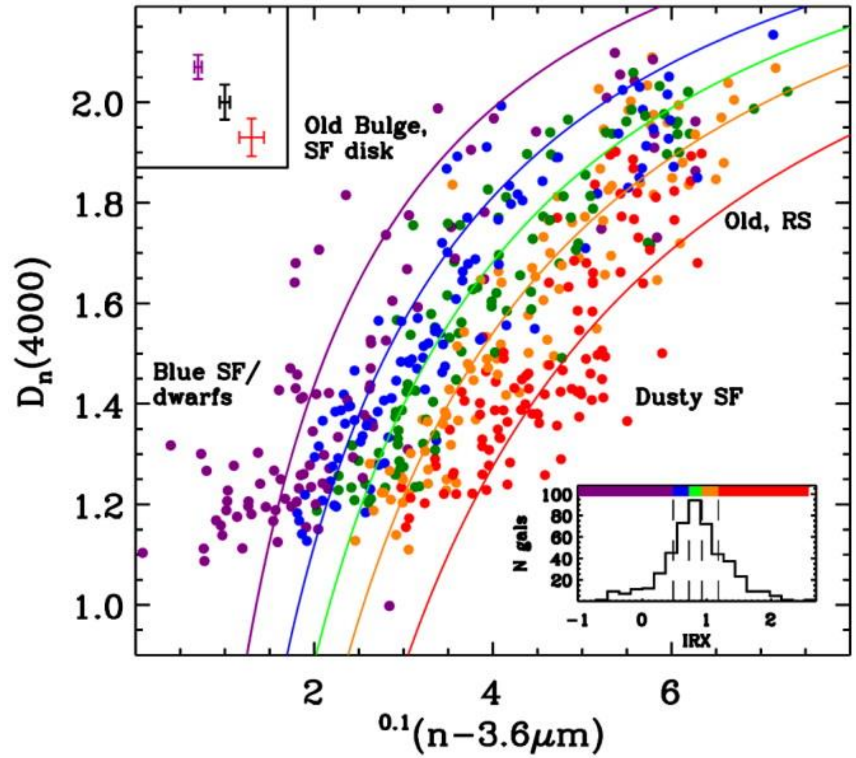

Johnson et al. 2006, ApJL 644, L109

HI Gas in Galaxies

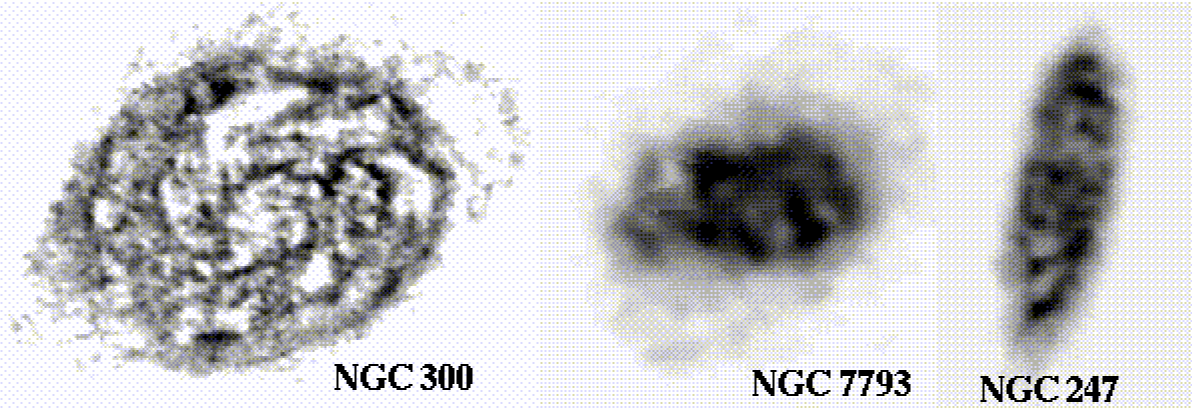

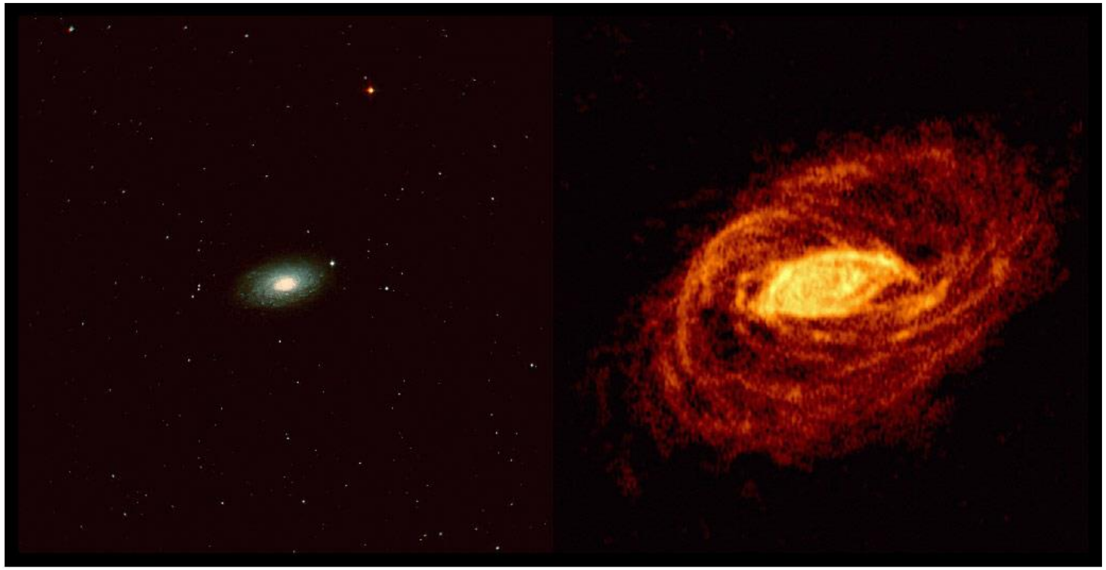

Optical and HI image of NGC5055
(Oosterloo et al.)

Generic star formation law

- Kennicutt 1998a,b (ARAA and ApJ 498, 541)

Numerous theoretical scenarios that produce a Schmidt law with $N = 1-2$ can be found in the literature (Larson 1992, and references therein). Simple self-gravitational models for disks can reproduce the large-scale star formation thresholds observed in galaxies (Quirk 1972; K89), and the same basic model is consistent with a Schmidt law at high densities with index $N \sim 1.5$ (Larson 1988, 1992; Elmegreen 1994). For example, in a simple self-gravitational picture in which the large-scale SFR is presumed to scale with the growth rate of perturbations in the gas disk, the SFR will scale as the gas density divided by the growth timescale:

$$\rho_{\rm SFR} \propto \frac{\rho_{\rm gas}}{(G\rho_{\rm gas})^{-0.5}} \propto \rho_{\rm gas}^{1.5} \,, \qquad (5)$$

$$\boxed{\Sigma_{SFR} = A\ \Sigma_{gas}^{\ n}}$$

where $\rho_{\rm gas}$ and $\rho_{\rm SFR}$ are the volume densities of gas and star formation. The corresponding scaling of the projected surface densities will depend on the scale height distribution of the gas, with $N = 1.5$ expected for a constant mean scale height, a reasonable approximation for the galaxies and starbursts considered here. Although this is hardly a robust derivation, it does show that a global Schmidt law with $N \sim 1.5$ is physically plausible.

In a variant of this argument, Silk (1997) and Elmegreen (1997) have suggested a generic form of the star formation law, in which the SFR surface density scales with the ratio of the gas density to the local dynamical timescale:

$$\Sigma_{\rm SFR} \propto \frac{\Sigma_{\rm gas}}{\tau_{\rm dyn}} \propto \Sigma_{\rm gas}\,\Omega_{\rm gas} \,, \qquad (6)$$

Global Schmidt Law

- Kennicutt 1998, ARAA 36, 189

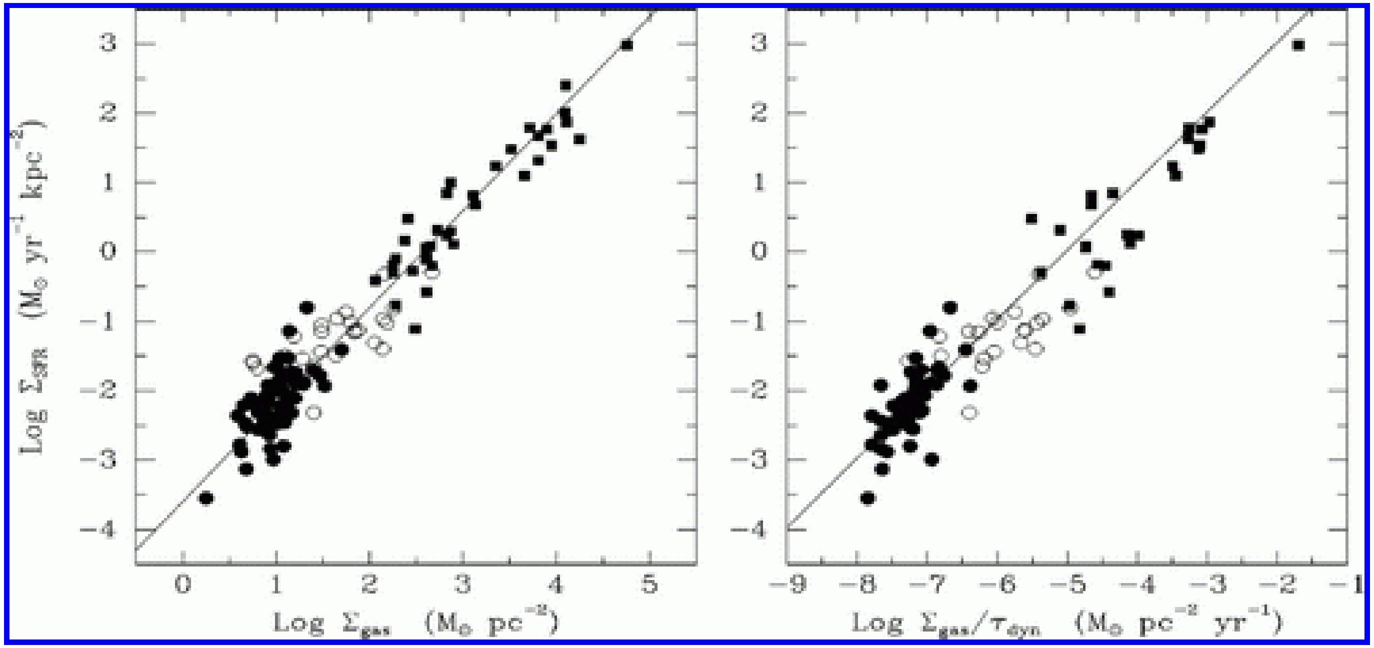

View larger version (72K)

Notice dynamic range in Σ's!

Figure 9 (*Left*) The global Schmidt law in galaxies. *Solid points* denote the normal spirals in Figure 5, *squares* denote the circumnuclear starbursts in Figure 7. The *open circles* show the SFRs and gas densities of the central regions of the normal disks. (*Right*) The same SFR data but plotted against the ratio of the gas density to the average orbital time in the disk. Both plots are adapted from Kennicutt (1998).

SFR versus Gas Surface Density

- Kennicutt 1998
  ARAA 36, 189

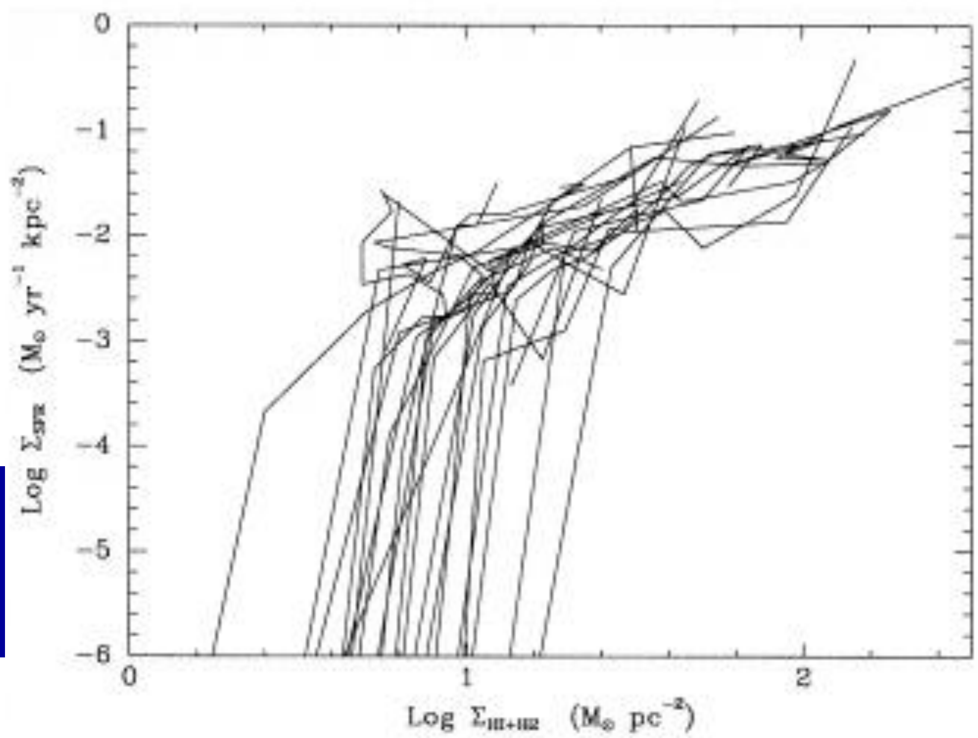

Schmidt law:

$\Sigma_{SFR} = A\ \Sigma^{n}_{gas}$

$$\Sigma_{SFR} = (2.5 \pm 0.7) \times 10^{-4} \left(\frac{\Sigma_{gas}}{1\ M_\odot\ \mathrm{pc}^{-2}} \right)^{1.4 \pm 0.15} M_\odot\ \mathrm{year}^{-1}\,\mathrm{kpc}^{-2}, \tag{7}$$

where Σ_{SFR} and Σ_{gas} are the disk-averaged SFR and gas surface densities, respectively.

Spiral Galaxies in THINGS — The HI Nearby Galaxy Survey

Coordinated multiwavelength programs
Numbers starting to accumulate

- WHISP (WSRT)
- VIVA (VLA; van Gorkom et al)
- THINGS (VLA; Walter et al.)
- Little THINGS (VLA; Hunter et al)
- ANGST(VLA; Ott et al.)
- FIGGS (GMRT; Begum et al.)

Future: EVLA + CARMA/ALMA + others

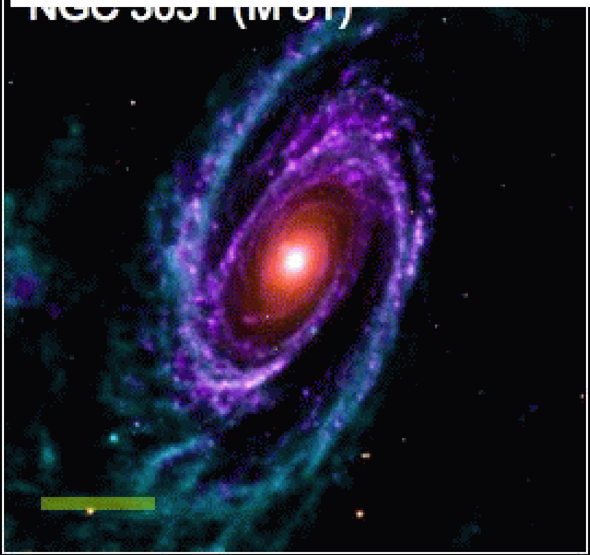

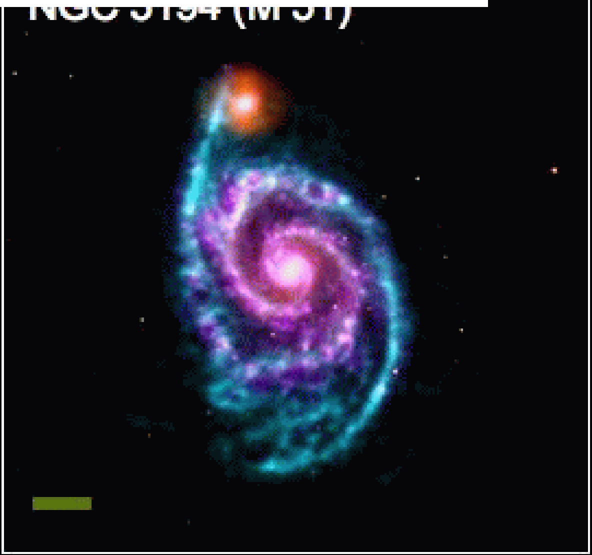

THINGS
The HI Nearby Galaxy Survey

color coding:
THINGS Atomic Hydrogen
(Very Large Array)
Old stars
(Spitzer Space Telescope)
Star Formation
(GALEX & Spitzer)

scale: 15,000 light years

Image credits:
VLA THINGS: Walter et al. 08
Spitzer SINGS: Kennicutt et al. 03
GALEX NGS: Gil de Paz et al. 07

Interactions

- Galaxy - galaxy interactions
- Galaxy – ICM interactions (where ICM)


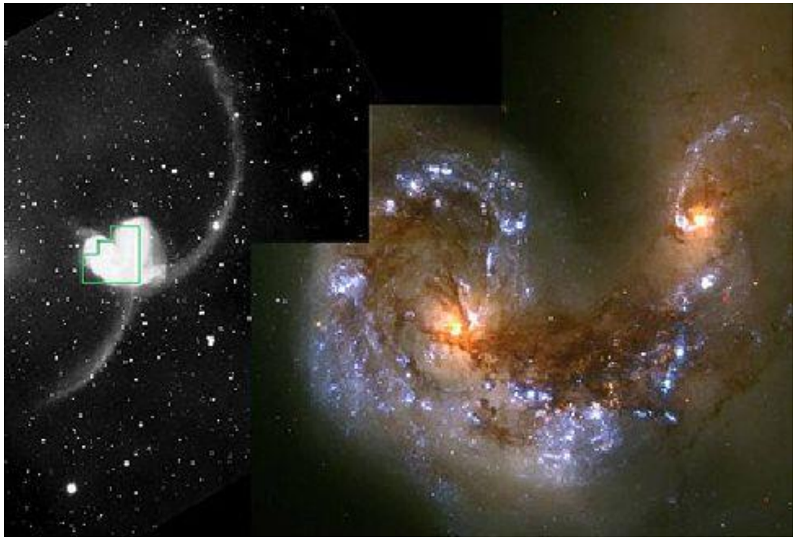
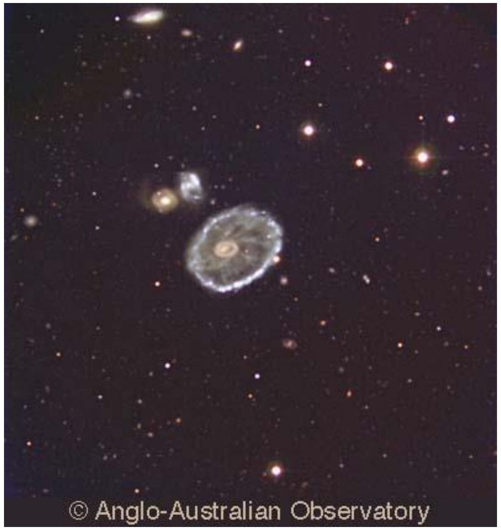


Interactions in distant clusters

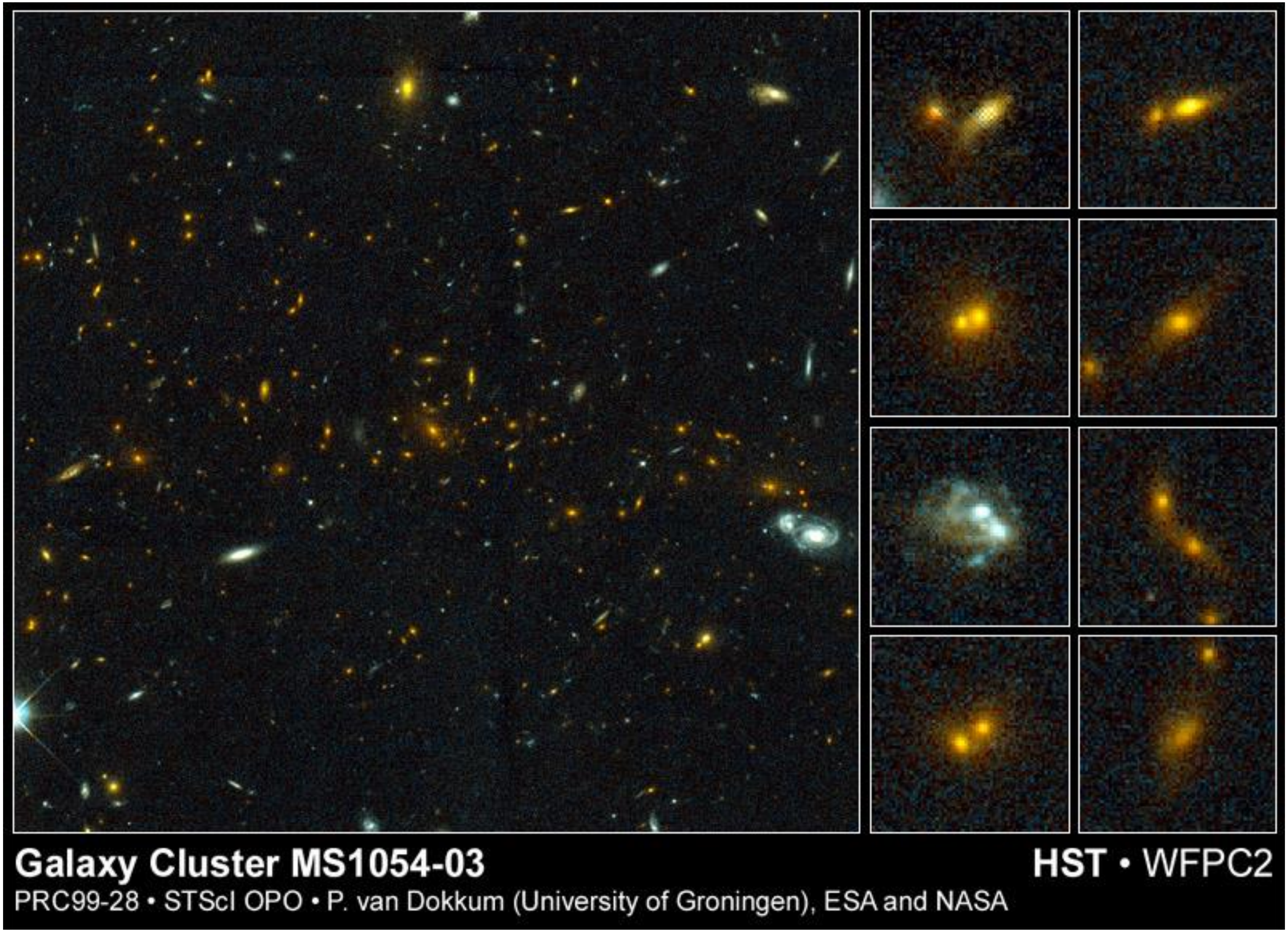

Quasar Host Galaxies

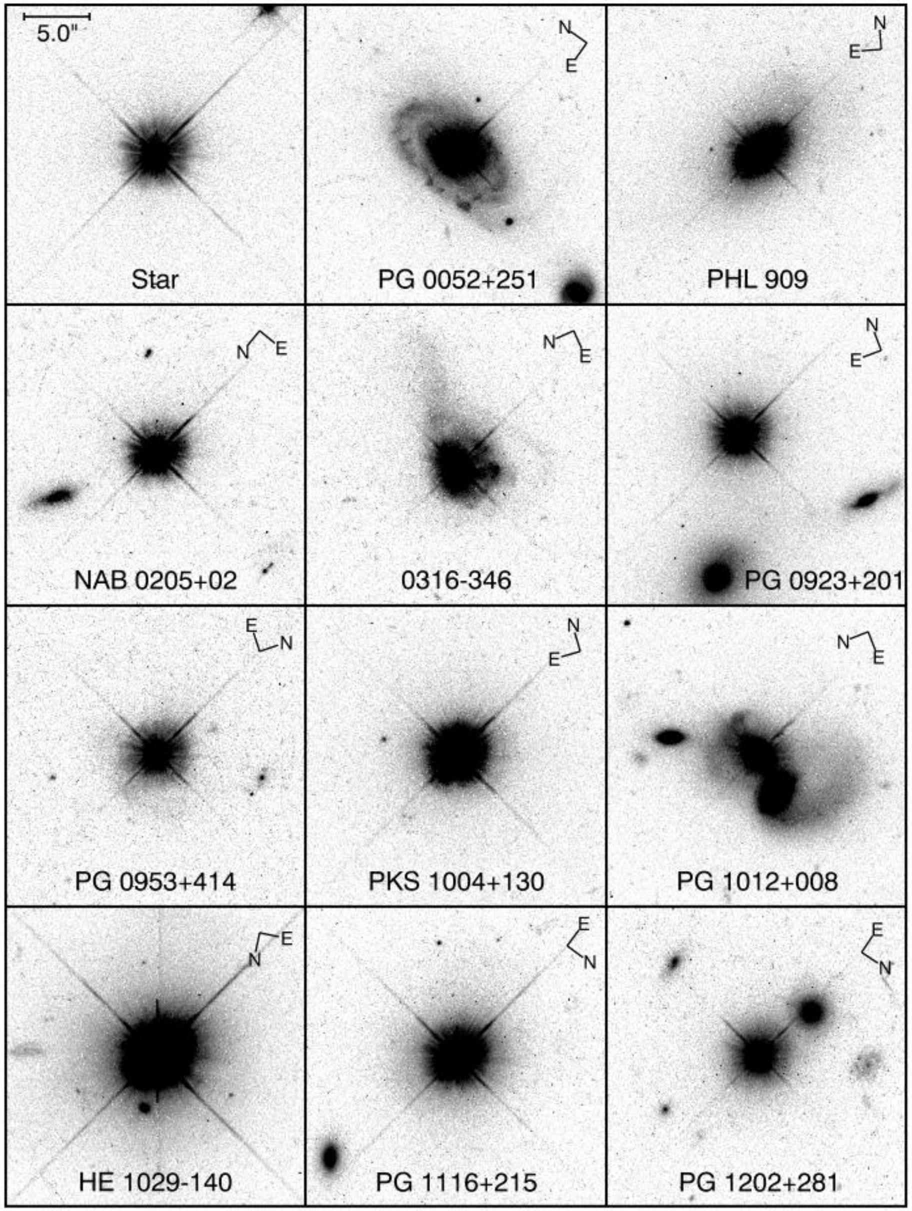

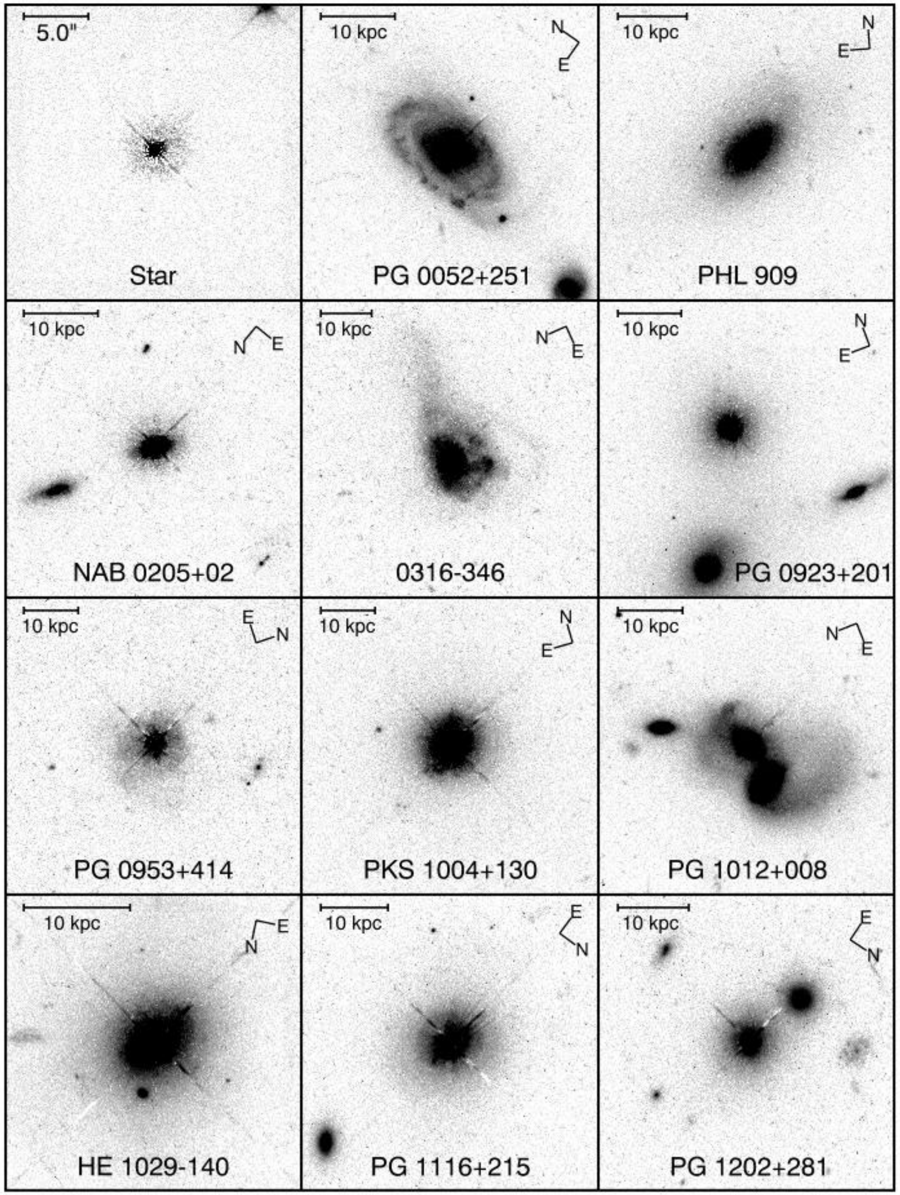

Morphological Alteration Mechanisms

Environment-independent

a. Galactic winds
b. Star formation without replenishment

II. Environment dependent

a. Galaxy-galaxy interactions
    i. Direct collisions
    ii. Tidal encounters
    iii. Mergers
b. Galaxy-intracluster medium interactions
    i. Ram pressure stripping
    ii. Thermal evaporation
    Iii. Turbulent viscous stripping
c. Galaxy-cluster interactions
    i. Harrassment

Galaxy-galaxy interactions

Barnes & Hernquist
See: http://www.ifa.hawaii.edu/~barnes

During tidal interactions and mergers, gas tends to be driven towards the centers of galaxies through gravitational torques on it by tidally induced stellar bars $\Rightarrow$ dissipation and shocks

- Starbursts
- Globular cluster formation
- Feeding of AGN

Low velocity encounters (Tides, mergers)

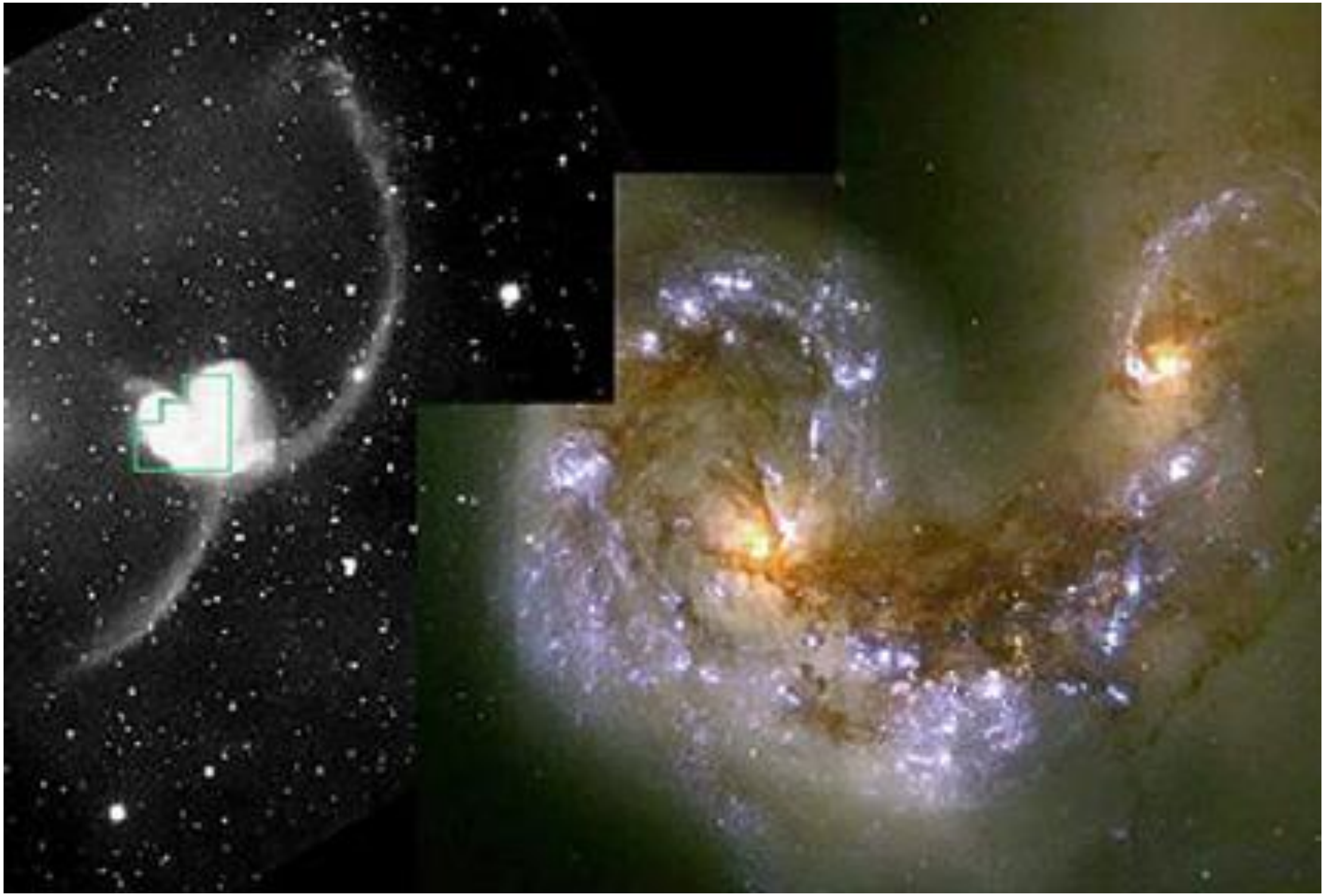

The Antennae: NGC 4038/9. Optical wide field (left) + HST (right)

The Antennae (as observed)

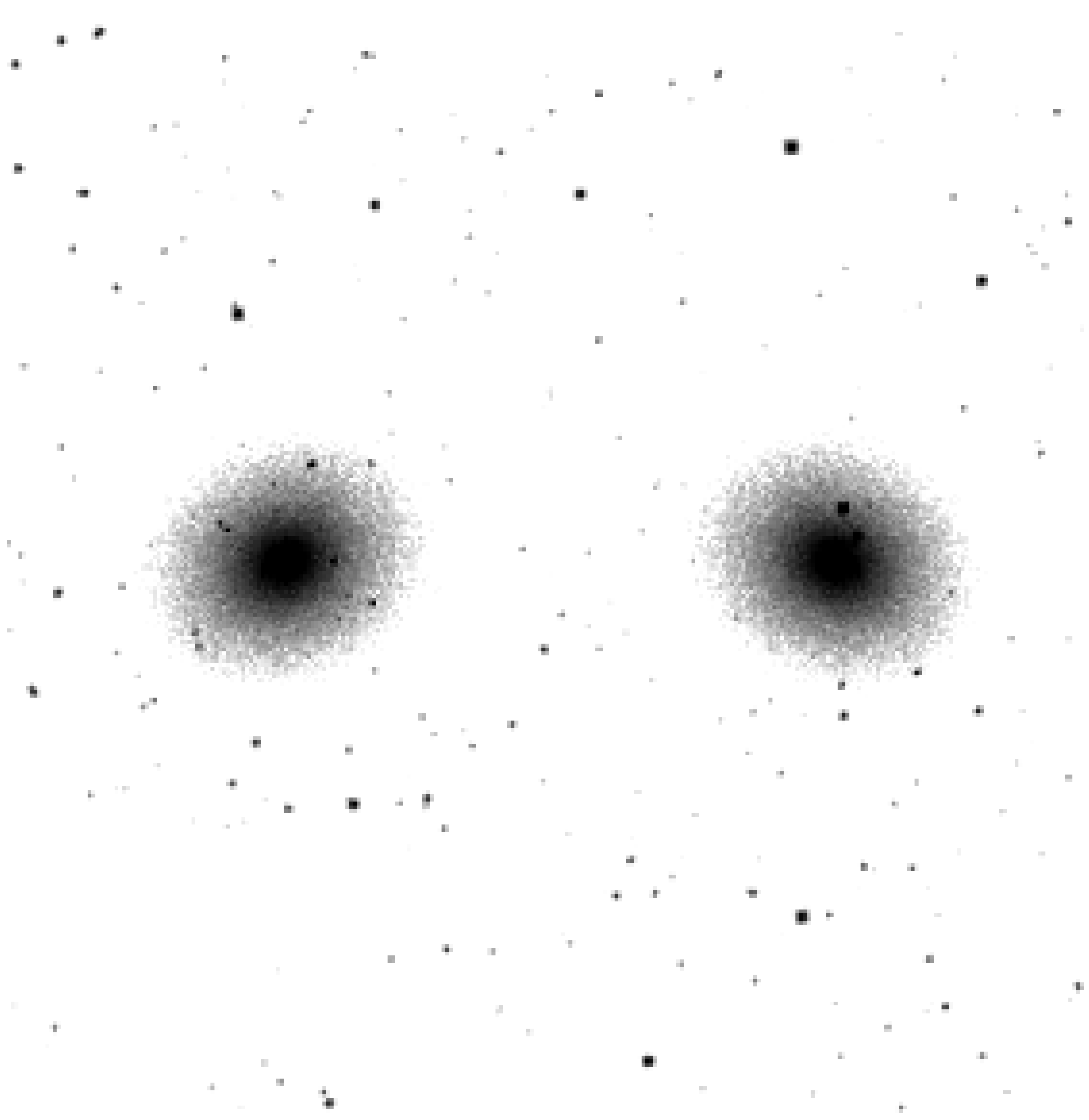

The Antennae (from the top)

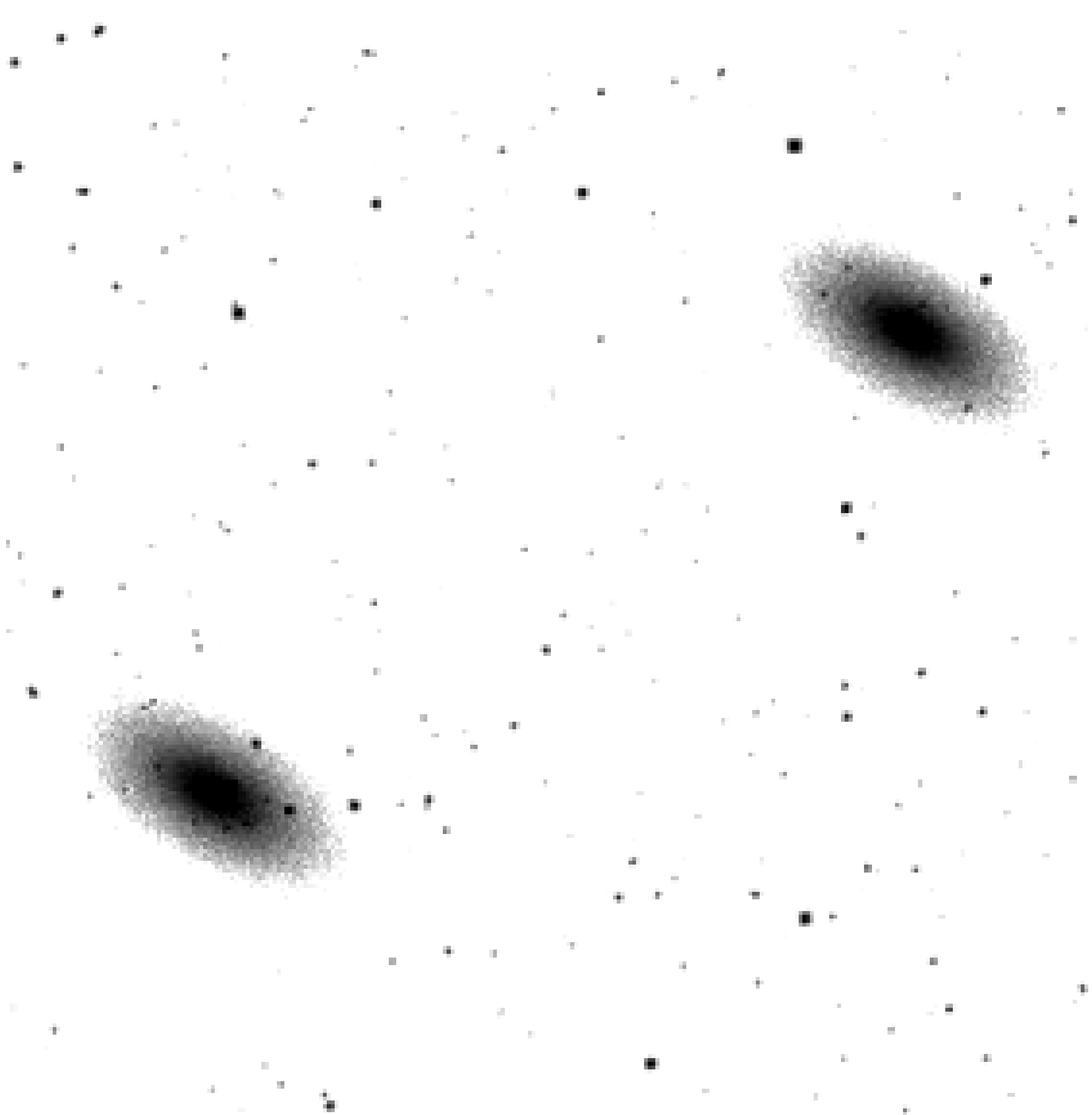

Toomre & Toomre 1972

- The galaxy's mass is concentrated at a point
- The outer disk particles are arranged in 5 rings
- They do not interact with each other (no self-gravity)
- All passages involve two galaxies that have a close, slow moving parabolic approach
- Each time unit is 100 million years

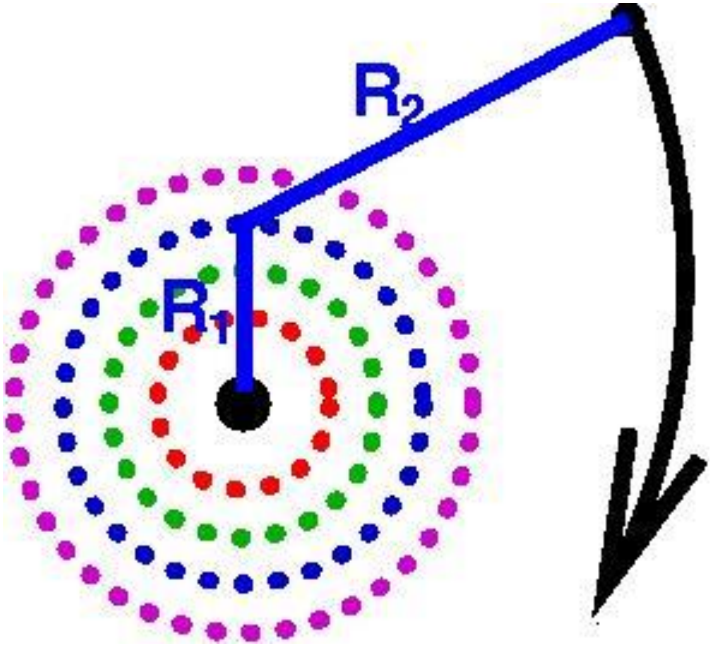

Although much more sophisticated codes exist today, T&T72 demonstrated the overall damage done by tides.

M81/M82 encounter

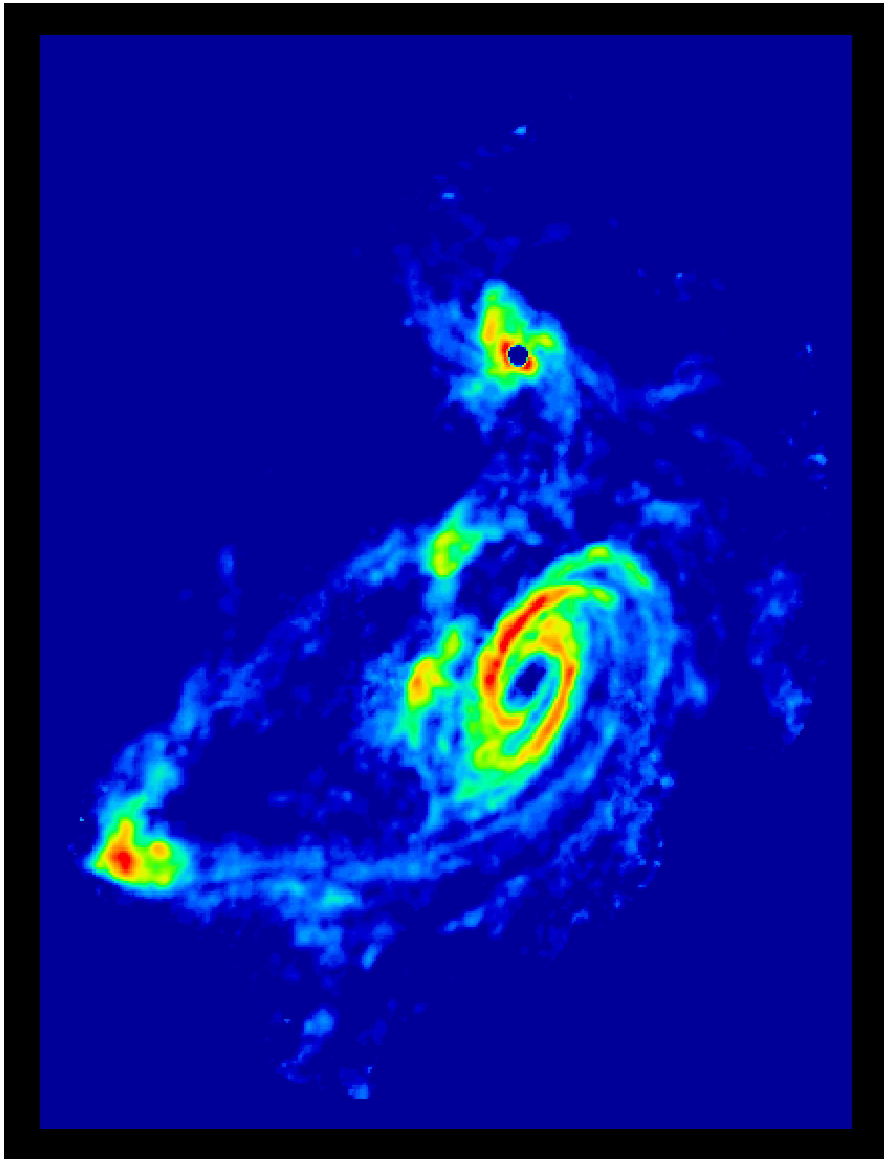

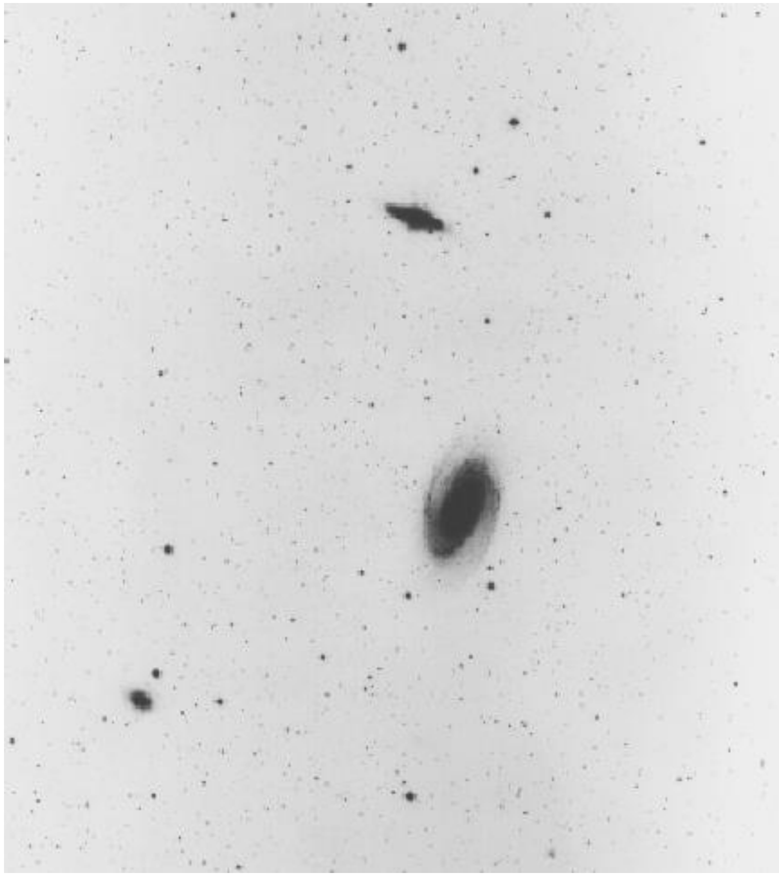

M81/M82 encounter

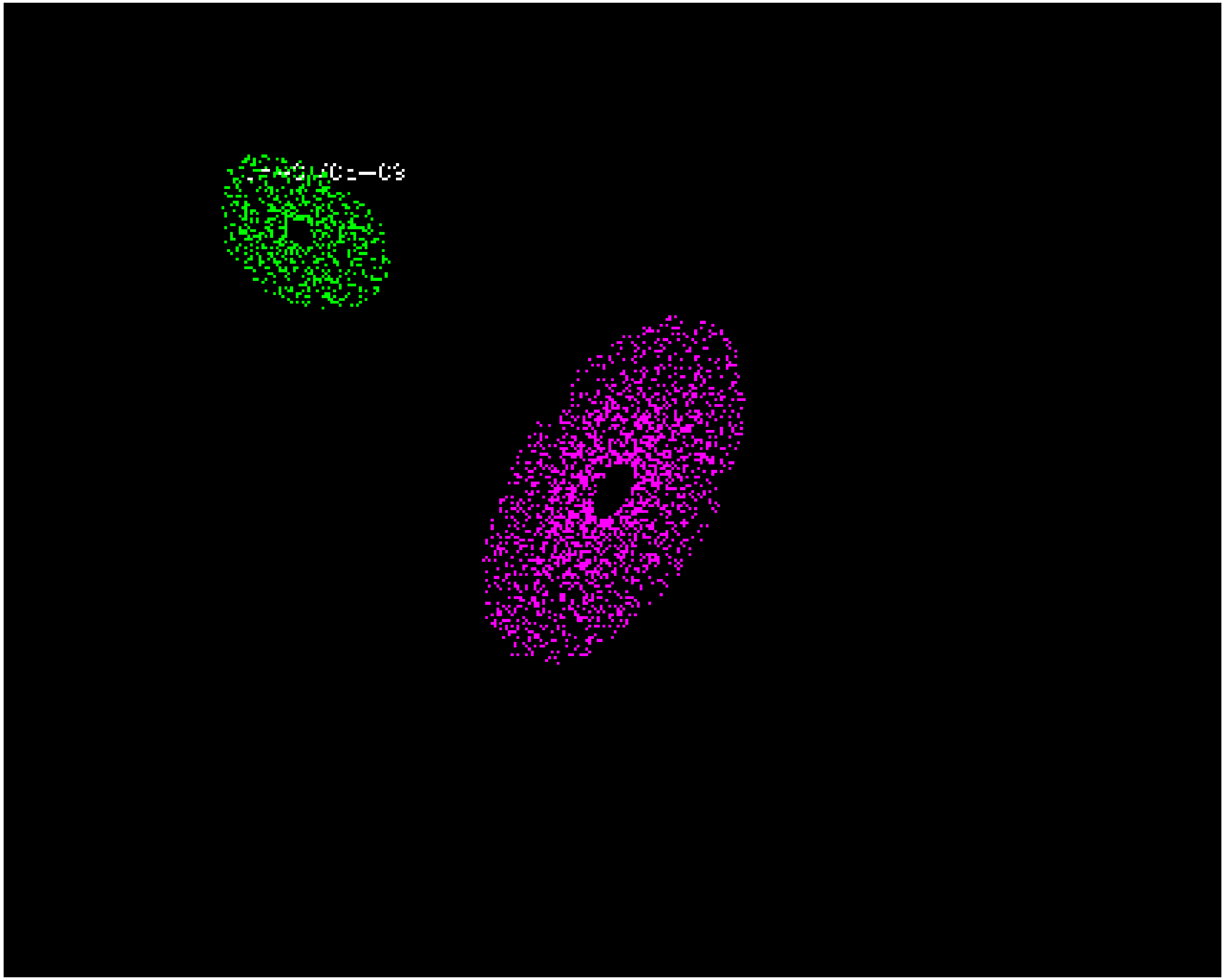

M81/M82 encounter

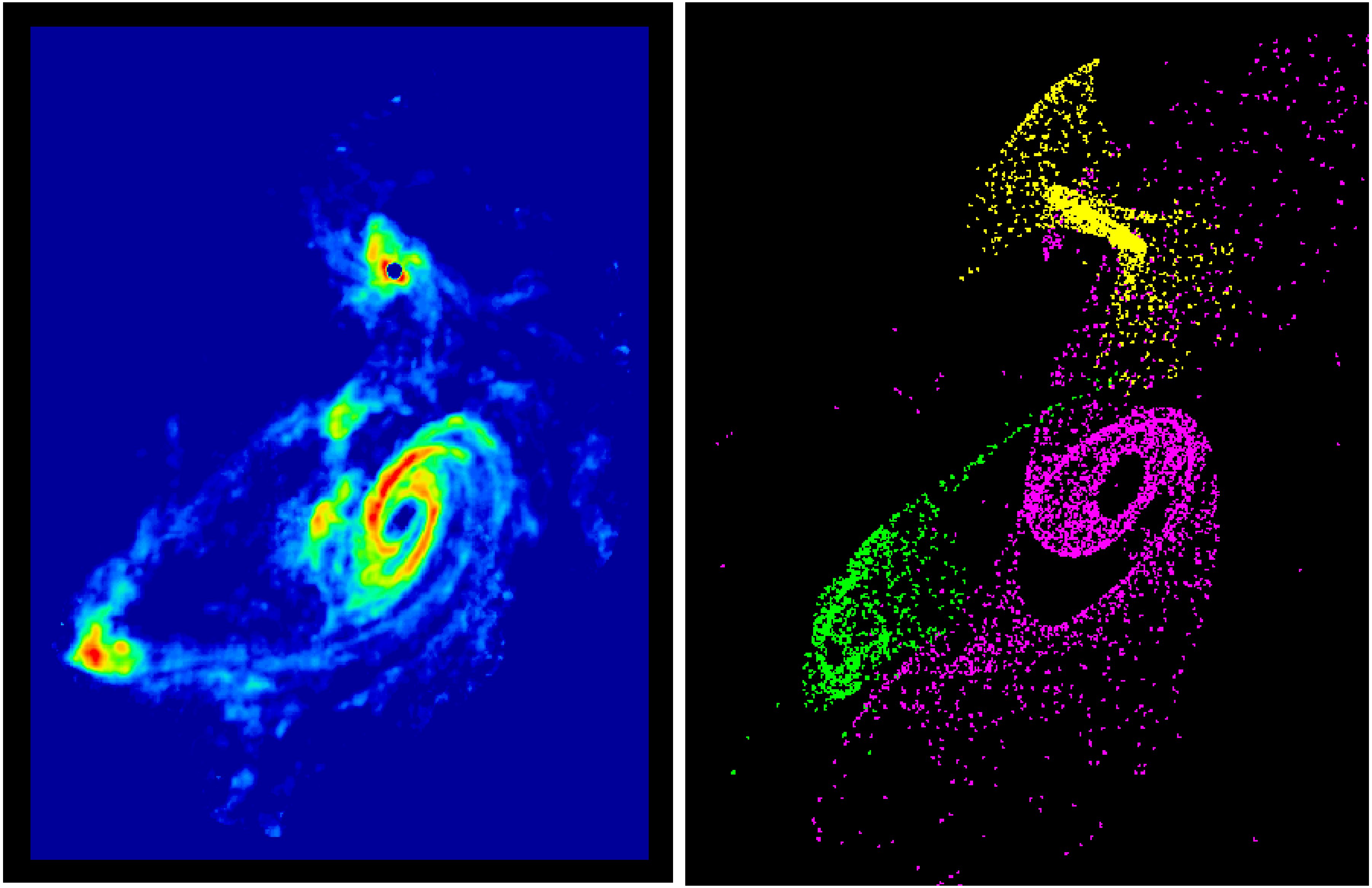

Toomre^2 results

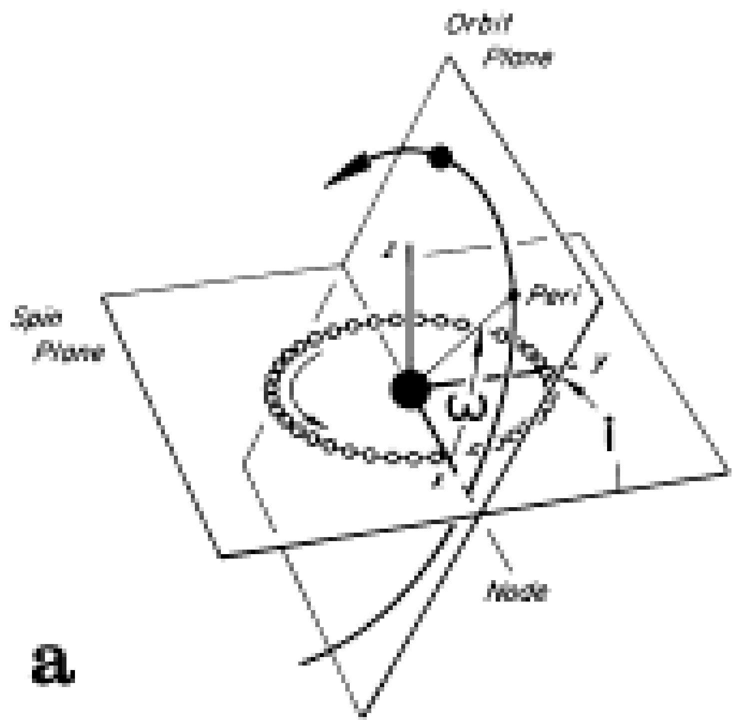

- Galaxy encounters are not accidental; most pairs are bound already
- Direct encounters cause more damage than retrograde ones
- Tails (nice) are easier to make than bridges (messy)
- Viewing geometry is critically important

Retrograde passages

Toomre & Toomre found that retrograde passage (ones in the opposite direction to a galaxy's spin) have little tidal effect. See Picture below

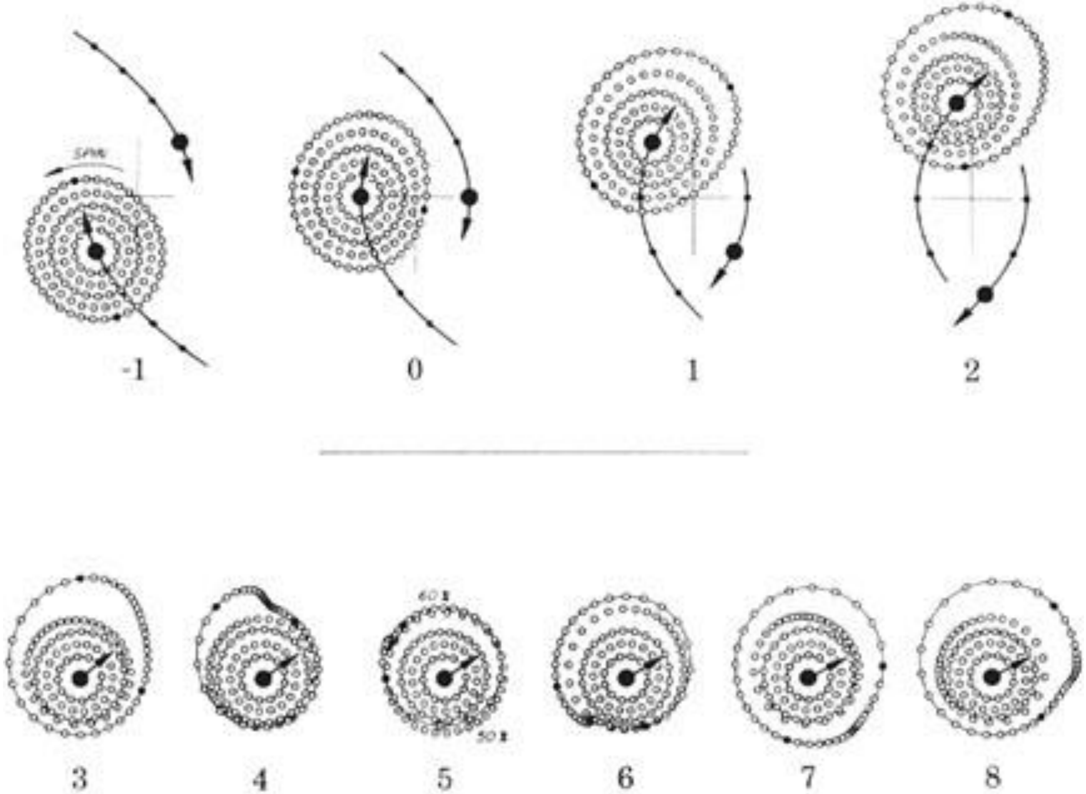

Flat retrograde ($i=180^\circ$) parabolic passage of a companion of equal mass.

TT72

- Direct passages are more effective
- More damage from equal mass companion

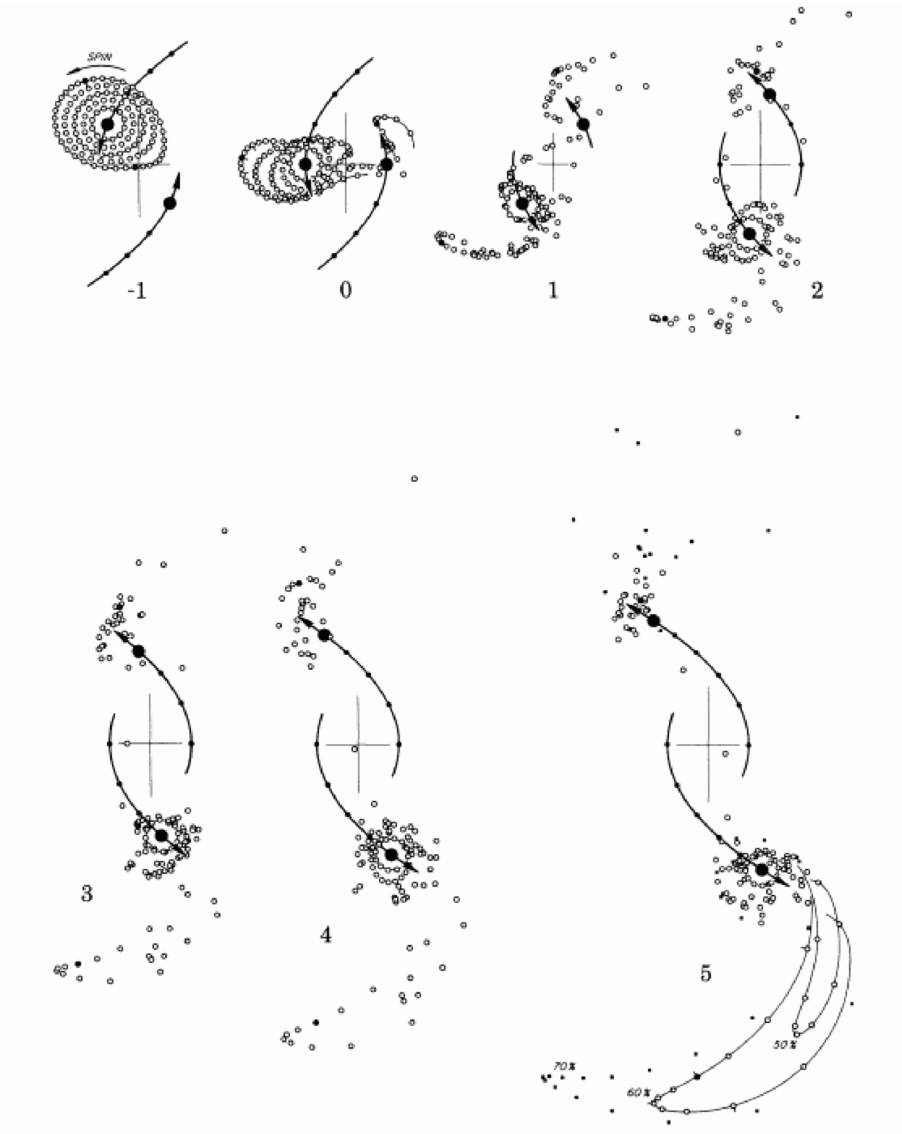

FIG. 2.—A flat direct ($i = 0°$) parabolic passage of a companion of equal mass

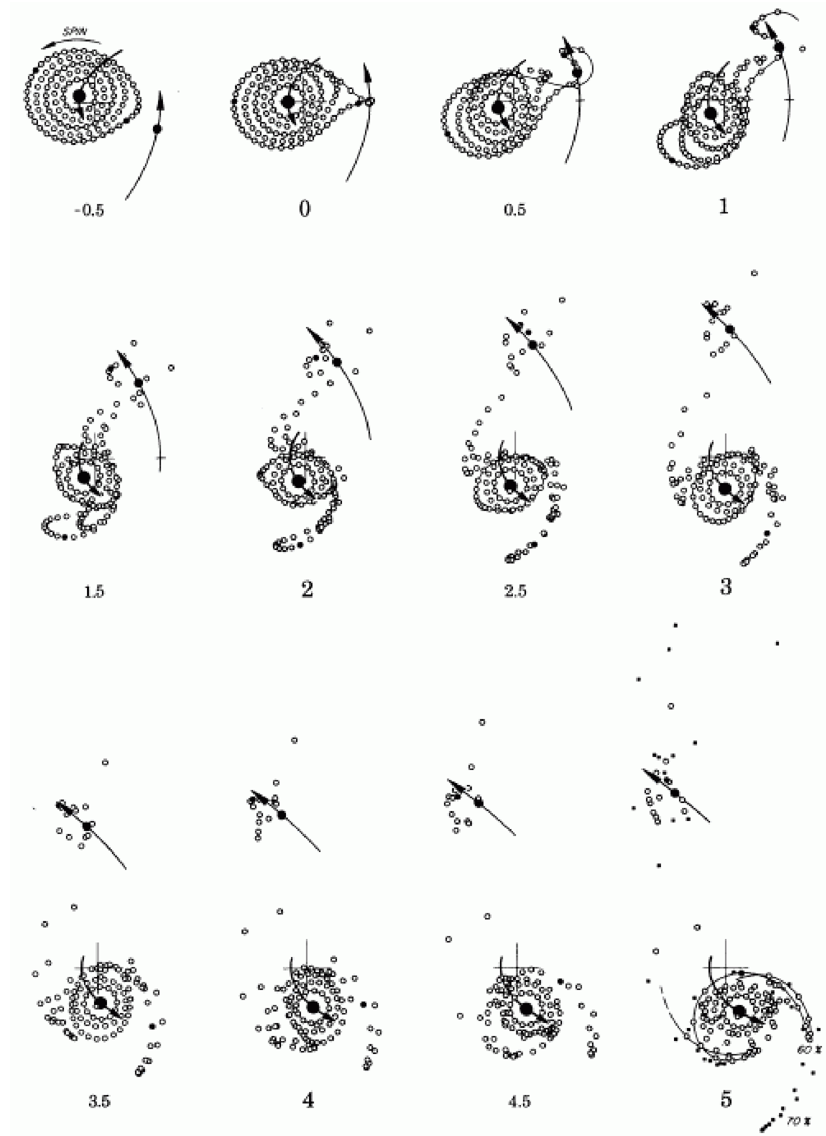

FIG. 4.—A flat direct ($i = 0°$) parabolic passage of a quarter-mass companion

Bridge Building and Inclination

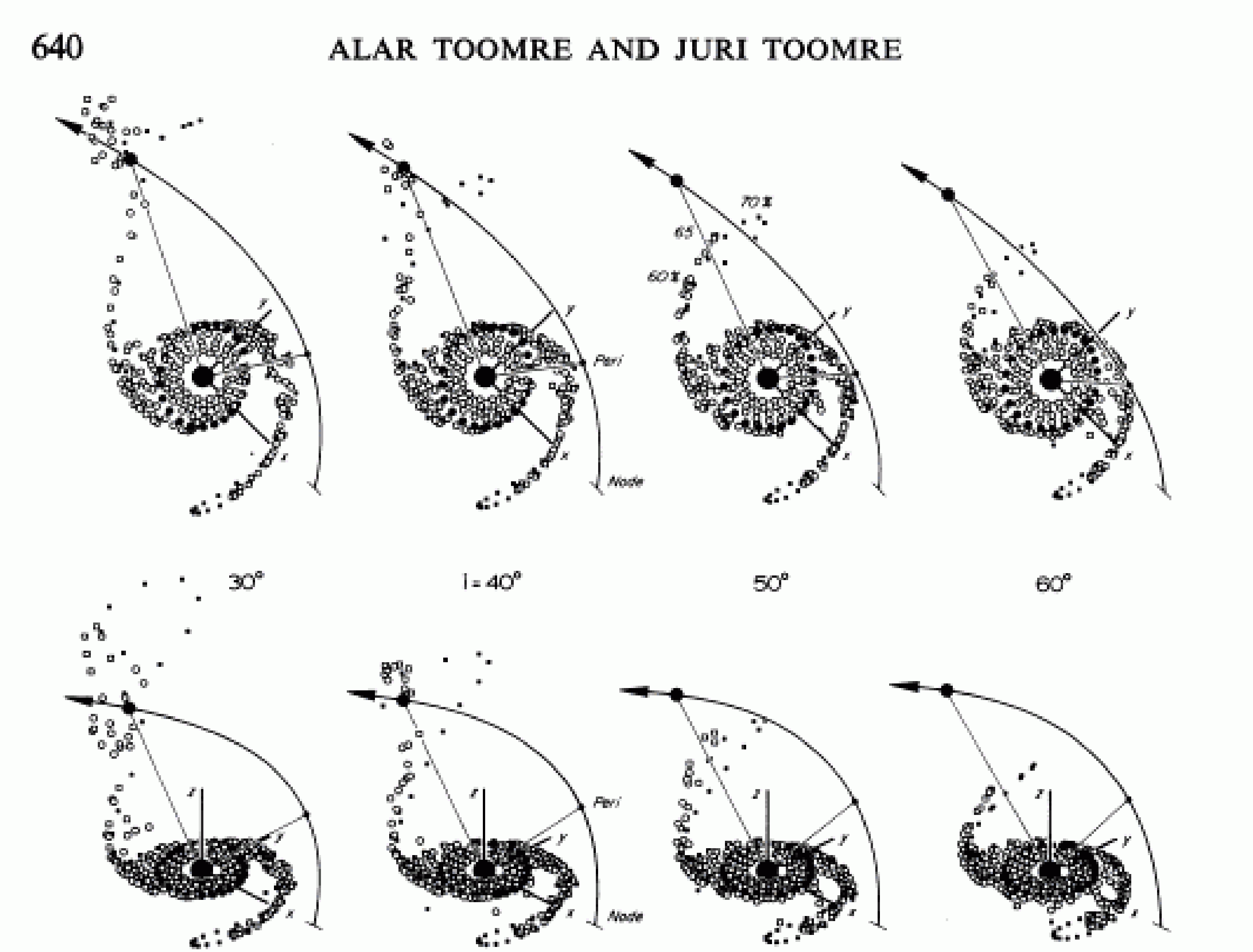

FIG. 13.—Results of four differently inclined passages of fixed argument $\omega = +60°$. The top row depicts the $\beta = 0°$ face-on appearances of these four severely perturbed disks at $t = 3.143$, whereas the bottom row shows how each object would look if viewed at tilt $\beta = 60°$ from the same longitude $\lambda = 45°$.

Tails

- Unlike bridges, tails involve some particles escaping towards infinity
- To form major tails, the galaxies should be similar in mass.
- Like bridges, tail making is less effective at higher inclination planes. Again, the difference between 0° and 30 ° is small.
- However, in higher inclinations, the tail is raised from the orbit plane. This allows the tails to be crossed, as in NGC 4038/9

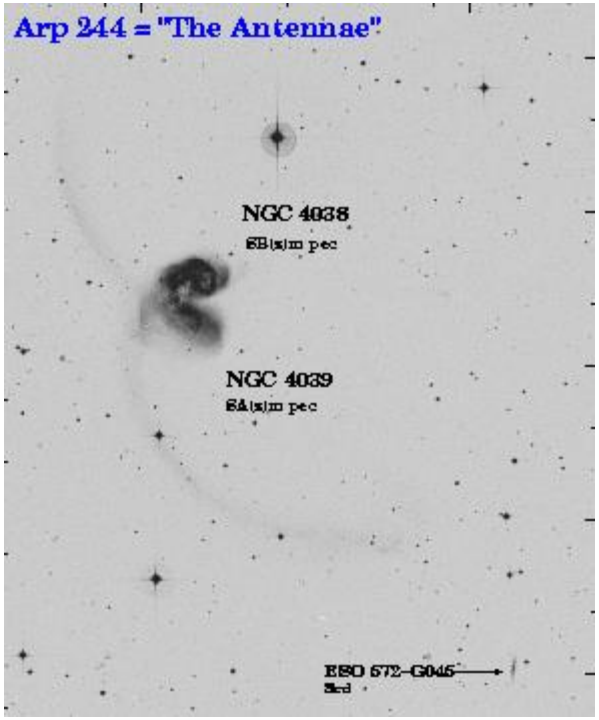

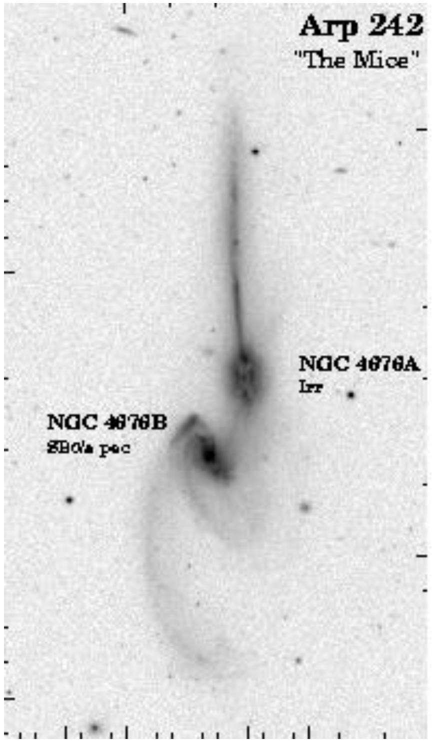

Gravitational encounters

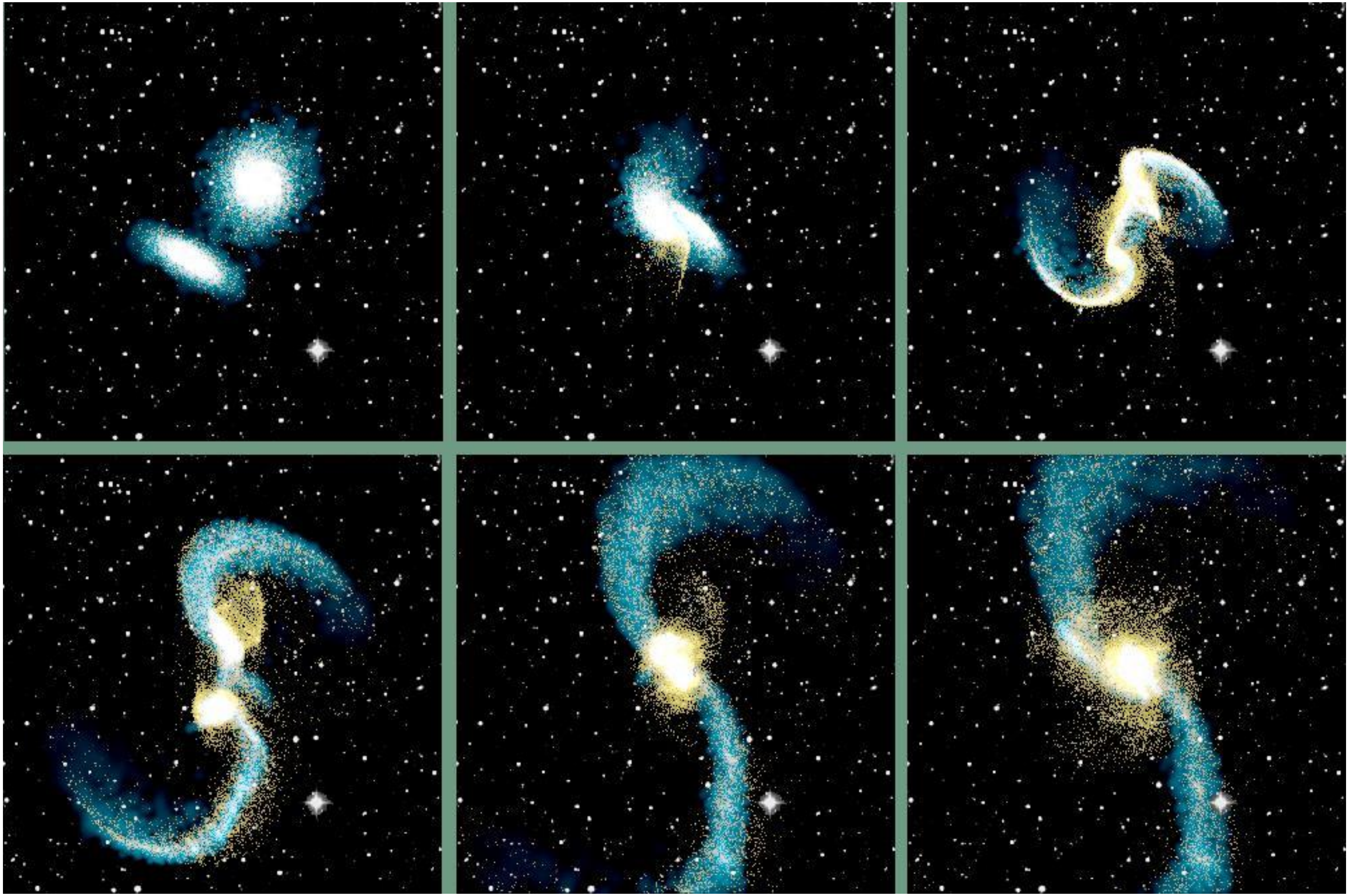

The Antennae

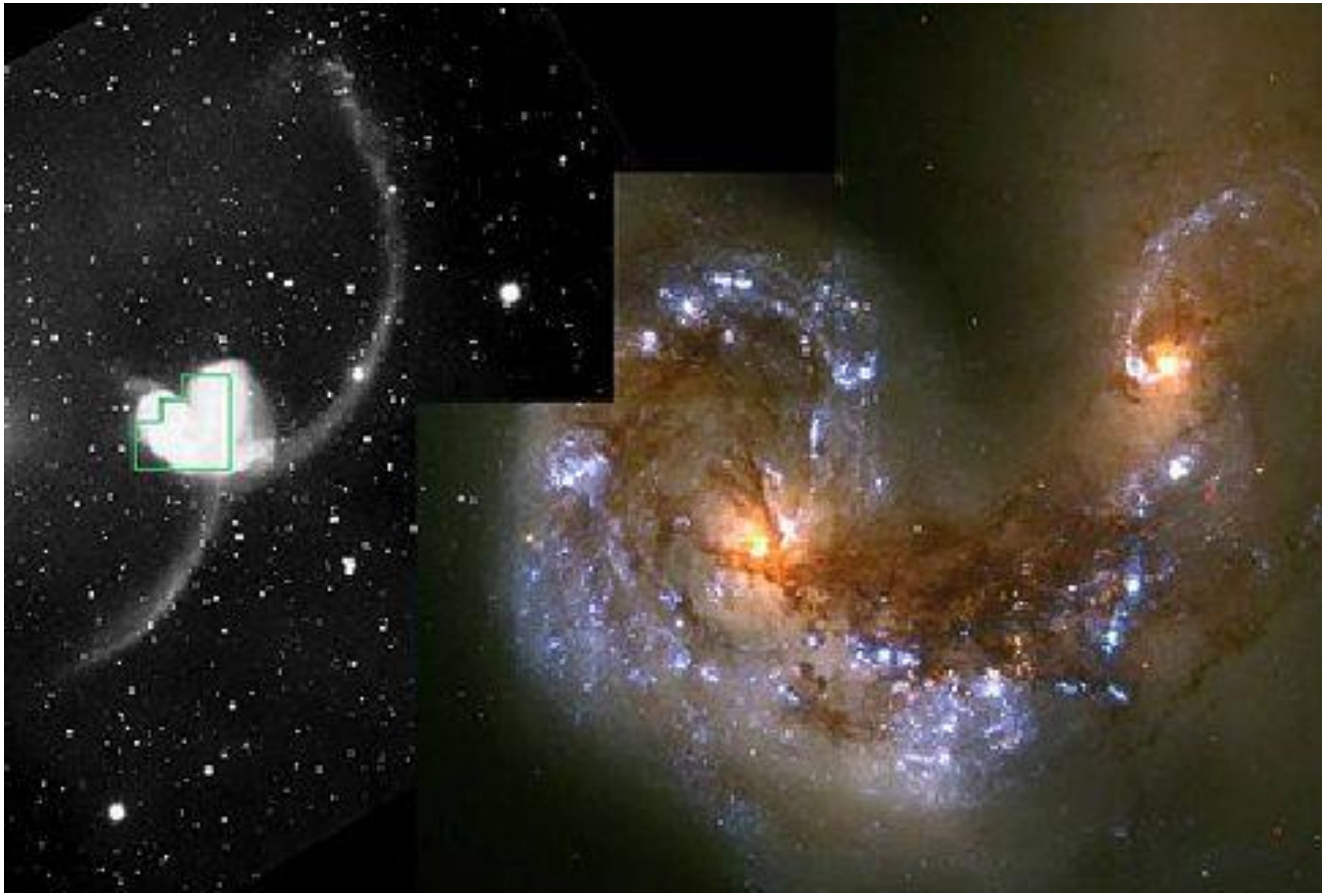

Encounter geometry

Barnes, 1988, ApJ 331, 699

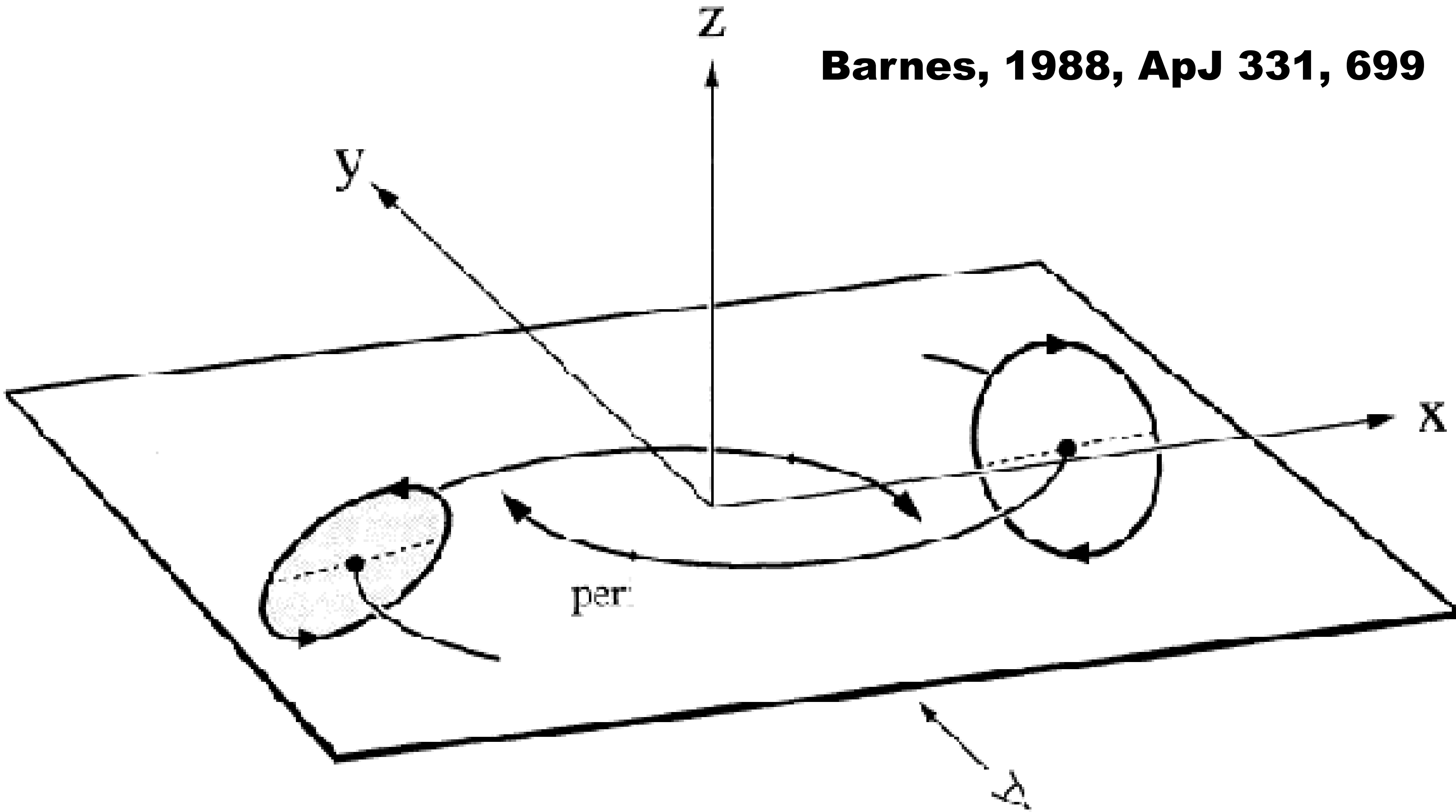

- Disks shown in their original position.
- Each disk inclined 60° with respect to orbital plane

The Antennae in HI

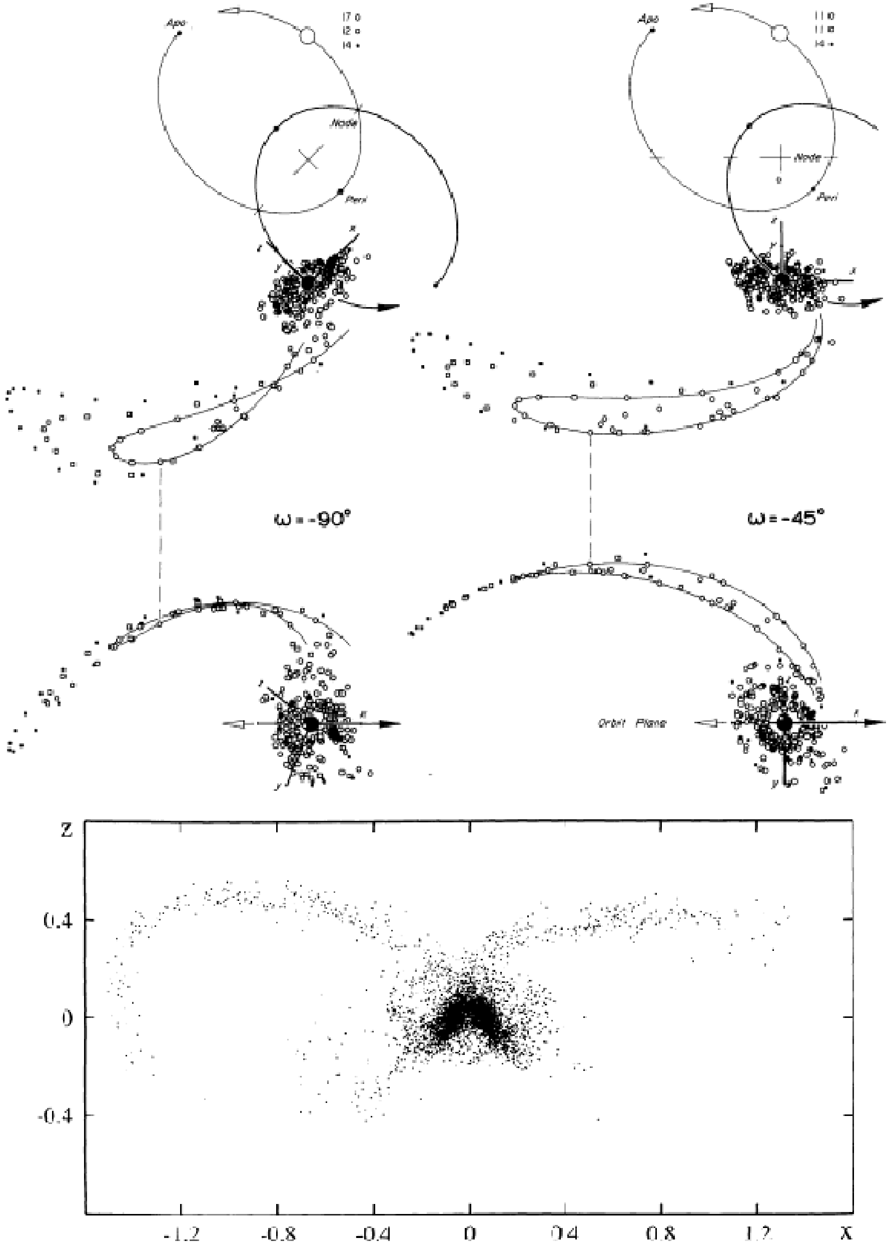

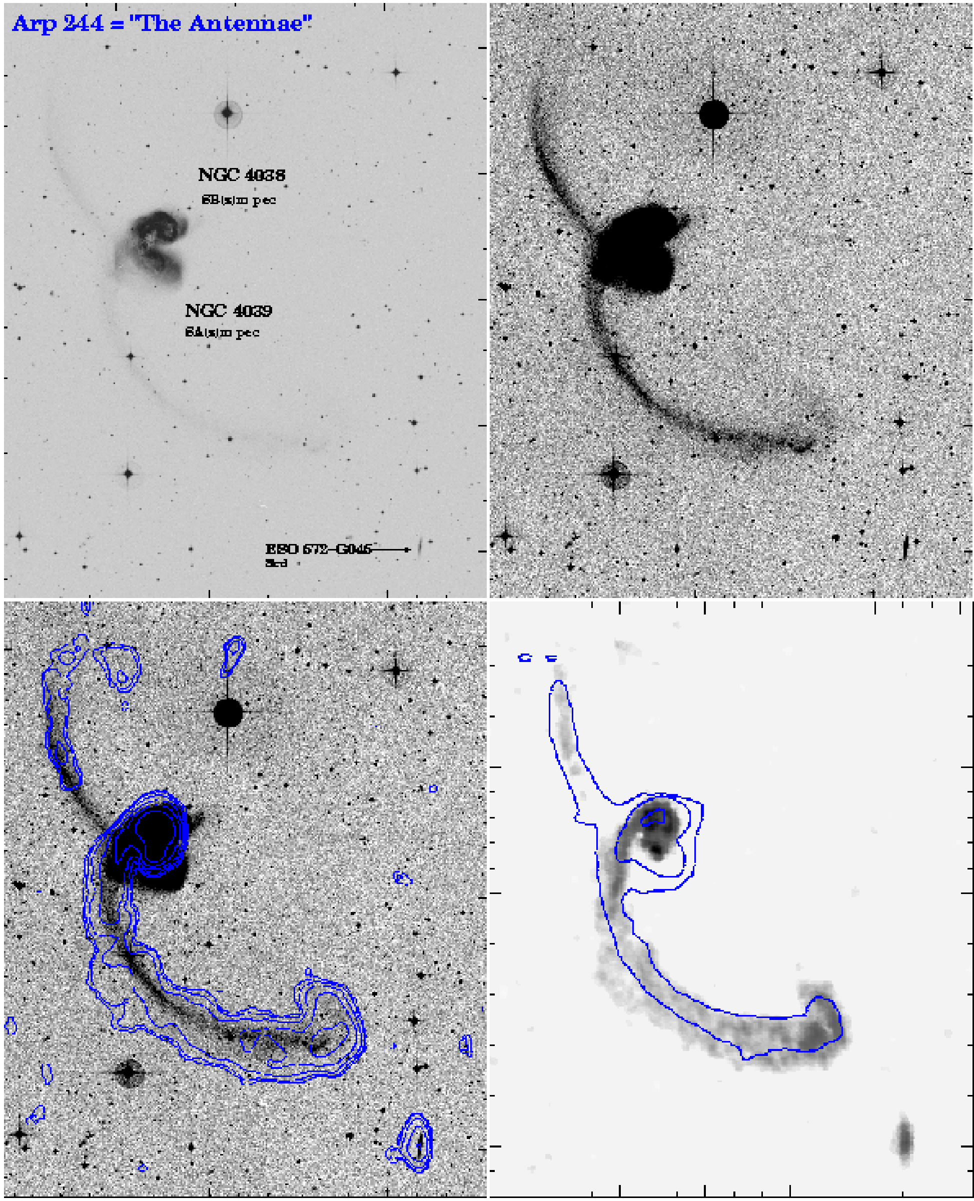

http://www.cv.nrao.edu/~jhibbard

M51

b) *M51 and NGC 5195*

Unlike the above, the most famous "bridge" linking two galaxies now seems definitely a fraud. Certainly both M51 (= NGC 5194) and its companion NGC 5195 show major signs of tidal damage. But as we are about to demonstrate, that damage only completes the proof that NGC 5195 lies at present well behind M51.

To begin, we would like it clearly understood here that our immediate concern is *not* with the magnificent spiral structure seen in M51 within, say, 2′.0 of its center. Rather, in our view much of the *explicit* tidal damage to M51 itself only commences

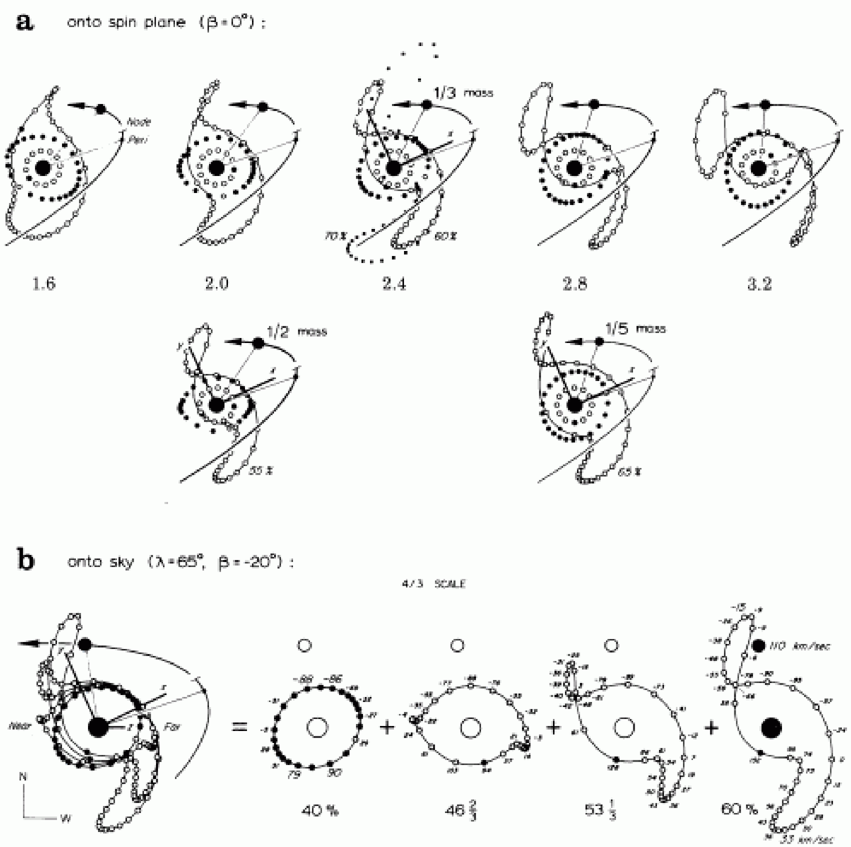

FIG. 20.—Auxiliary studies of M51. (*a*) The top row offers five face-on ($\beta = 0°$) views of the evolving shapes of three test-particle rings of initial radii 0.2, 0.4, and $0.6 R_{\min}$, after being perturbed by an inclined $i = -70°$, $\omega = -15°$, elliptic $e = 0.8$ passage of a companion of one-third mass. Also shown, at times $t = 2.0$ and 2.8, are the corresponding shapes from instances where the mass ratio of the satellite to the primary was assumed one-half and one-fifth; in those cases, the original radius of the outermost ring was altered to 0.55 and $0.65 R_{\min}$, respectively. (*b*) Slightly tilted ($\lambda = 65°$, $\beta = -20°$) and $\frac{4}{3}$-enlarged view of the above $t = 2.4$ configuration. It excludes the 0.2 and $0.7 R_{\min}$ particles, but it includes two additional rings from 7/15 and 8/15 $R_{\min}$. The left-hand picture has been decomposed on the right into its four constituent rings; the italicized numbers there are the Doppler velocities of various particles, relative to the primary, obtained after scaling the similar speed of the satellite to $+110\ \mathrm{km\ s^{-1}}$.

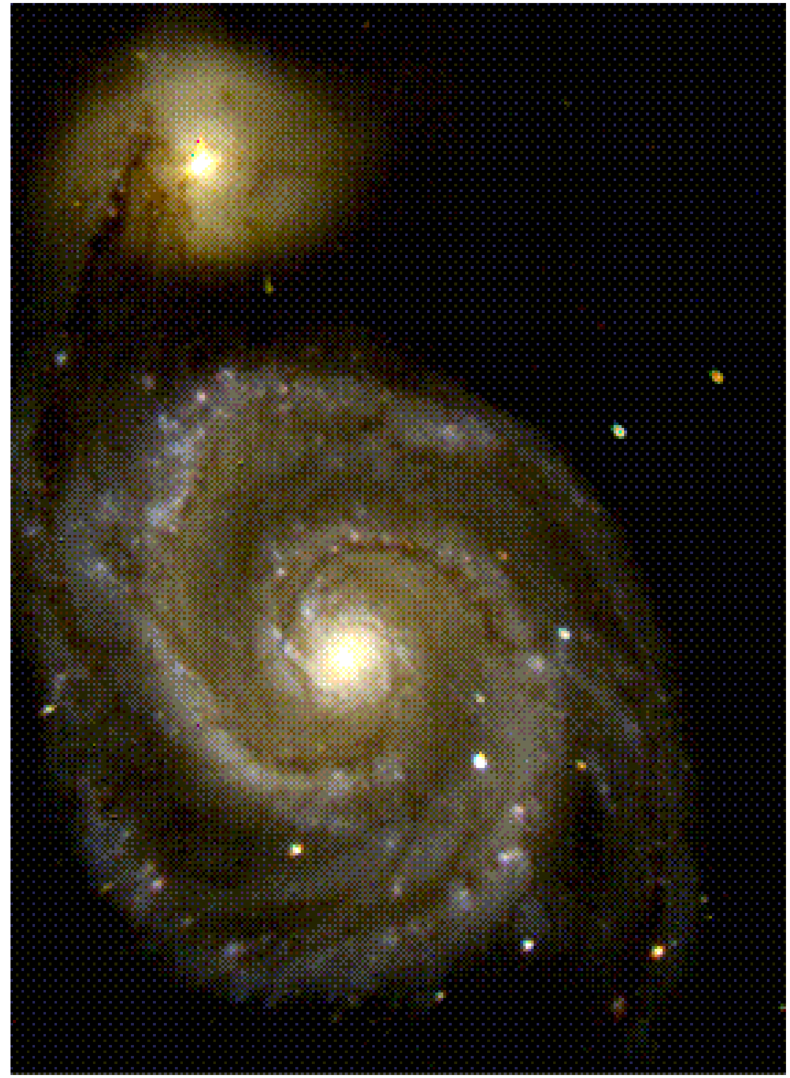

M51

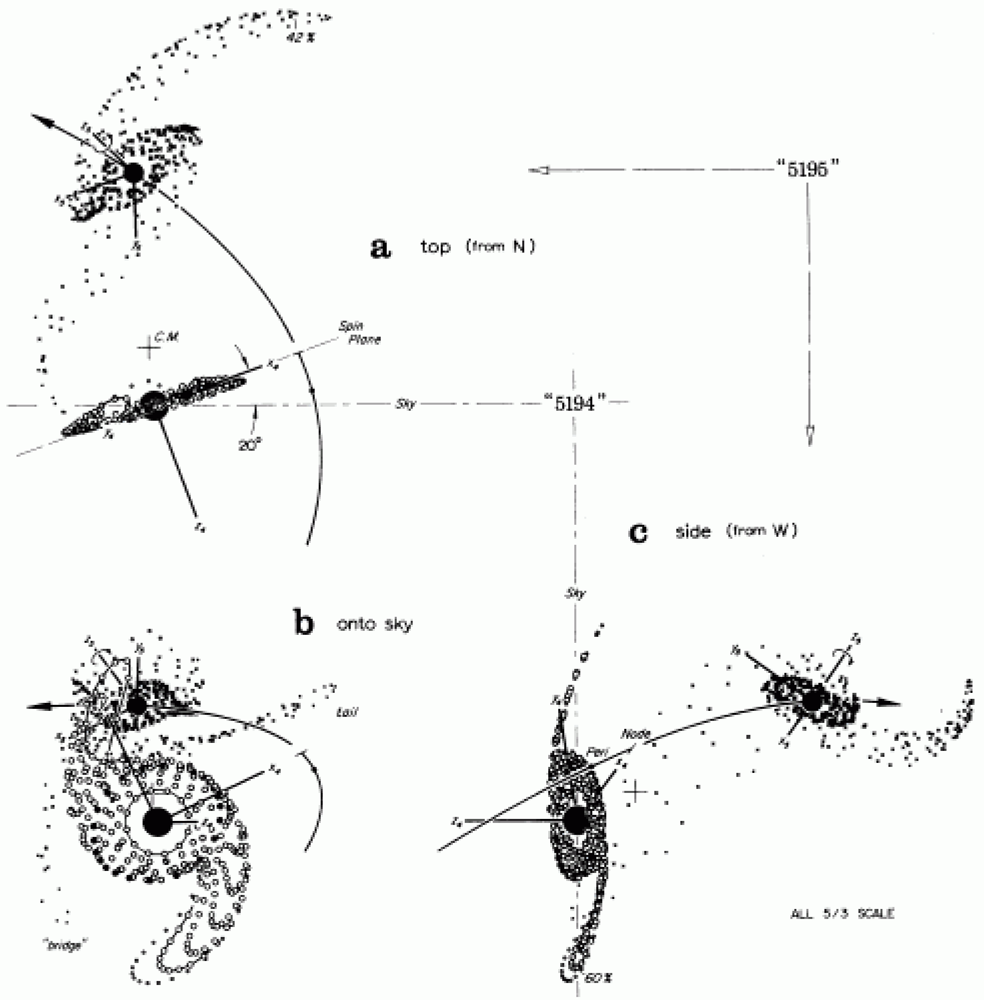

FIG. 21.—Model of the recent encounter between M51 and NGC 5195. Shown here at $t = 2.4$ are three mutually orthogonal views of the consequences of a highly elliptic $e = 0.8$ passage of a supposedly disklike "5195." This satellite was chosen to be one-third as massive, and of exactly 0.7 times the linear dimensions, of the "5194" primary—which itself contains particles from initial radii $0.2(0.05)0.4(0.033)0.633 R_{\min}$. The orbit plane differs by an angle $i_4 = -70°$ from the initial spin plane of the larger disk and by $i_5 = -60°$ from that of the smaller; however, the arguments $\omega_4 = \omega_5 = -15°$ of the pericenters were here kept identical, to make the above nodal axes x_4 and x_5 exactly antiparallel. The three views show the combined system as it would appear not only (*b*) to us ($\lambda_4 = 65°$, $\beta_4 = -20°$), but also edge-on to our sky from (*a*) the "north" ($-25°$, $90°$) and (*c*) the "west" ($65°$, $70°$) directions.

M51

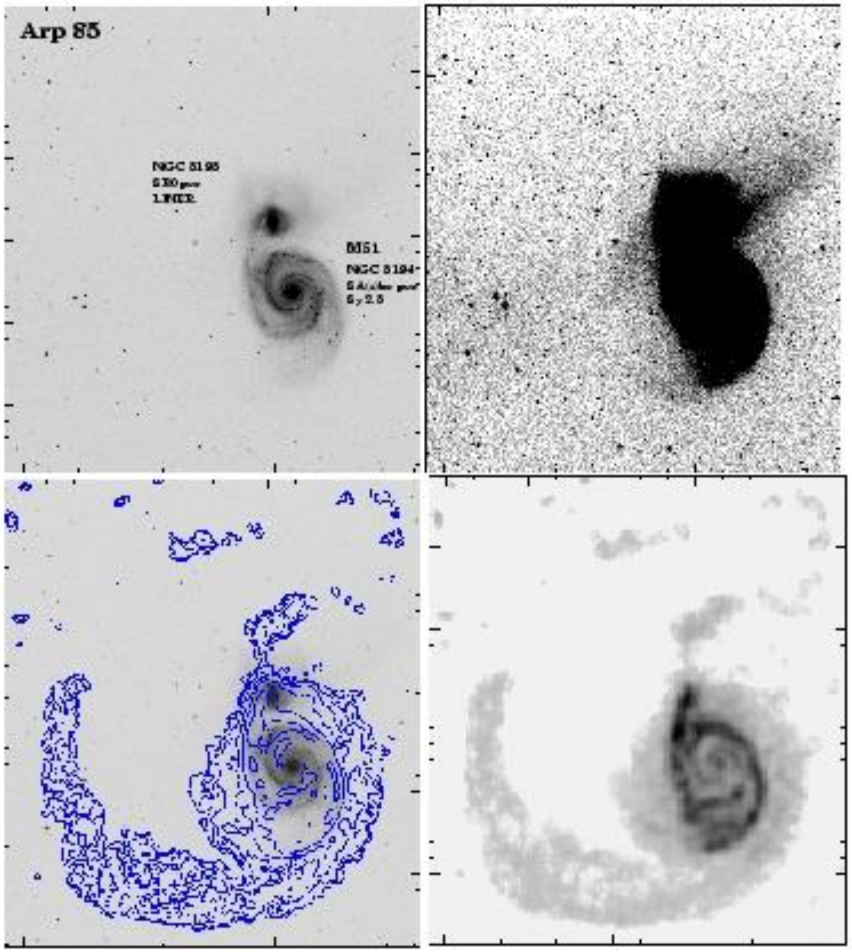

Figure 1. **M51: The Whirlpool Galaxy.**
HI: VLA C+D-array, 34″ resolution, contours=4×10^{19} cm^{-2} $\times 2^n$.
Optical: DSS, FOV=26′ × 29′.
Reference: Rots, A. H., Bosma, A., van der Hulst, J. M., Athanassoula, E., & Crane, P. C. 1990, AJ, 100, 387. See also Miller, Bregman & Wakker, these

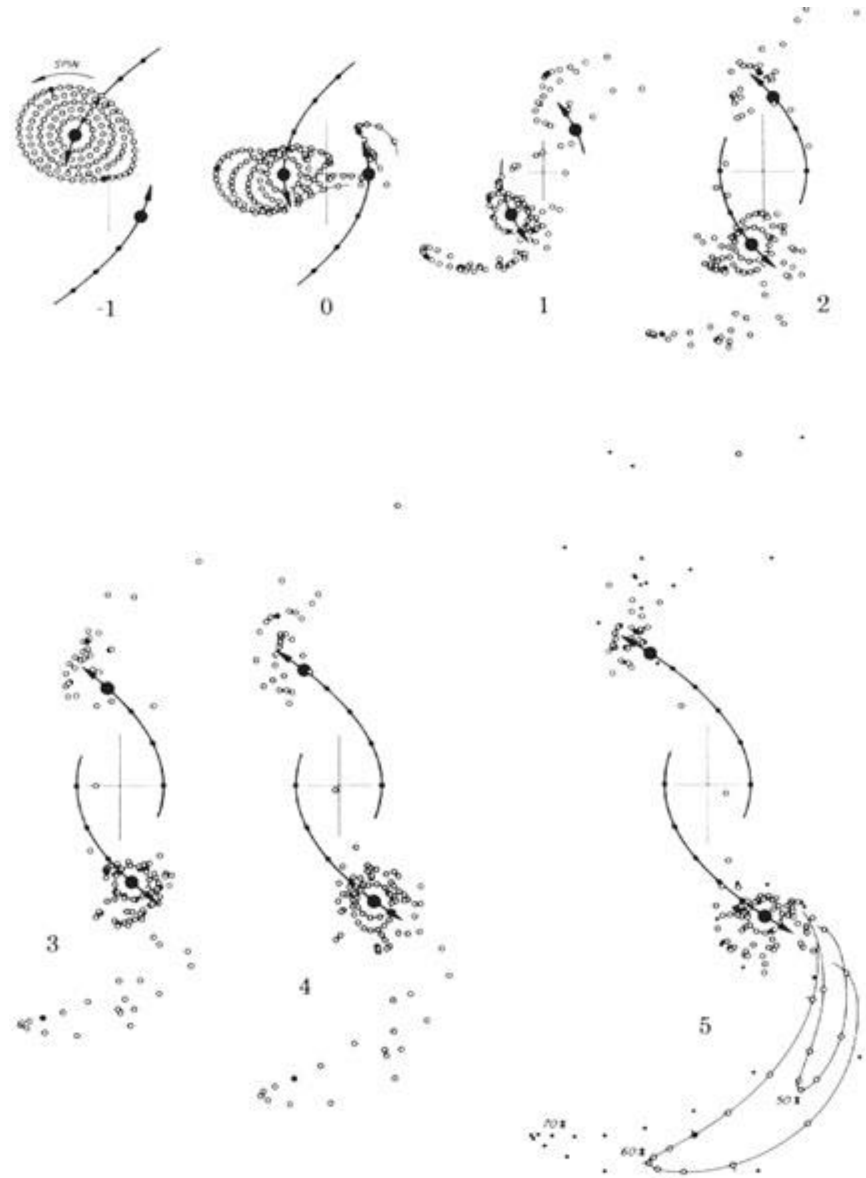

"The Mice"

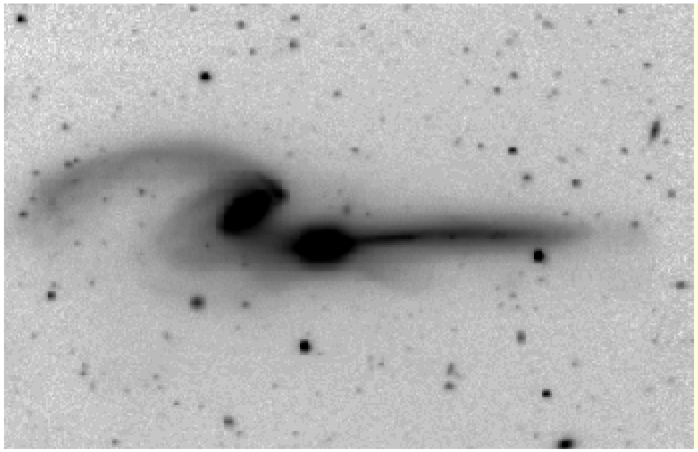

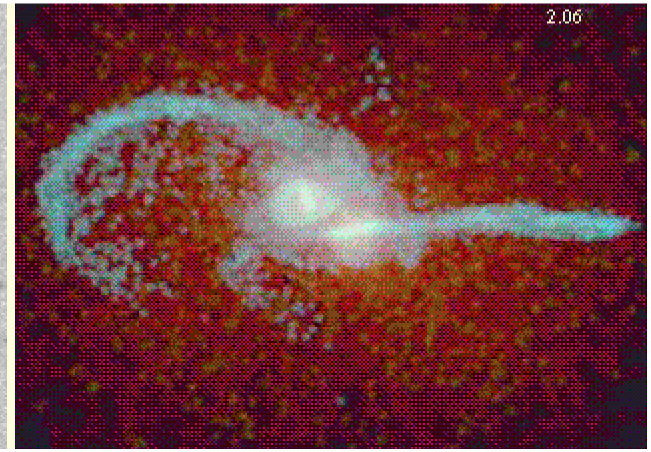

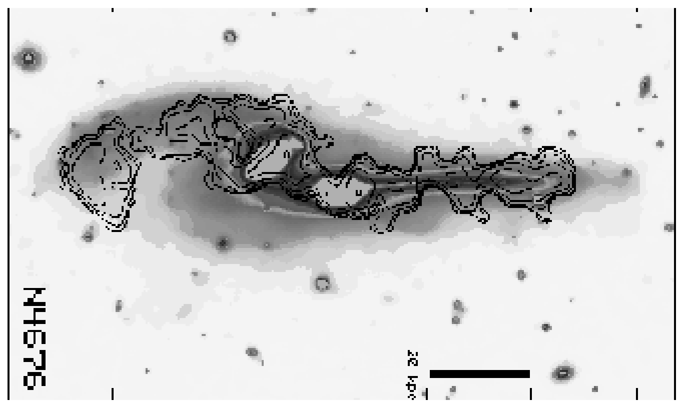

TT72: The Mice

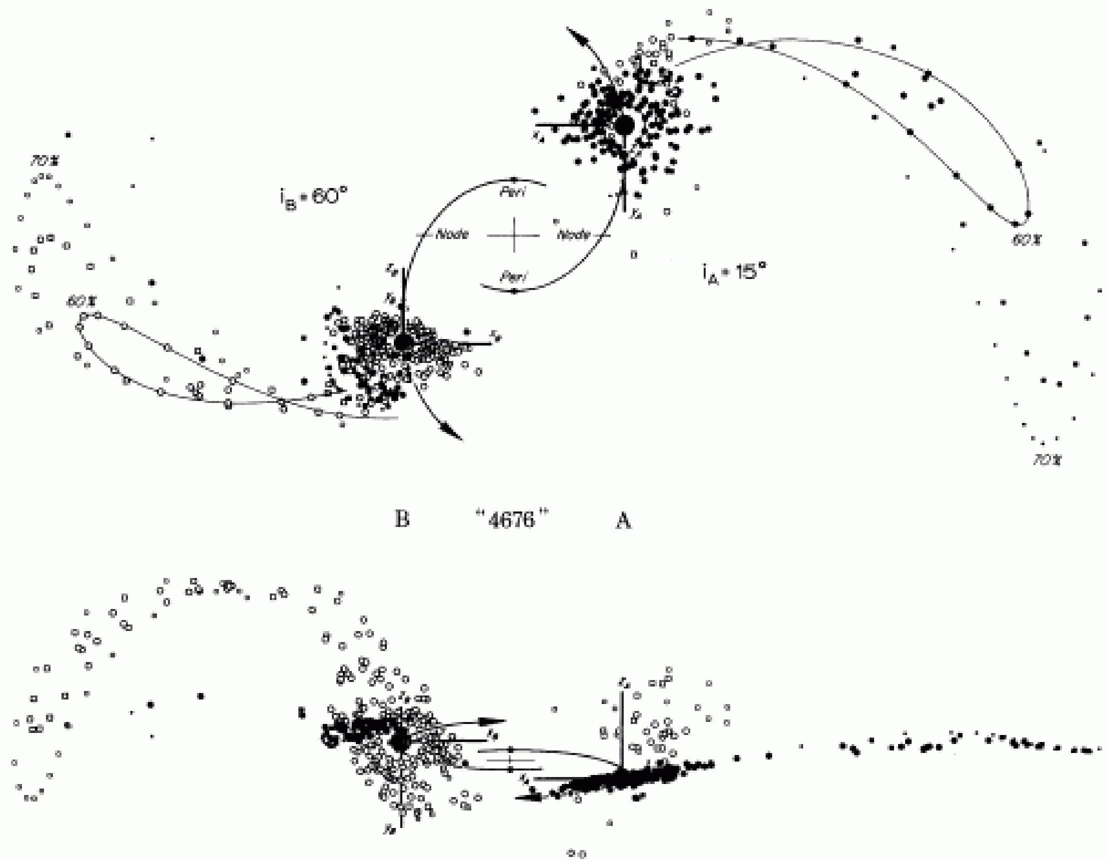

FIG. 22.—Model of NGC 4676. In this reconstruction, two equal disks of radius $0.7R_{\min}$ experienced an $e = 0.6$ elliptic encounter, having begun flat and circular at the time $t = -16.4$ of the last apocenter. As viewed from either disk, the adopted node-to-peri angles $\omega_A = \omega_B = -90°$ were identical, but the inclinations differed considerably: $i_A = 15°$, $i_B = 60°$. The resulting composite object at $t = 6.086$ (cf. fig. 18) is shown projected onto the orbit plane in the upper diagram. It is viewed nearly edge-on to the same—from $\lambda_A = 180°$, $\beta_A = 85°$ or $\lambda_B = 0°$, $\beta_B = 160°$—in the lower diagram meant to simulate our actual view of that pair of galaxies. The filled and open symbols distinguish particles originally from disks A and B, respectively.

The Mice: a driven system

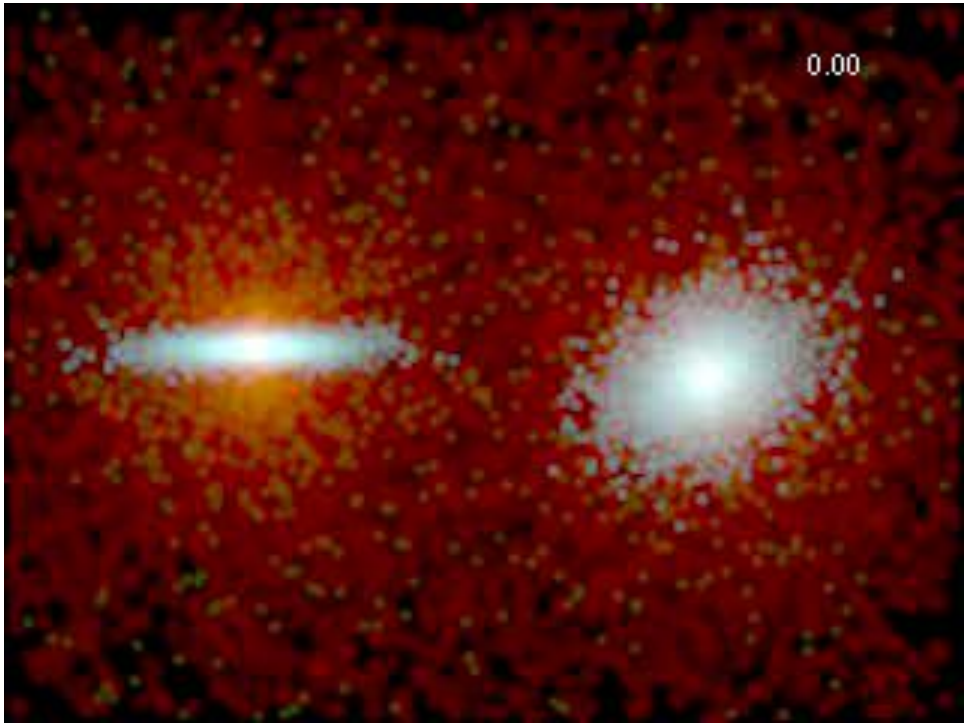

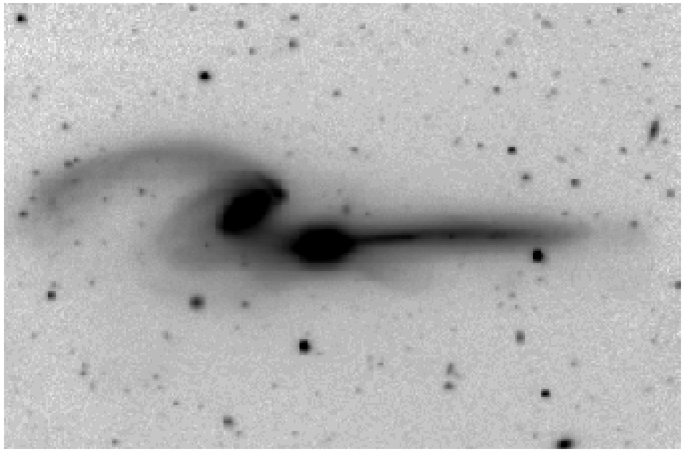

The Mice: a driven system: J. Barnes

Mice encounter (J. Barnes)

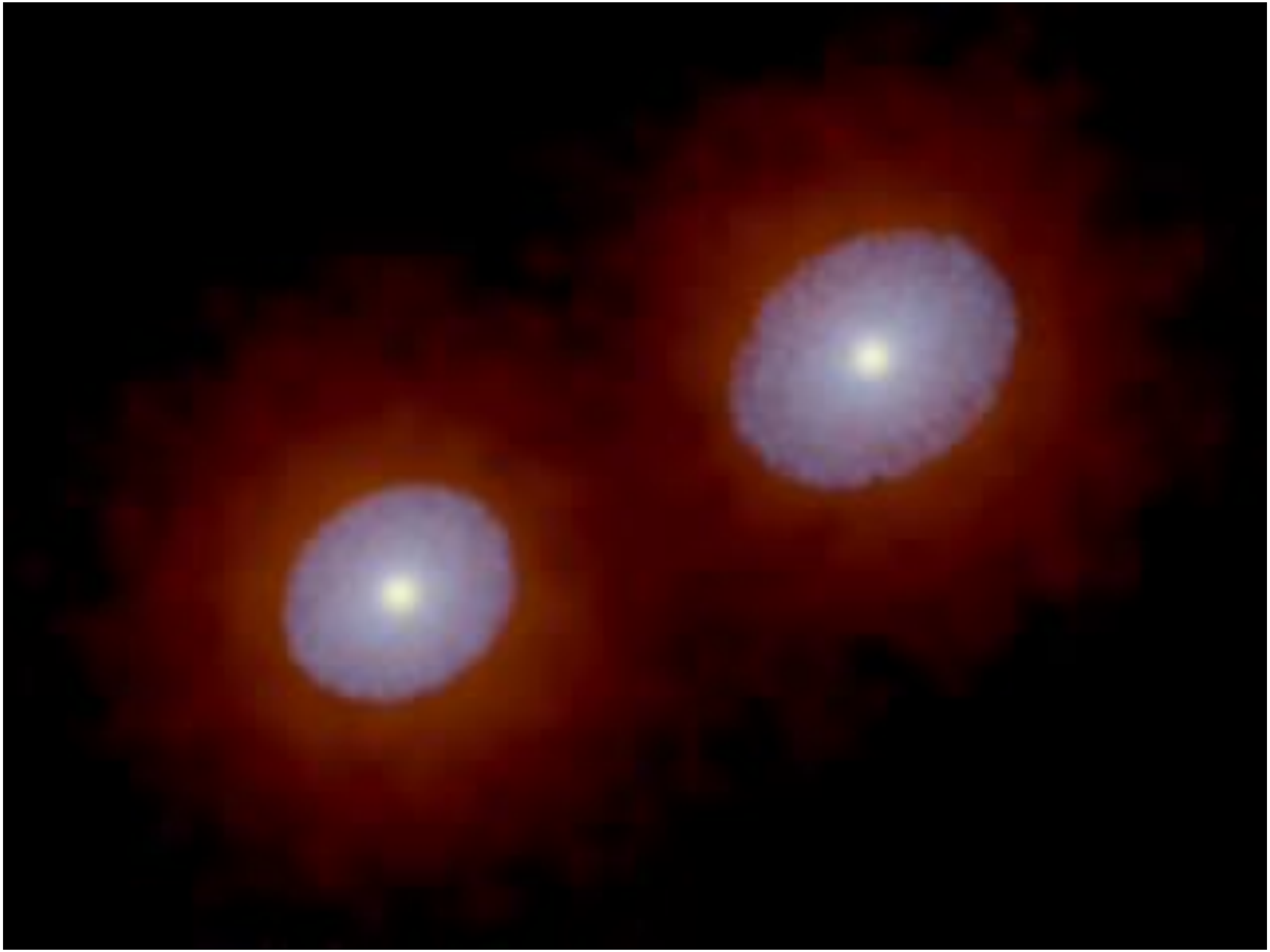

Chris Mihos' Cartwheel movie

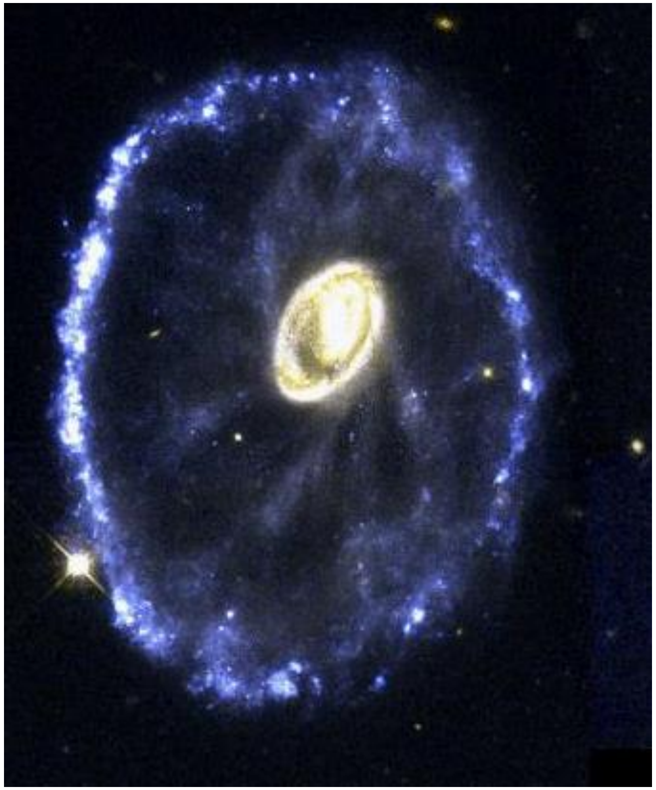

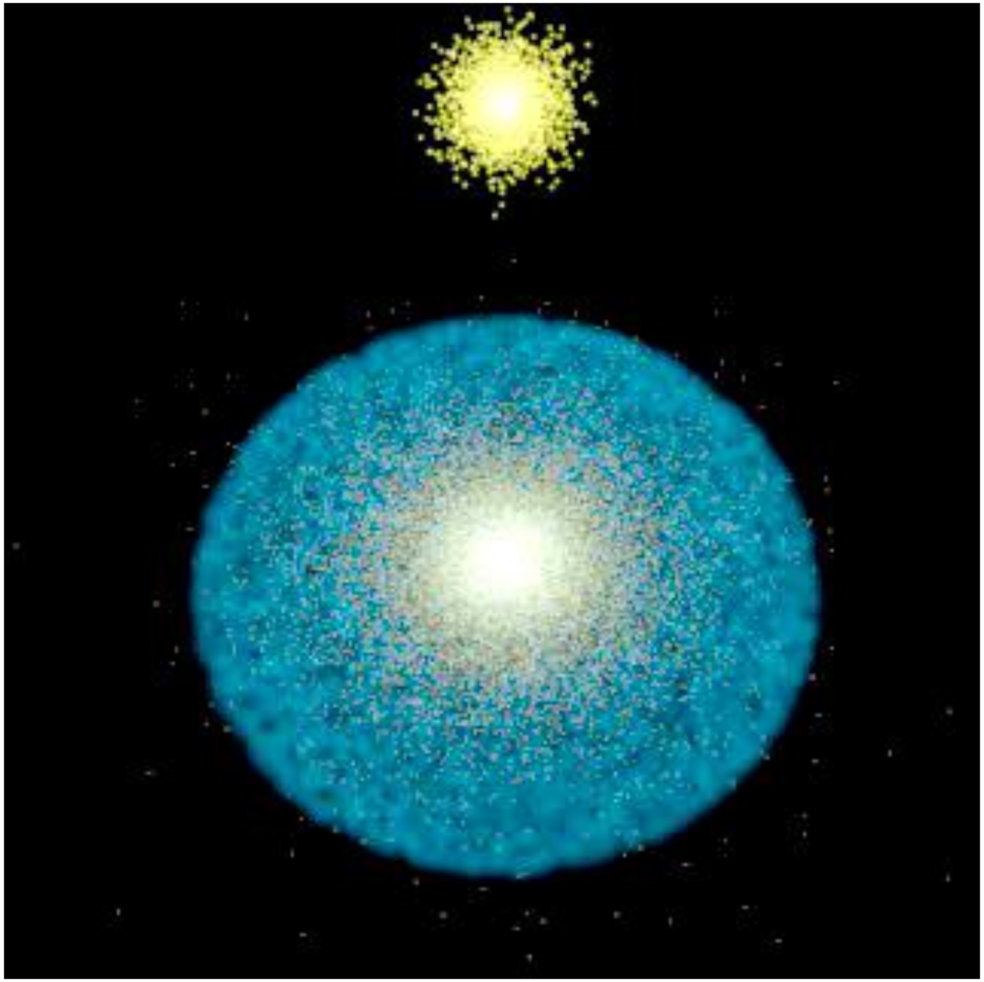

Cartwheel: A head-on collision

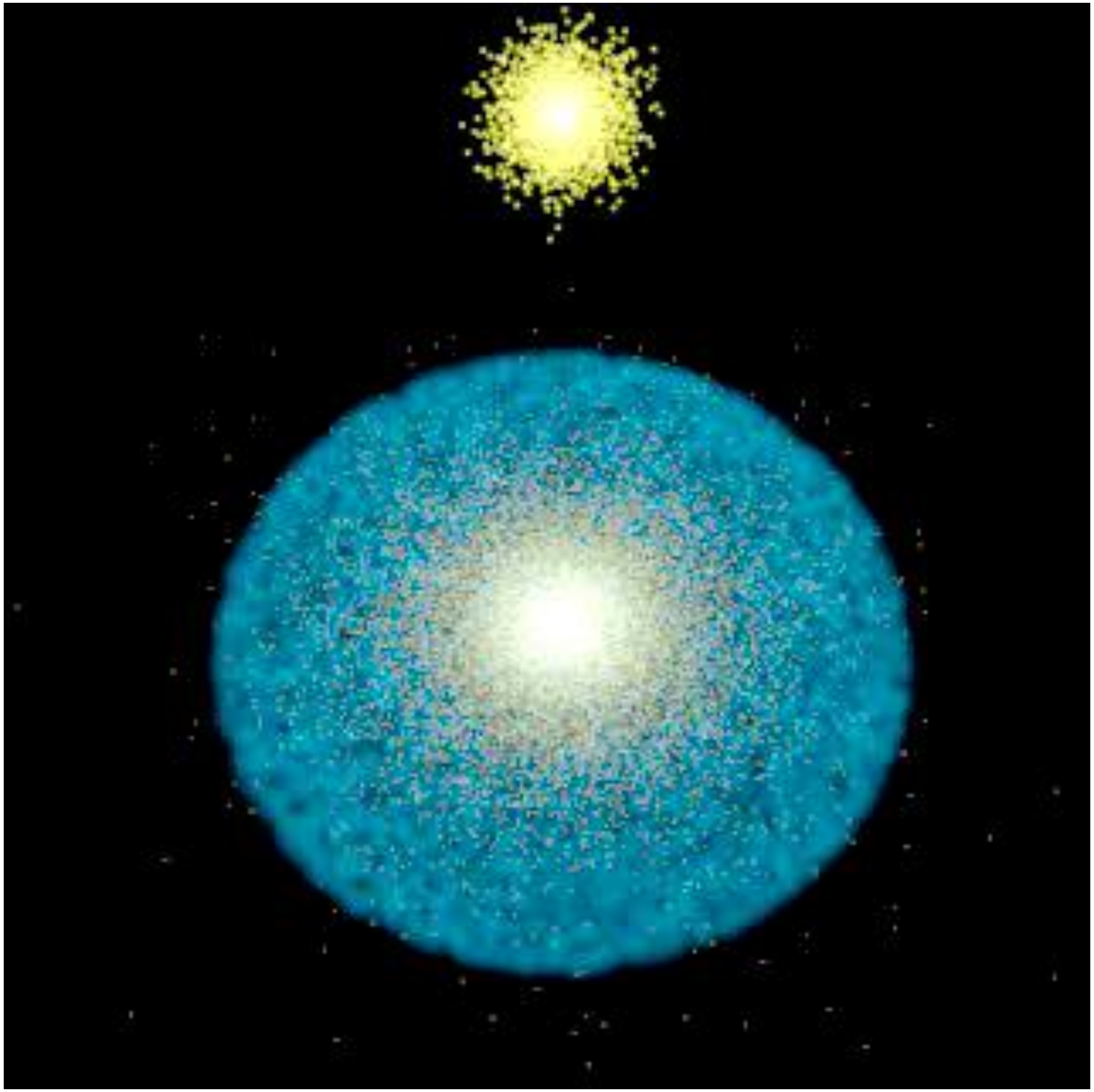

How likely are encounters?

- Slow encounters are unlikely in dense clusters
- Simulated passages are unlikely to be hyperbolic
- Tails and bridges are the least observed in dense clusters
- Close encounters unlikely in loose groups
- Therefore, most tidal effects must have been created by galaxies gravitationally bound

The Magellanic Clouds

- The Magellanic Clouds are contained within a common HI envelope.
- The Magellanic Stream traces their interaction with the MW.

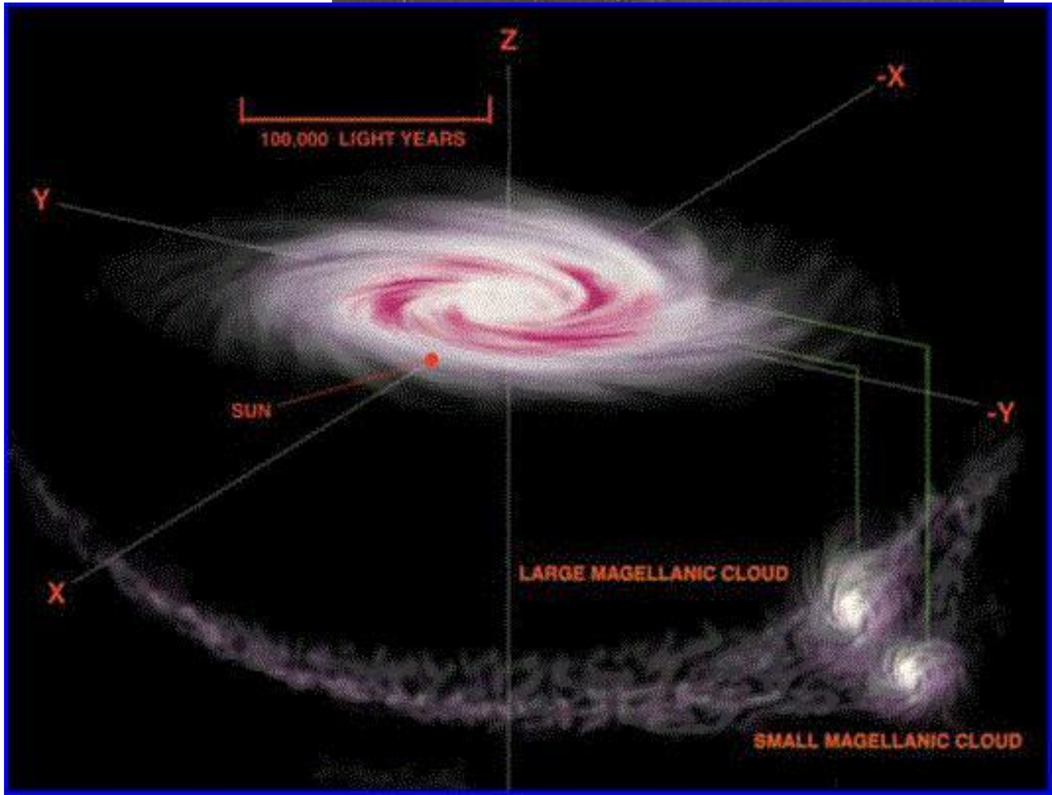

cD N4881 in Coma

cD = "cluster diffuse"

Much brighter than next brightest galaxy

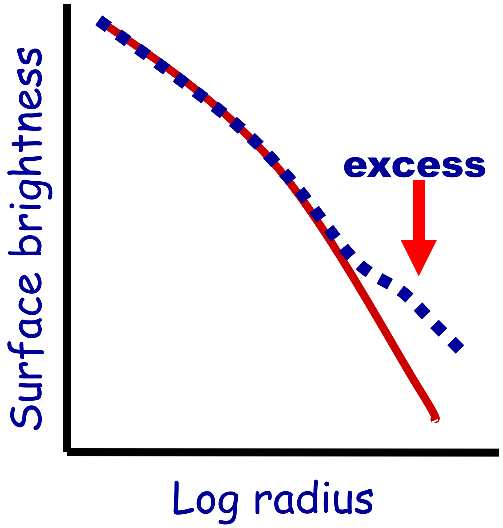

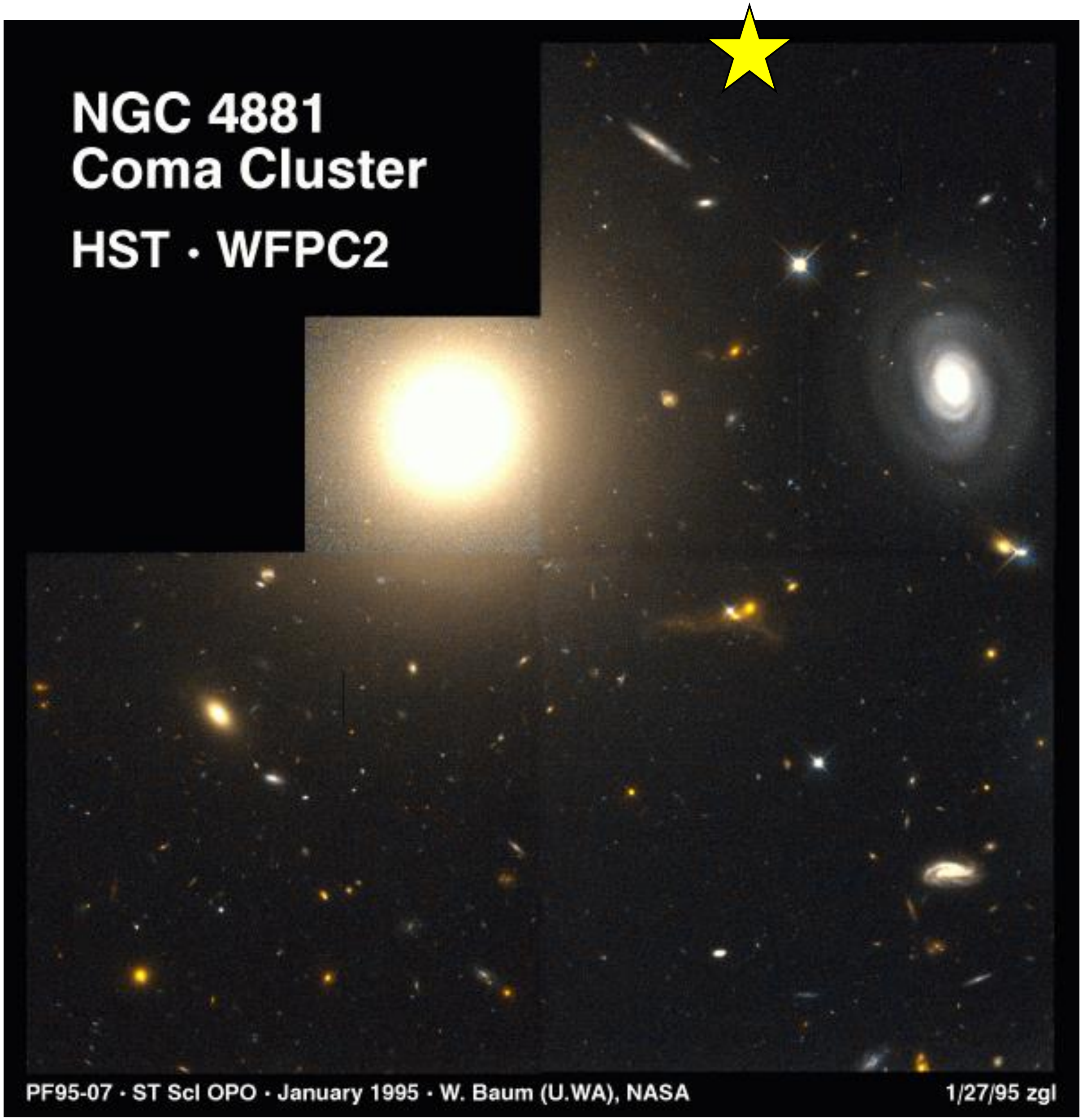

cD surface brightness profile

- cD galaxy in the cluster A496
- Note the excess light at $R^{1/4} > 2$

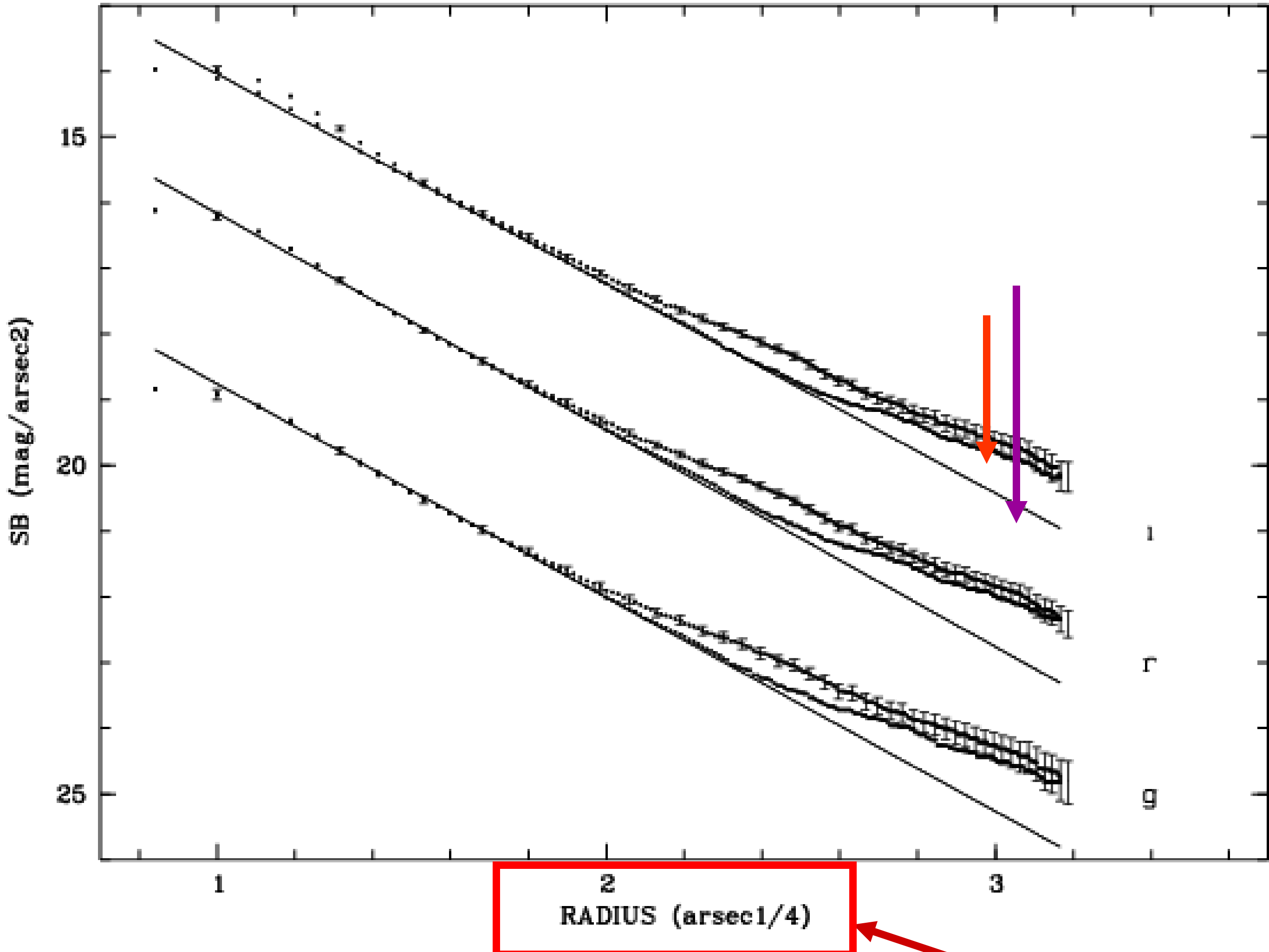

$$SB(r) = SB(r_{eff}) \exp(-7.67[(r/r_{eff})^{1/4} - 1])$$

where r_{eff} is the effective radius

Morretti et al.

cD galaxies

- In the cores of regular rich clusters (or at a density enhancement)
  - *Local* conditions are important
- Offset (too bright) from the luminosity function of normal galaxies
- Extensive (~1Mpc) stellar envelopes of low surface brightness
- Many have multiple nuclei

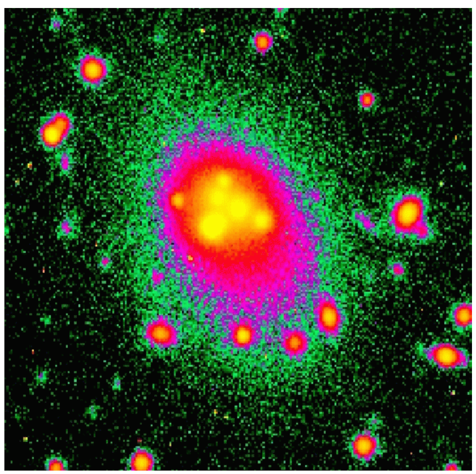

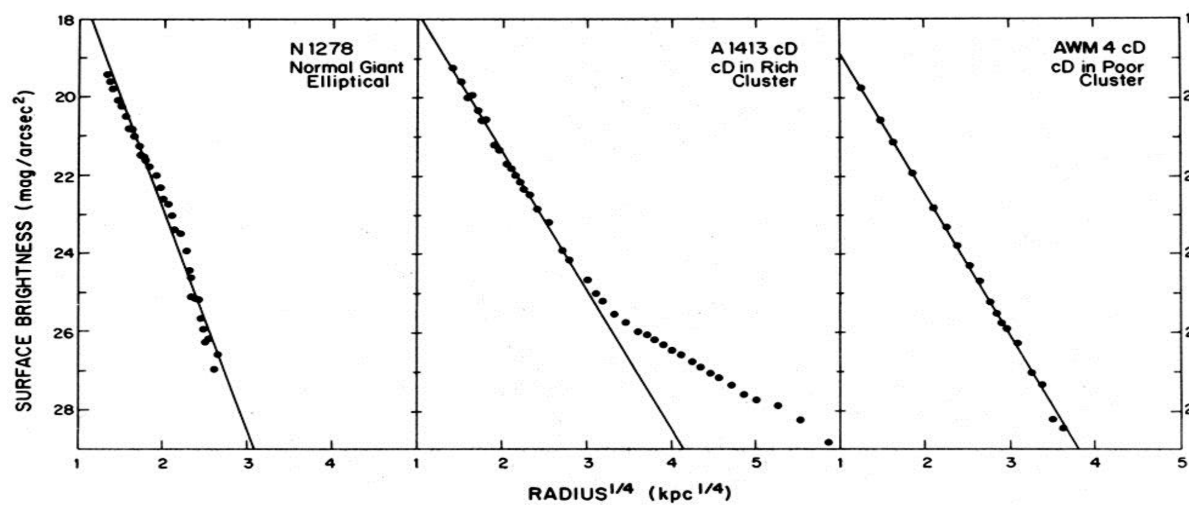

cD galaxy in Abell 3827

)

How do cD's form?

- Galactic Cannibalism (Ostriker & Hausman, 1977)
  - Dynamical friction brings massive galaxies to the center of clusters
  - Merger of these massive galaxies in the cluster cores
  - Giant galaxy then swallows other galaxies going through the core

Centaurus A

Dynamical friction

- Suppose an object of mass M is moving within a sea of other objects of mass m, with $m < M$.
- As M moves forward, the other objects are pulled towards it, with the closest ones feeling the strongest force.
- This produces a region of enhanced density along the path of M, including a wake trailing it.
- Dynamical friction = net gravitational force on M due to others that opposes its motion.
- Kinetic energy is transferred from M to surroundings, thus reducing its speed.

Cartoon of dynamical friction

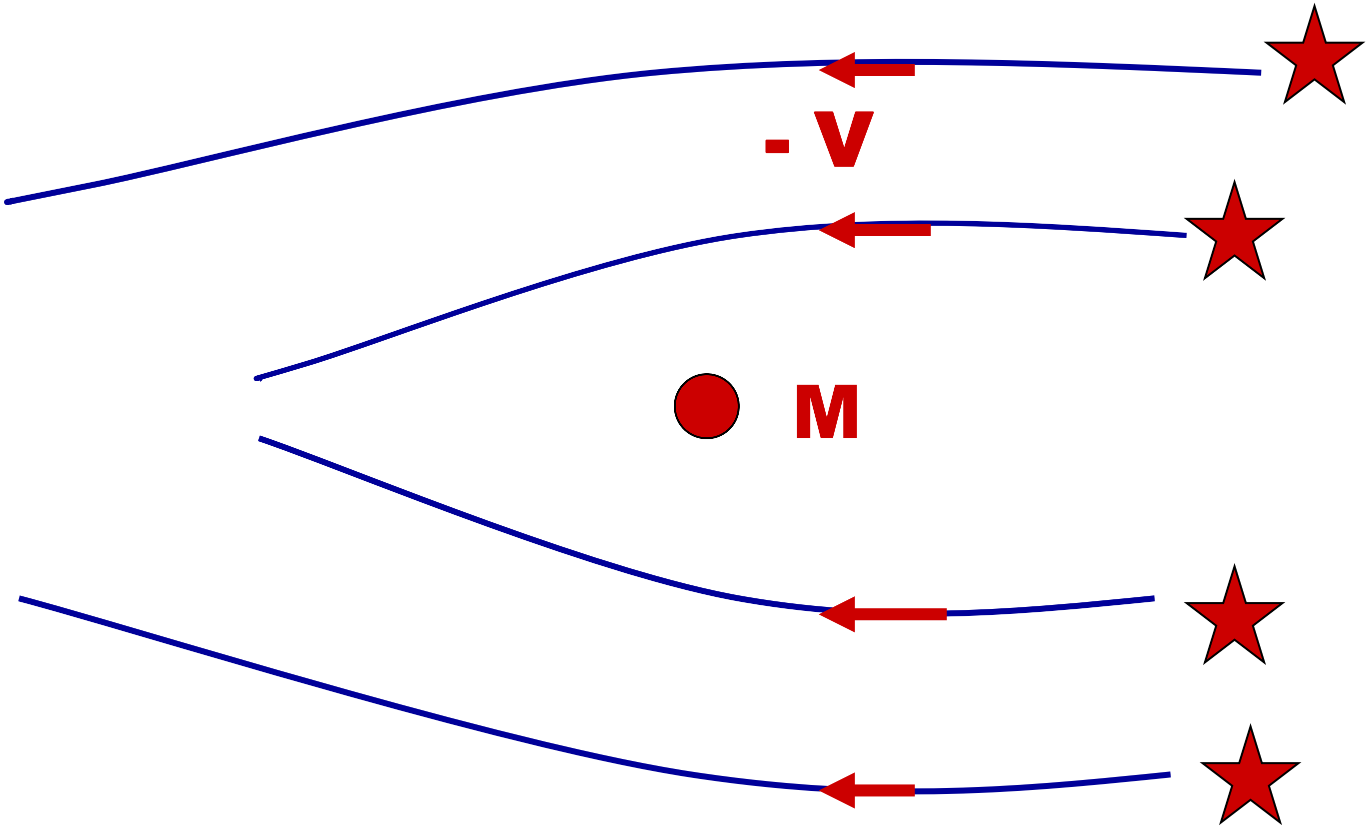

Mass M sees stars approach at velocity –V
Stars are deflected a bit by M
Slight excess of mass behind mass M

Galaxy harassment

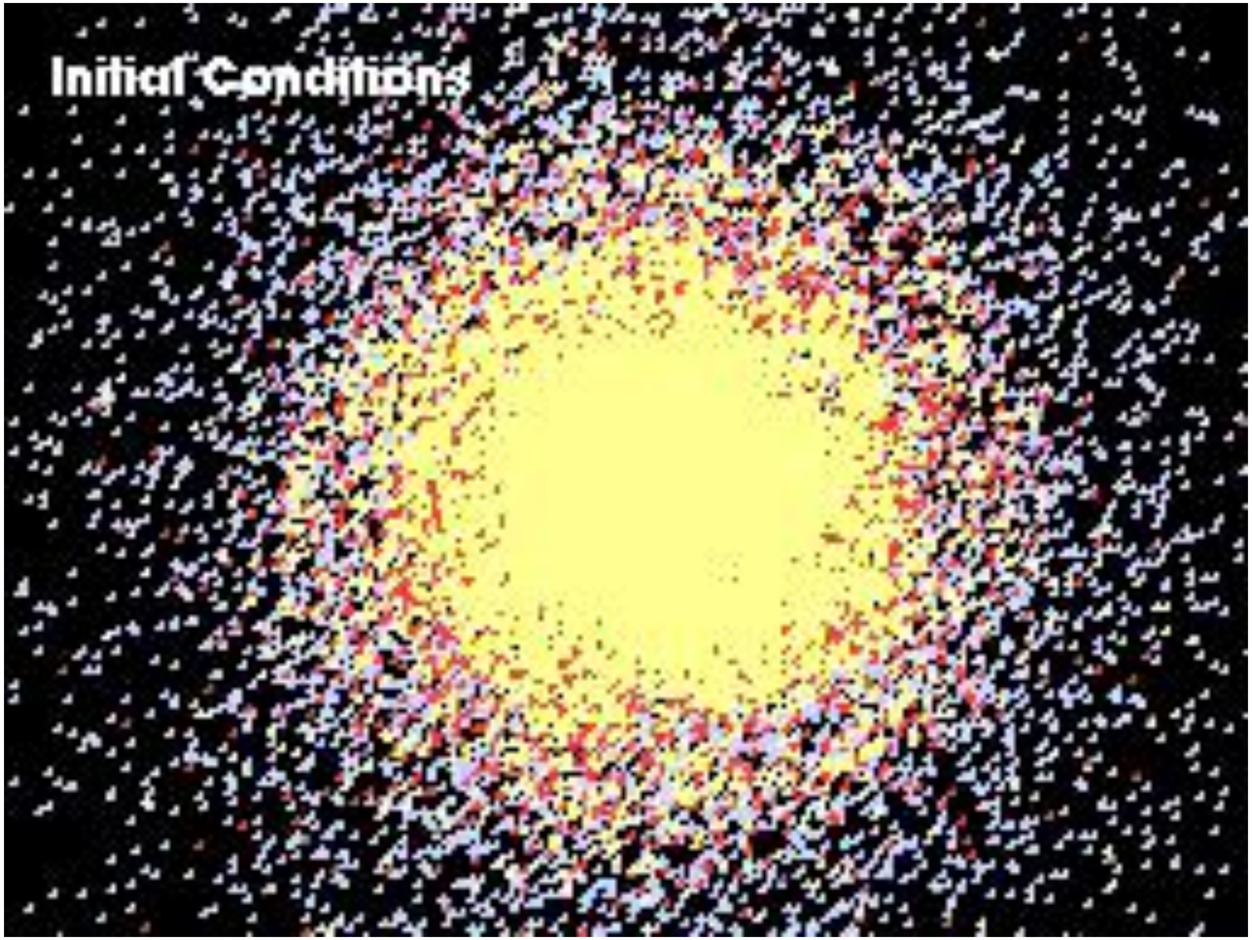

Multiple rapid encounters in a cluster may also seriously impact galaxy evolution.

Animation courtesty of G. Lake

Harassment

- Supporting evidence:
  - Intra cluster diffuse light (ICL)
    - Intergalactic stars, ~10-40% of the cluster stellar population (Feldmeier et al., 2003)
  - Tidal debris
    - e.g. Plumes and arc-like structures
    - The amount of tidal debris and ICL depends on local density, which supports the merger scenario (Combes, 2004)
  - Rings of star formation that are more common than two-armed spirals (Oemler et al., 1997)
    - Due to bars triggered during tidal interactions?

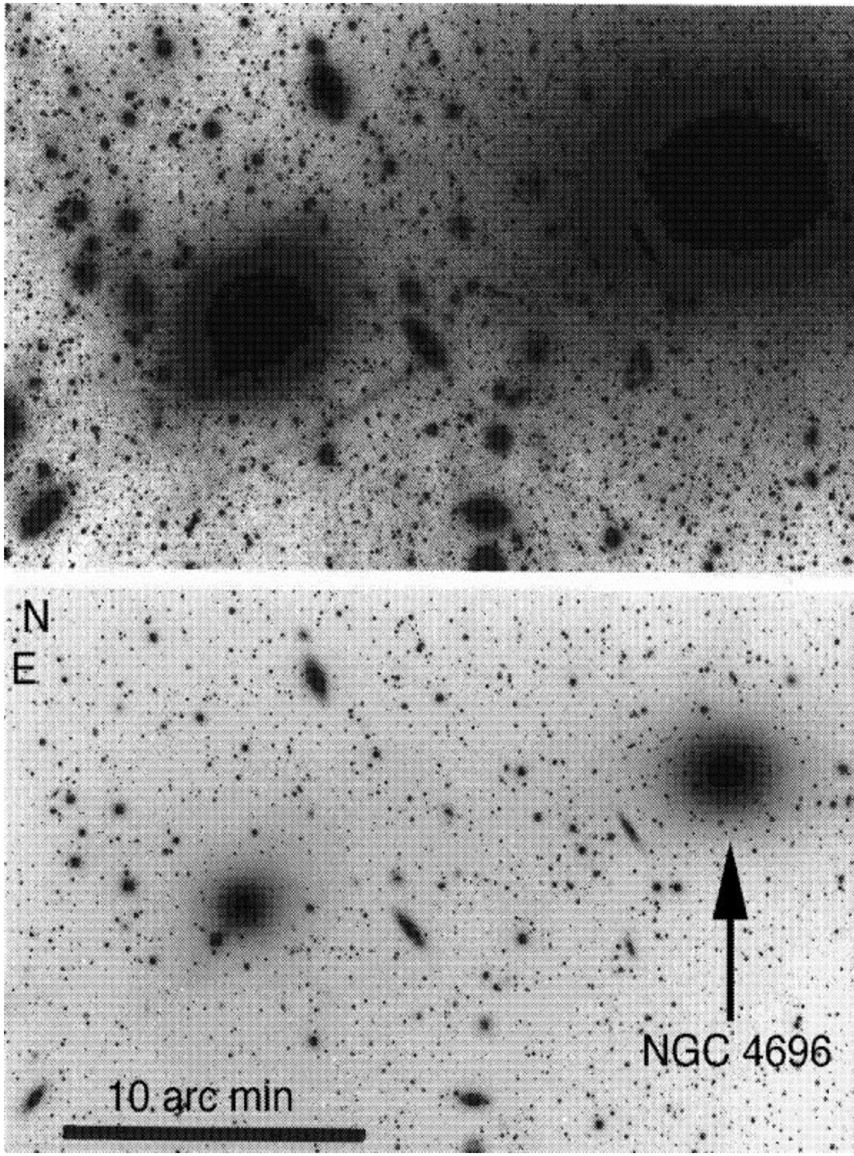

Ram pressure sweeping

- Spirals in Virgo are HI deficient.
- Hydrodynamical simulations show effectiveness of ram pressure stripping
- Stripping occurs if

  $\rho_{ICM}V^2 > 2\pi G\, \Sigma_{gas}\Sigma_{stars}$

- Gravitational "restoring" force of stars and gas in galaxy
- Σ is surface density

- Ram pressure exerted by stationary gas on moving galaxy
- V is velocity of galaxy with respect to cluster

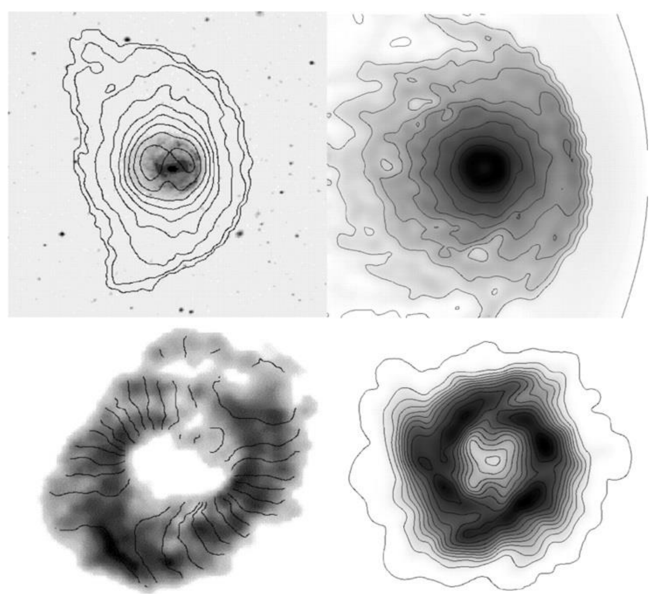

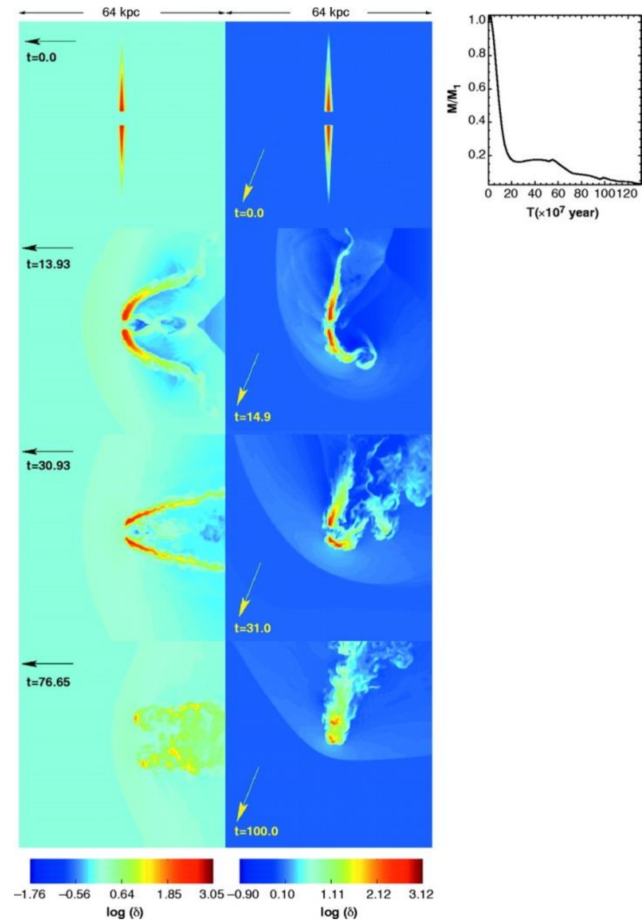

Vollmer et al. 2001

Ram Pressure Stripping

- Ram Pressure Stripping can remove the gas supply of galaxies that pass through clusters
  - Interaction between ISM and ICM
  - Could explain metal content of the ICM
  - Episodes of starburst?

Animation by Bengt Vollmer

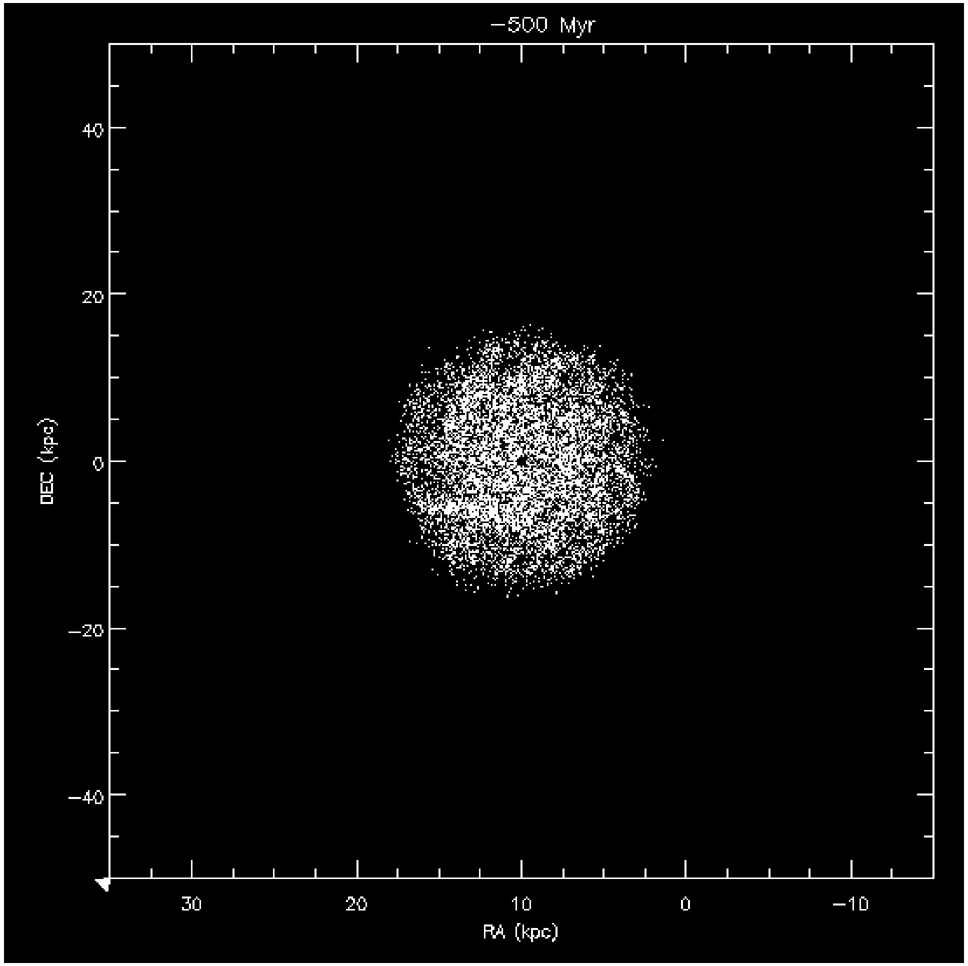

Formation of a cluster like Virgo

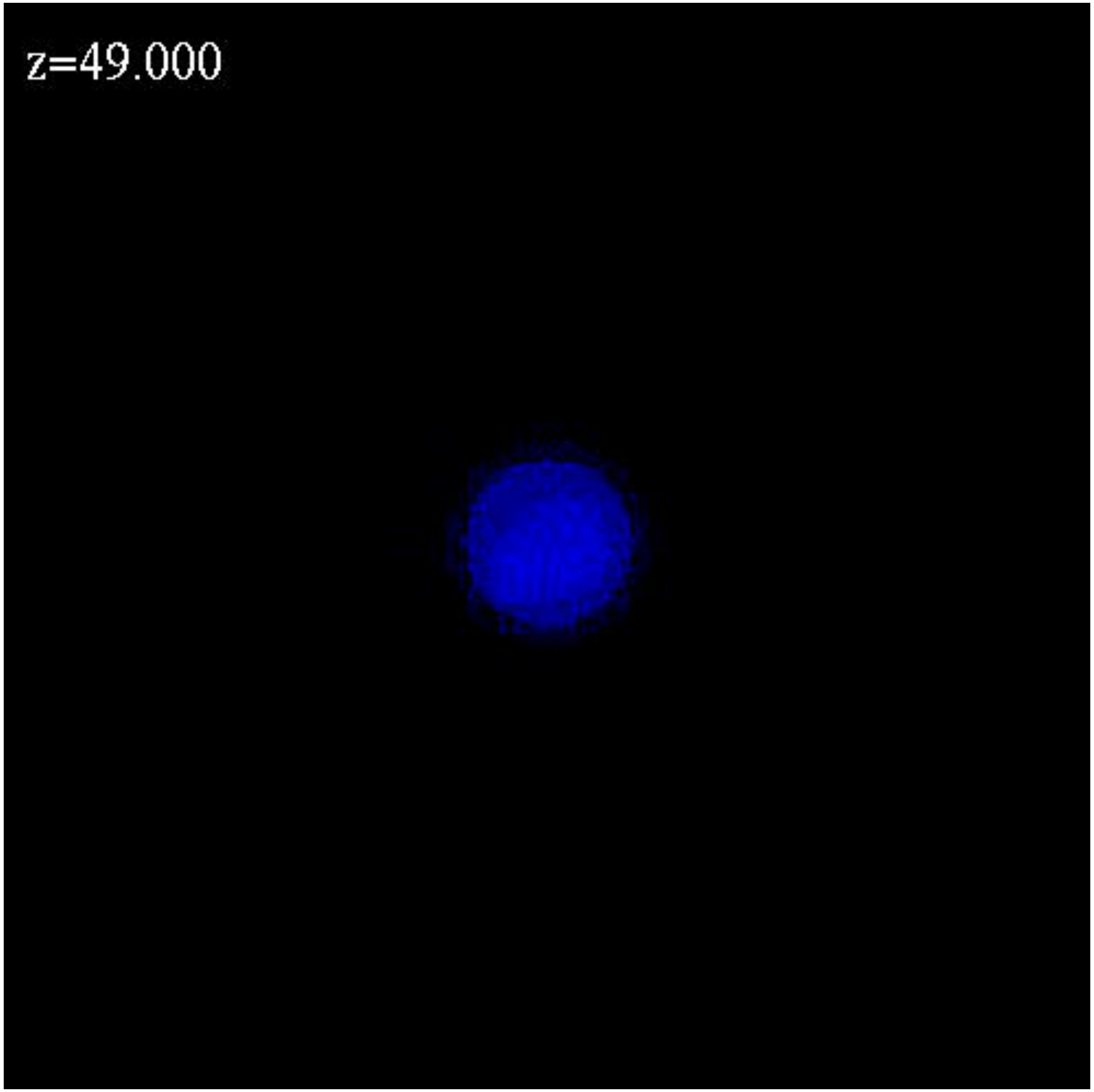

Simulation by
Ben Moore

HI Deficiency:

- HI standard of "normalcy":
  324 isolated galaxies
  Haynes & Giovanelli 1984
- Extended to smaller objects
  Solanes et al. 2002

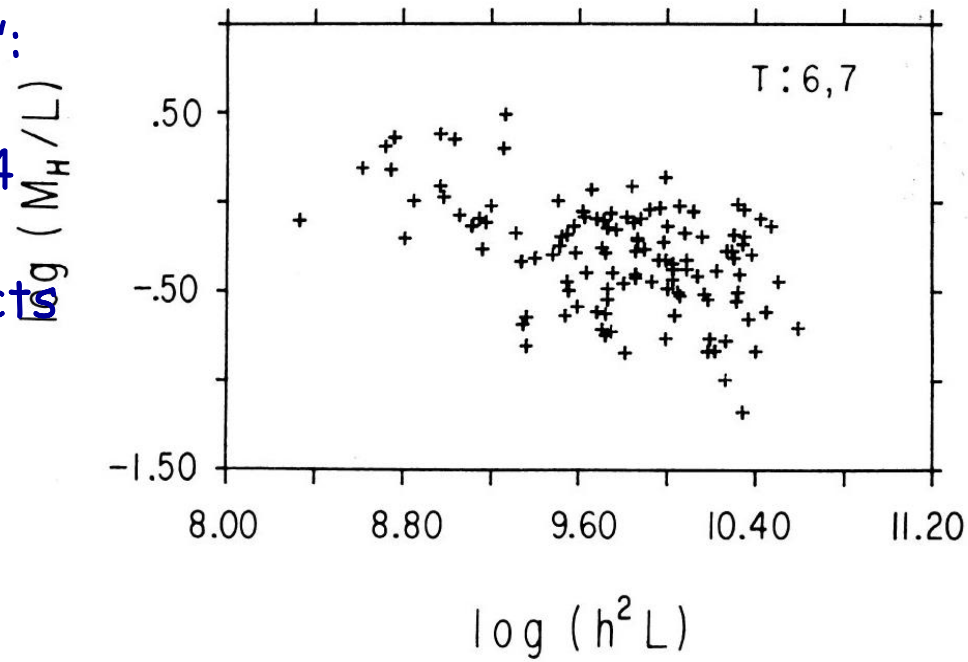

<DEF> $Def_{HI} = \log[\,M(HI{:}D)_{pred}\,] - \log[\,M(HI{:}D)_{obs}\,]$

(positive for systems more deficient than isolated galaxies of same type)

HI deficiency in Virgo

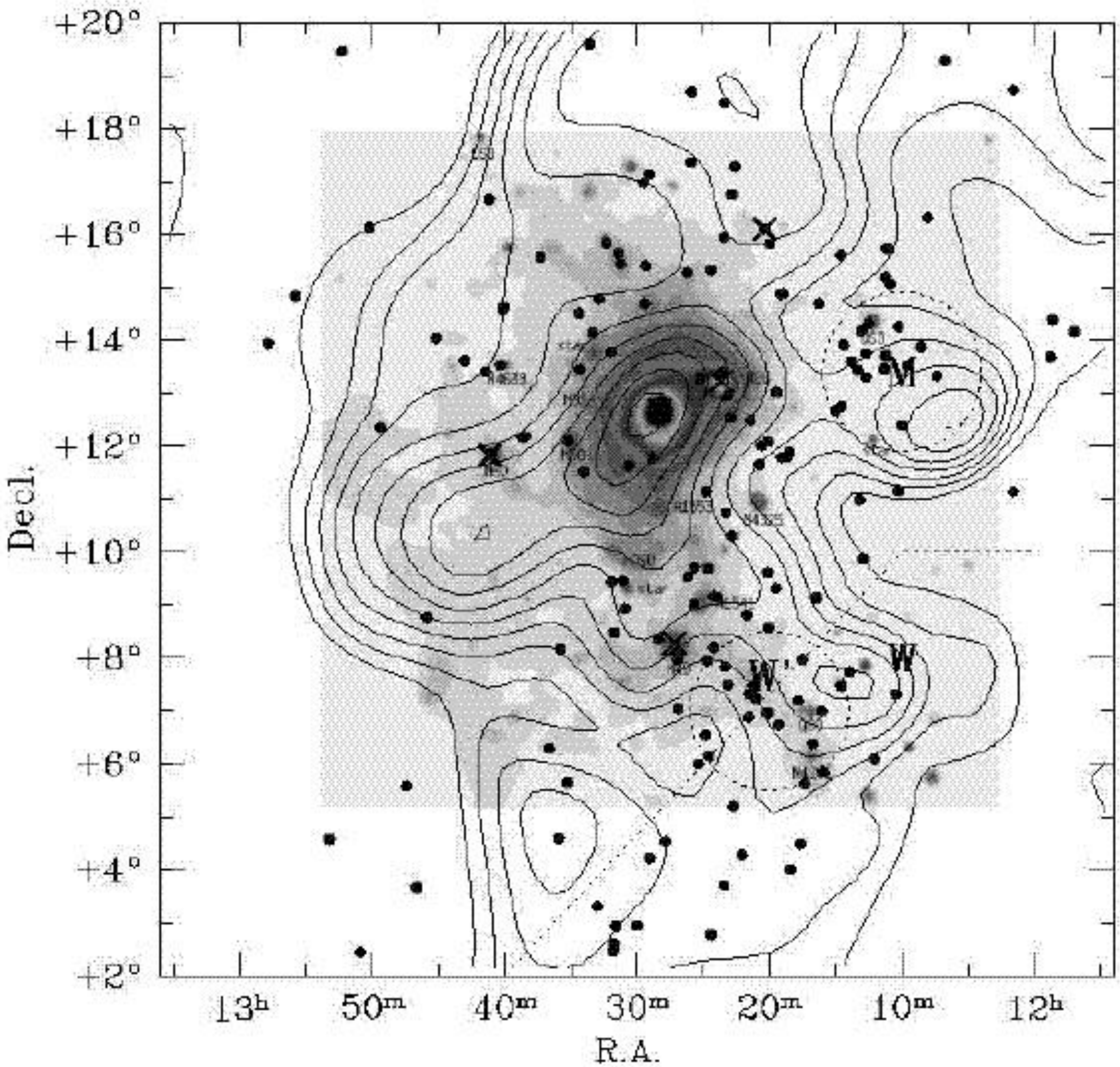

Dots: galaxies w/ measured HI

Contours: HI deficiency

Grey map: ROSAT 0.4-2.4 keV

Solanes et al. 2002

Galaxies embedded in the hot X-ray gas are deficient in their HI relative to isolated galaxies of the same size and morphology.